

https://dspace.org/

Corrosion behaviour of Pt-based superalloys intended for high temperature applications.

Maledi, Nthabiseng Beauty

2008-07-10T07:36:07Z
http://hdl.handle.net/10539/5020

Downloaded from a DSpace repository. https://dspace.org/

Corrosion behaviour of Pt-based superalloys intended for high temperature applications

Nthabiseng Beauty Maledi

A dissertation submitted to the Faculty of Engineering and the Built Environment, University of the Witwatersrand, in fulfillment of the requirements for the degree of Masters of Science in Engineering.

Johannesburg, 2007

Declaration

I declare that this dissertation is my own unaided work. It is being submitted for the degree of Masters of Science in the University of the Witwatersrand, Johannesburg. It has not been submitted before for any degree or examination in any other University.

Signature: N.B Maledi

……..

November 2007

ABSTRACT

Innovations towards the development of new high temperature alloys led to the development of ternary and quaternary Pt-based superalloys with similar structure to Ni-based superalloys (NBSA). These alloys are to be used in the gas turbine industry. This report presents the work that involved aggressive environmental interactions of Pt-based superalloys with molten salt and reducing environments at high temperatures. The work was to serve as materials selection criterion for the developed high temperature alloys. Hot corrosion was conducted at ±950ºC in molten Na_2SO_4 salt. The controlled mixed gas (0.2%SO_2-N_2) environment test was performed at 900ºC. Characterisation methods that were used included SEM, Raman, XRD and optical microscopy. The performance of Pt-based superalloys was outstanding, under both test conditions, outperforming the benchmark alloys. Alloy RS1 [Pt-Al-Cr] showed better performance over other investigated Pt-based superalloys and the benchmark alloys in molten salt. Exceptional behaviour was exhibited by alloy RS2 [Pt-Al-Ru] in the mixed gas environment. The uncoated alloy was unable to form a protective oxide scale, which led to the failure of the single crystal alloy. The coated alloy suffered serious degradation under 0.2%SO_2-N_2 conditions due to the formation of undesirable brittle phases. Ternary Pt-based superalloys are encouraging for further development as the next high temperature alloys in the gas turbine industry.

Dedications

This dissertation is dedicated to my loving daughter Keamogetswe Maledi

O boitumelo ba pelo ya me…..

ACKNOWLEDGEMENTS

I would like to thank everyone who contributed positively towards the success of my work. I appreciate the influence my supervisor had towards this work, his resourcefulness, support and guidance towards the success of this research work.

Many thanks to Dr Michelle Sephton, for her contribution and influence as my first supervisor who initiated this corrosion work. Wishing you success in your endeavors.

Gratitude to Dr Lesley Cornish, for helping me complete my studies, and giving me the opportunity to be part of the Advanced Materials Group at Mintek. I am grateful for the opportunity that was presented to me to attend the workshop in Germany. I truly learned a lot from the visit. You've made my dreams possible, you are truly God sent.

Not forgetting the Advanced Materials team: Thanks to Lizelle Glaner for preparing the samples. Dr Alistair Doughglas for your devotion in helping me complete my analysis. Lesley Chown and Rainer Süss for editing my conference paper. You have a true team spirit and best of luck for the future.

Sincere thanks to Professor Witcomb for cutting my samples, as small as they were, and for the time you spent working on the images. To our warm spirited

technician, Mr Aubrey Xoseka for developing the SEM pictures in the dark room and your special magic touch with metallographic preparation. Rudolph Erasmus for spending endless hours on the Raman spectroscopy, I appreciate the effort in characterising the samples.

Thanks to CSIR for preparing and donating coated samples. Thanks to Mintek for the financial support towards my studies and for supplying samples for this investigation.

Lastly, I would like to thank the people who did not have technical support but showed a lot of interest in my work. To my family, for the support and encouragement, especially for baby-sitting on my behalf, when I could not. To Jerome, for your understanding, devotion and eagerness to help. God bless.

CONTRIBUTIONS FROM THIS STUDY

1. Maledi, N.B., Potgieter, J.H., Sephton, M., Cornish, L.A., Chown, L., Süss, R., Hot corrosion behaviour of Pt-alloys intended for application in the next generation of gas turbines, *2nd International Platinum Conference "Platinum Surges Ahead"* South African Institute of Mining and Metallurgy SAIMM conference, Symposium Series S45, pp 81-90, Sun City, South Africa, 12th -18th October 2006

2. Maledi, N.B., Potgieter, J.H., Cornish, L.A., Chown, L., Süss, R., The performance of coatings compared to Pt-based superalloys intended for high temperature applications subjected to hot corrosion: A review, *8thInternational Corrosion Conference***,** South African Institute of Mining and Metallurgy SAIMM conference, Johannesburg, South Africa, 14th -15th November 2006

TABLE OF CONTENTS

Declaration.....ii
ABSTRACT.....iii
Dedications.....iv
ACKNOWLEDGEMENTS.....v
CONTRIBUTIONS FROM THIS STUDY.....vii
TABLE OF CONTENTS.....viii
List of figures.....xi
List of tables.....xiv
Chapter I.....1
1. *INTRODUCTION*.....1
1.1 BACKGROUND.....3
1.2 MOTIVATION.....3
1.3 HYPOTHESIS.....4
1.4 SPECIFIC OBJECTIVES OF THIS INVESTIGATION.....4
1.5 APPROACH OF THE INVESTIGATION.....5
1.6 GENERAL LAYOUT.....5
Chapter II.....7
2. ***Literature Review***.....7
2.1 INTRODUCTION.....7
2.2 STRENGTHENING MECHANISMS AND DEVELOPMENTS OF NBSAs.....10
2.3 CHEMICAL COMPOSITION AND THE EFFECT OF ALLOYING ELEMENTS.12
2.4 PROCESSING TECHNIQUES OF NBSAs.....14
2.4.1 Coatings and blade cooling in gas turbines.....16
2.5 HIGH TEMPERATURE MECHANICAL PROPERTIES.....19
2.5.1 Creep resistance.....19
2.5.2 Good tensile strength.....20
2.5.3 Thermal expansion.....21
2.5.4 Thermal conductivity.....21
2.5.5 Low density.....21
2.5.6 Surface stability.....21
2.5.6.1 *Oxidation*.....22
2.5.6.2 *Hot corrosion*.....23
2.6 FACTORS AFFECTING HOT CORROSION.....28
2.6.1 Alloy composition.....28
2.6.2 Temperature.....29
2.6.3 Gas composition.....29
2.6.4 Salt composition and deposition rate.....29
2.7 HOT CORROSION MECHANISMS.....30
2.8 LABORATORY TESTS USED TO STUDY HOT CORROSION.....31

Chapter III **33**

3. *Development of Platinum-based superalloys* **33**

3.1 INTRODUCTION 33
3.1.1 Ceramics 33
3.1.2 Intermetallics 34
3.1.3 Refractory metals 35
3.1.4 Composites 35
3.1.5 Platimun group metals-(PGMs) 35
3.2 MICROSTRUCTURE AND THE EFFECT OF ALLOYING ELEMENTS IN THE INVESTIGATED ALLOYS 36
3.3 MECHANICAL PROPERTIES OF Pt-BASED SUPERALLOYS 39

Chapter IV **43**

4. ***Experimental procedure*** **43**

4.1 INTRODUCTION 43
4.2 INVESTIGATED MATERIALS 44
4.3 EXPERIMENTAL PROCEDURE 46
4.3.1 Crucible test 46
4.3.2 Sulphidation test 47
4.4 MATERIALS CHARACTERISATION 48
4.4.1 Scanning electron microscope with X-ray dispersive spectrometry 48
4.4.2 X-ray diffraction 48
4.4.3 Raman spectroscopy 48
4.4.4 Optical microscopy 49

Chapter V **50**

5. ***Results*** **50**

5.1 HOT CORROSION RESULTS 50
5.1.1 Corrosion kinetics 50
5.1.2 Corrosion morphologies and cross sectional analysis 54
5.1.3 X-ray diffraction analysis 68
5.1.4 Raman analysis 73
5.2 SULPHIDATION RESULTS 76
5.2.1 Corrosion kinetics obtained after sulphidation 76
5.2.2 SEM analysis with EDS performed on cross sections of the investigated alloys after sulphidation 77
5.2.3 X-ray diffraction analysis after sulphidation 92
5.2.4 Raman analysis 99

Chapter VI **107**

6. ***Discussions*** **107**

6.1 HOT CORROSION 107
6.1.1 Degradation of the investigated alloys 107
6.1.2 Possible mechanism of failure 110
6.1.3 Role of alloying elements in corrosion resistance 112
6.2 SULPHIDATION 114

Chapter VII **118**

7. ***Conclusions and recommendations*** **118**

7.1 Conclusions 118
7.2 Recommendation 120
7.2 Contributions of this research 121
8. REFERENCES 122

LIST OF FIGURES

Figure 2.1 Different materials used in the aerospace industry 8
Figure 2.2 A fcc crystal structure of the γ' precipitate. 10
Figure 2.3 Yield strength versus temperature indicates capabilities of the γ'–phase with increasing temperature 11
Figure 2.4 Processing techniques developed to increase working temperatures in gas turbines 15
Figure 2.5 Ellingham diagram of oxides plotted against partial pressures. 22
Figure 2.6 Equilibrium phase diagram for Na_2SO_4-V_2O_5 25
Figure 2.7 Typical microstructure of type I hot corrosion 27
Figure 2.8 Three corrosion mechanisms showing a) Non-layered hot corrosion b) Transition type hot corrosion c) Layered hot corrosion. 28
Figure 2.9 Calculated solubilities of metal oxides at 1200 K in molten Na_2SO_4 salt 30
Figure 2.10 Burner rig test configuration showing a sample during the test 32
Figure 3.1 Binary phase diagram of Pt-Al system 36
Figure 3.2 (a) Pt-based superalloys: SEM-BSE of optimum $Pt_{84}Al_{11}Ru_2Cr_3$ alloy 38
Figure 3.2 (b) NBSA Cuboidal γ' precipitates of MAR-M200 alloy 38
Figure 3.3 Stress rupture strength of an ODS alloy (PM2000) and ternary Pt-based superalloys at 1300ºC in air 40
Figure 3.4 Stress rupture strength of an ODS alloy (PM2000) and ternary Pt-based superalloys at 1300ºC and 30 MPa 41
Figure 3.5 Material loss of various high temperature alloys 42
Figure 4.1 Cross section of a coated Ni-based superalloy in as polished condition showing a thin coating applied on the surface of the alloy 45
Figure 5.1 Corrosion kinetics of uncoated Ni-based superalloy (CMSX-4) after exposure to molten Na_2SO_4 salt at 950ºC 51
Figure 5.2 Corrosion kinetics of the coated nickel based superalloy after exposing the sample to molten Na_2SO_4 salt at 950ºC 52
Figure 5.3 Corrosion kinetics of Pt-based superalloys in molten salts at 950ºC for duration of 792 hours 53
Figure 5.4 Cumulative weight gains of Pt-based superalloys after 792 hours in molten salt 54
Figure 5.5 Secondary electron micrograph showing corrosion morphology of the coated NBSA that resulted after hot corrosion in molten Na_2SO_4 salt at 950ºC 55
Figure 5.6 Secondary electron image of the corrosion morphology of the uncoated CMSX-4 after hot corrosion at 950ºC with a crack running across the surface of the alloy 56
Figure 5.7 EDS analysis performed on the surface of the uncoated alloy that was exposed to molten salt at 950ºC 56
Figure 5.8 Secondary electron image of alloy P421 with non-protective oxide scale after hot corrosion at 950ºC after 540 hours 57
Figure 5.9 Secondary electron image of crystal structured corrosion morphology on alloy P421 after undergoing hot corrosion at 950ºC for 792 hours 58

Figure 5.10 Secondary electron image of the surface morphology on alloy P420 after exposure to molten Na_2SO_4 salt for a period of 540 hours 59
Figure 5.11 Secondary electron image of the corrosion morphology of alloy P420 after hot corrosion at 950ºC for 792 hours 60
Figure 5.12 Secondary electron image showing a porous oxide scale on the surface of alloy RS1 after hot corrosion in molten salt for 540 hours 61
Figure 5.13 Secondary electron image with a porous oxide scale on the surface of alloy RS1 after hot corrosion in molten salt for 792 hours 61
Figure 5.14 Secondary electron image of the corrosion morphology that resulted on the surface of alloy RS2 after hot corrosion at 950ºC for 540 hours 62
Figure 5.15 Secondary electron image of corrosion morphology that resulted on the surface of alloy RS2 at 950ºC for 792 hours 62
Figure 5.16 Secondary electron image of the corrosion morphology of alloy RS3 after hot corrosion in molten Na_2SO_4 salt at 950ºC for duration of 540 hours 63
Figure 5.17 Secondary electron image of corrosion morphology of alloy RS3 after hot corrosion in molten Na_2SO_4 salt at 950ºC for duration of 792 hours 63
Figure 5.18 SEM scan obtained after performing cross sectional analysis on the surface of the alloy RS2. 64
Figure 5.19 Cross sectional morphology of the uncoated alloy after hot corrosion attack in molten Na_2SO_4 salt 65
Figure 5.20 SEM scan obtained after performing cross sectional analysis on the surface of the uncoated alloy 65
Figure 5.21 Secondary electron micrograph of the cross section of alloy RS1 after hot corrosion test at 950°C 66
Figure 5.22 Secondary electron micrograph of the cross section of alloy RS2 after hot corrosion test at 950°C 67
Figure 5.23 Secondary electron micrograph of the cross section of alloy RS3 after hot corrosion test at 950°C 67
Figure 5.24 X-ray diffraction pattern on the scale of alloy RS1 after hot corrosion 68
Figure 5.25 X-ray diffraction pattern on the scale of alloy RS2 after hot corrosion 69
Figure 5.26 X-ray difraction patterns on the surface of alloy RS3 after hot corrosion 69
Figure 5.27 X-ray diffraction patterns on alloy P420 after hot corrosion at 950°C 70
Figure 5.28 X-ray diffraction patterns on the surface of alloy P421 after hot corrosion.. 71
Figure 5.29 X-ray diffraction patterns on the surface of the coated Ni-based superalloy after hot corrosion 72
Figure 5.30 X-ray diffraction patterns on the surface of uncoated Ni-based superalloy after hot corrosion 73
Figure 5.31 Raman spectra obtained from the five Pt-based superalloys after hot corrosion investigations at 950 °C 74
Figure 5.32 Raman spectra obtained from the uncoated CMSX-4 alloy after hot corrosion investigations at 950 °C 75
Figure 5.33 Raman spectra of the coated NBSA after hot corrosion test at 950°C 76
Figure 5.34 Corrosion kinetics of the seven investigated alloys after sulphidation in a 0.2% SO_2-N_2 gaseous environment 77
Figure 5.35 SEM image showing cross section of alloy RS1 after the sulphidation test in 0.2% SO_2-N_2 gas at 900ºC 78

Figure 5.36 Secondary electron images of the cross section of aloy RS1 at 30 000X magnification after the sulphidation test, showing the effect and depth of attack by 0.2%SO_2-N_2 gas 78
Figure 5.37 SEM image showing the external oxide layer that formed on the surface of alloy RS1 79
Figure 5.38 EDS analysis performed on the external scale that formed on the surface of alloy RS1 after the sulphidation test in 0.2% SO_2-N_2 environment 80
Figure 5.39 Secondary electron image of alloy RS2 after sulphidation test 81
Figure 5.40 Cross section of alloy RS2 at 14 000X magnification with an Al_2O_3 scale forming on the surface of the alloy 81
Figure 5.41 EDS analysis performed on the external scale of alloy RS2 81
Figure 5.42 Secondary image of cross section of alloy RS3 after sulphidation test 82
Figure 5.43 EDS analysis performed on the dark area in the corroded section on alloy RS3 83
Figure 5.44 Secondary image of alloy P420 after sulphidation test in 0.2% SO_2-N_2 environment 84
Figure 5.45 Secondary electron image of alloy P420 with the dendritic structure below the corroded area 85
Figure 5.46 Transverse section of corroded alloy P421 after the sulphidation test at 900°C 86
Figure 5.47 Transverse section of alloy P421 across the corroded area of alloy P421 after sulphidation test at 900°C 86
Figure 5.48 Transverse section of alloy P421 showing the Al depleted area after exposing the alloy to 0.2% SO_2-N_2 environment 86
Figure 5.49 Cross section showing the different phases formed when the alloy was exposed to 0.2% SO_2-N_2 atmosphere 87
Figure 5.50 EDS analysis performed on the external scale of the coated alloy after sulphidation test 88
Figure 5.51 Inter-diffusion zone at high magnification showing the coated Ni-based superalloy after 60 hours in a 0.2% SO_2-N_2 atmosphere 89
Figure 5.52 EDS analysis performed on the needle-like phases that formed between the substrate and the coating 89
Figure 5.53 EDS analysis performed on the coated alloy in the area below the Al_2O_3 scale 90
Figure 5.54 Secondary image of the cross section of the uncoated Ni-based superalloy after sulphidation test 91
Figure 5.55 XRD spectrum performed on the coated Ni-based superalloy before and after corrosion in controlled atmosphere constituting of 0.2% SO_2-N_2 at 900°C for a period of 60 hours 92
Figure 5.56 XRD pattern on the uncoated Ni-based superalloy after exposure to 0.2% SO_2-N_2 atmosphere 93
Figure 5.57 XRD spectra performed on the external surface of alloy RS1 before and after exposure to 0.2% SO_2-N_2 atmosphere at 900ºC for a period of 60 hours 94
Figure 5.58 XRD spectrum performed on the external scale of alloy RS2 [Pt-Al-Ru] before and after exposure to 0.2% SO_2-N_2 atmosphere at 900°C for a period of 60 hours 95

Figure 5.59 XRD spectrum performed on the external surface of alloy RS3 [Pt-Al-Cr-Ru] before and after exposure to a 0.2% SO_2-N_2 atmosphere at 900°C for a period of 60 hours 96
Figure 5.60 XRD spectrum performed on the external surface of alloy P420 [Pt-Al-6Co] before and after exposure to a 0.2% SO_2-N_2 atmosphere for a period of 60 hours .. 97
Figure 5.61 XRD pattern of alloy P421 in as-cast condition and after exposing the alloy to a gaseous environment of 0.2% SO_2-N_2 for a duration of 60 hours 98
Figure 5.62 Raman spectra collected on the external surface of the uncoated alloy after sulphidisation at 900°C for a period of 60 hours 100
Figure 5.63 Raman spectra collected on the external surface of the coated alloy after sulphidisation at 900°C for a period of 60 hours 101
Figure 5.64 Raman spectra collected on the external surface of alloy RS1 after sulphidisation at 900°C for a period of 60 hours 102
Figure 5.65 Raman spectra collected on the external surface of alloy RS2 after sulphidisation at 900°C for a period of 60 hours 103
Figure 5.66 Raman spectra collected on the external surface of alloy RS3 after sulphidisation at 900°C for a period of 60 hours 103
Figure 5.67 Raman spectra collected on the external surface of alloy P420 after sulphidisation at 900°C for a period of 60 hours 105
Figure 5.68 Raman spectra collected on the external surface of alloy P421 after sulphidisation at 900°C for a period of 60 hours 105
Figure 6.1 Cross section of alloy RS3 showing fluxing of the external scale when the alloy was immersed in molten Na_2SO_4 salt 111
Figure 6.2 Spallation around the cracks on the surface of alloy P420 that was subjected to molten salts at 950°C for a period of 540 hours 113
Figure 6.3 EDS spot analysis performed on the needles formed 116

LIST OF TABLES

Table 2.1 Norminal chemical composition of commercial NBSAs 12
Table 2.2 Effects of various alloying elements in NBSAs 14
Table 2.3 Properties and applications of NBSAs at 870 ºC..... 20
Table 2.4 Kinetics of Cr, Al, and Si oxides at 1200 ºC 23
Table 2.5 High temperature processes with respective corrosion mode..... 26
Table 3.1 Properties of ceramics material compared to Nimonic, a nickel based superalloy 34
Table 3.2 Misfit calculations of the developed Pt-based superalloys..... 38
Table 3.3 Hardness results of the five Pt-based superalloys used in the investigation..... 40
Table 4.1 Nominal chemical composition of selected Pt-based alloys (at%) investigated 45
Table 4.2 Nominal chemical composition of CMSX-4 (wt%) 45
Table 5.1 Peak positions in cm^{-1} by Raman spectra on surface of the uncoated NBSA .. 75
Table 5.2 Peak positions found on the surface of Pt-based superalloys after exposing the alloys to a corrosive gas..... 102
Table 5.3 Raman shifts of the corroded alloy P420 exposed to 0.2% SO_2-N_2 corrosive gas at 900 °C 104

1. INTRODUCTION

The development of high temperature materials in gas turbines is largely influenced by an ongoing demand to increase the operating temperatures of jet engines. High temperature operations allows for enhanced efficiencies, which result in marked economical benefit through reduced fuel consumptions. With the law becoming more stringent towards pollution, increasing operating temperatures will also allow for significant reduction of both noise and air pollution.

The currently used nickel based superalloys (NBSAs) have reached their application limit in the aerospace industry. These alloys are operating at critical temperatures of 1100°C (90% of the alloy's melting point) [Hüller *et al.,* 2005]. It is intended to operate gas turbines at higher temperatures, exceeding 1300°C, so that better performance can be obtained [Saltykov *et al.,* 2004; Pint *et al*., 2006]. However, the desired temperatures are too high for NBSAs to withstand. This has led to new innovative research, aimed at developing novel materials to replace NBSAs. Previously it was difficult to engineer superalloys with both strength and corrosion resistance [Gurrappa, 2003]. Therefore the newly developed materials are to incorporate high temperature properties, which include high strength, creep and corrosion resistance.

Pt-based superalloys are amongst the numerous alloys that have been selected and developed for application in gas turbine blades. Pt was selected because of the element's high melting point (1769°C), similar fcc crystal structure to Ni, and better environmental resistance. In recent developments, Pt was mainly used in the gas turbine industry as an alloying element in

diffusion coatings. However, there is a demand to further develop Pt-based superalloys as structural material to replace NBSAs. The shortcomings of using Pt are the element's high cost and high density. The cost of Pt could be a disadvantage, since it has been noted that in other applications, alternative cheaper materials have been used to replace Pt. Density play a significant role during designing of gas turbines, especially where rotating components are concerned [Bradley, 1979; Carter, 2005]. Lightweight materials are desired because centrifugal forces can be diminished at low densities, therefore the heavy metal could have adverse effects towards the development of Pt-based superalloys. However, it is believed that the high cost could be compensated by the good properties of the alloy, while alloying additions could slightly reduce the density of Pt-based superalloys.

High temperature corrosion becomes significant and more aggressive with increasing temperatures [Yoshiba, 1993]. Generally coatings are a preferred choice in combating degradation due to the aggressive environment, but coatings are not completely reliable. When subjected to high stresses, coatings loose adhesion from the substrate and spall off [Dragos *et al.,* 2005]. It is therefore important and practical for the substrate to have inherent corrosion resistance [Pint *et al*., 2006].

Hot corrosion forms as a result of the formation of molten salt deposits from impurities in the air and fuel. Even at low concentrations, these particulates can cause serious degradation to these expensive materials. This work investigates hot corrosion behaviour of the developed ternary and quaternary polycrystalline Pt-based

superalloys and compares the behaviour to a coated and uncoated NBSA, CMSX-4[1] single crystal.

1.1 Background

The demand for heat resistant materials during World War II led to the birth of three classes of superalloys, Fe, Co and Ni-based superalloys. Amongst the three classes, NBSAs are the commonly used and desirable group in the aerospace industry due to their unique combination of high temperature properties. Since the development of NBSAs, the alloys underwent various microstructural modifications through metallurgical processes, which were aimed at improving the alloy's strength, creep properties and corrosion resistance. Coatings and cooling schemes were introduced to increase the working temperatures and also prevent the alloys from degradation in the corrosive environment. The degradation of high temperature material is due to the presence of impurities and gaseous environments that are a result of incomplete combustion reactions that takes place. Gas turbine materials are also subjected to stresses that could lead to failure.

1.2 Motivation

The Pt-industry has recently focused on finding new opportunities and uses for Pt. Presently, Pt finds its primary applications in the jewellery, automotive, coatings, glass, medical, chemical and electrical industries. The current research is aimed at using Pt as a replacement material in aerospace engines. The aerospace industry is a multi-billion dollar industry that presents great opportunities for high temperature materials. The world's fleet is on the rise with intentions to build bigger and better performing crafts, and similar trends are expected to be maintained for many years to come. This implies that there will be a high demand for high

[1] A second generation single crystal superalloy

strength materials with good mechanical and corrosion properties. Pt-based superalloys have shown successful performance in many high temperature applications, and are expected to have good properties in gas turbines as well. The trend in developing NBSAs has been geared towards increasing strength, with decreasing corrosion resistance. Now an alloy with better properties and more corrosion resistance is to be employed aimed to benefit the industry by savings on fuel, with less application of coatings, overcoming previous problem NBSAs could not address. Pt is recyclable, meaning the lifetime of the blade will be increased and environmental issues that arise during extraction of the metal will be eliminated. Turbine blades are not the only target market. Other areas of interest include the coating and the glass industries.

1.3 Hypothesis

Pt has good corrosion resistance in many high temperature applications. Addition of Pt in aluminide modified coatings has tremendously improved corrosion resistance of coatings in gas turbines. It is expected that Pt-based superalloys are likely to offer better corrosion resistance compared to alternative materials. Furthermore, Pt-based superalloys might not have to rely on coatings for them to be able to withstand the aggressive environments encountered in gas turbines.

1.4 Specific Objectives of this Investigation

Mechanical and oxidation properties of Pt-based superalloys were evaluated in previous work. Hot corrosion of Pt-based superalloys, another important high temperature property, was pending. The objective of the study was to help select suitable materials to be used in the aerospace industry. Corrosion behaviour of Pt-based superalloys of various chemical compositions was investigated in aggressive environments (molten salts and gaseous

environment). The selected Pt-based superalloys are to be ranked according to their resistance. The effect of alloying elements and the failure mechanism will be addressed.

1.5 Approach of the investigation

A cost effective method that was adopted in evaluating hot corrosion behaviour of Pt-based superalloys, was the crucible test or the molten salt test. This method was used because the test is aggressive and usually used to rank alloys, which was the main purpose of the study. Another test that was devised was the controlled atmosphere test, where the materials of interest were subjected to one of the corrosive gases at high temperatures. In both the tests, weight loss measurements were employed.

1.6 General layout

Chapter II gives an overview of superalloys, the development of microstructural properties, strengthening mechanisms and high temperature mechanical properties of NBSAs.

Chapter III describes the work conducted at Mintek toward the development of Pt-based superalloys. The work was aimed at selecting suitable ternary and quaternary alloys for further investigations. Mechanical properties such as creep, oxidation and
compression tests were evaluated and some of the results are presented.

Chapter IV describes the methodology of the weight loss test that was conducted in molten sodium sulphate salt and the effect of corrosive gases on the investigated alloys (sulphidation test). Characterisation techniques involved are discussed.

Chapter V presents corrosion kinetics, corrosion morphologies and characterisation results that were obtained during the investigation.

Chapter VI discusses the results obtained.

Chapter VII summarises the main findings of the investigation, conclusions drawn and recommendations.

2.1 INTRODUCTION

Superalloys are engineering materials based on group VIIIA elements (Fe, Co and Ni), designed to have outstanding properties and capabilities to withstand aggressive high temperature environments. Superalloys were developed in the United States during the early 1930s, as a result of the need for heat resistant materials [Sims *et al.*, 1972]. The aerospace industry is one of the largest users and developers of high temperature materials. Nickel based superalloys (NBSAs) comprise over 70% of an aircraft engine weight [Bradley, 1979; Bowman, 2000; Cornish *et al.*, 2003]. Figure 2.1 indicates other different materials such as titanium, aluminum, steel and composites used for different components in aerospace.

NBSAs are used in a wide range of applications, which includes components such as discs, bolts, shafts, cases, vanes, blades, burner cans, after burners and thrust reversers [Bradley, 1979]. Other high temperature applications includes marine, industrial, steam power plant, aircraft, rocket engines, petrochemical equipment and nuclear reactors [Sims *et al*., 1987; Callister, 1999].

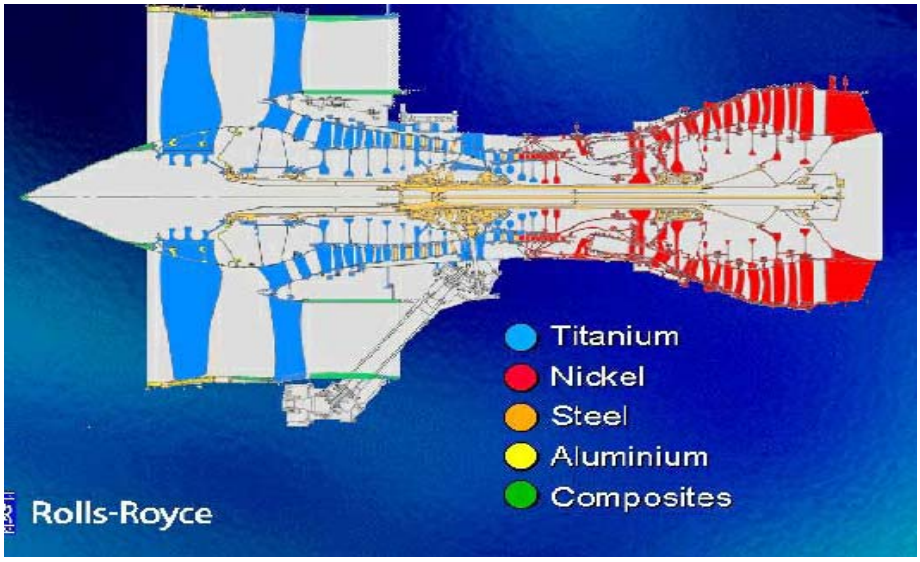


Figure 2.1 Different materials used in the aerospace industry [Bhadesia, 2003]

The successful application of NBSAs at high temperature is attributed to a number of mechanical properties the alloys possess. This includes properties such as creep resistance, high melting points, good thermal fatigue strength, and surface stability [Sims *et al*., 1972; Ashby and Jones, 1988]. All these factors are usually incorporated in the design, thus making superalloys complex materials.

There has been a constant temperature increase since the introduction of high temperature materials. Early age gas turbines were designed to operate at 700 ºC, and today, high turbine entry temperatures exceeding 1100 ºC are easily achieved [Ashby and Jones, 1988; Konter and Thumann, 2001; Pint *et al*., 2006] with fourth generation single crystal alloys. Essentially, increasing the inlet temperature improves the performance of the turbine engine [Gurrappa and Rao, 2006]. Other benefits include reduced fuel consumption and reduced emissions of gases such as NO_x, CO_2, H_2O, HC, CO and SO_x that pose a threat to the environment.

Thermodynamic efficiency of gas turbines is based on the Brayton cycle, expressed as follows:

$$\eta \approx 1 - \frac{\Delta T_2}{\Delta T_1} \qquad (2.1)$$

Where, T_1 and T_2 are absolute temperatures of the heat source and heat sink respectively. From the above expression it can be noted that better efficiencies are obtained by increasing working temperatures. However, NBSAs have reached their limit, as the materials are operating at near melting point temperature. Any further temperature increases will result in melting of the alloy and subsequent premature failures [Chatterjee *et al.*, 2001], hence the need for a high strength material with higher melting point.

Ceramics, composites, refractory materials, intermetallics and Platinum Group Metals (PGMs) have all been investigated as suitable materials to replace NBSAs. Commercialisation of the aforementioned alloys has not reached full scale, hence coatings are likely to assume an important role in driving temperatures even higher [Gurrappa and Rao, 2006]. The development of these alloys is discussed in other sections of the paper.

Mechanical and corrosion properties form an integral part of the design or development of any new material that is to be used in the aerospace complex applications. Therefore, both these temperature dependant properties are to be taken into considered during material selection processes [Yoshiba, 1993; Deb *et al.,* 1996]. Previous developments of

NBSAs were based at enhancing creep properties, which could compromise the corrosion resistance of the alloys.

2.2 STRENGTHENING MECHANISMS AND DEVELOPMENTS OF NBSAs

Strength is one of the primary properties required in high temperature materials and improved strength has been associated with microstructural properties of NBSAs. NBSAs are characterised by their unique microstructure which comprises the austenitic γ-phase (Ni matrix); an intermetallic, ordered cuboidal fcc precipitate, γ′–phase (Ni_3 (Al, Ti)) and carbide particles [Sims *et al.*, 1972; Hertzberg, 1989]. The γ-phase is the continuous phase with high concentration of solid solution alloying elements. The γ′–phase, shown in figure 2.2, imparts strength to the matrix without lowering fracture toughness of the alloy [Brandl *et al.,* 1998], while carbide particles reduce grain boundary mobility.

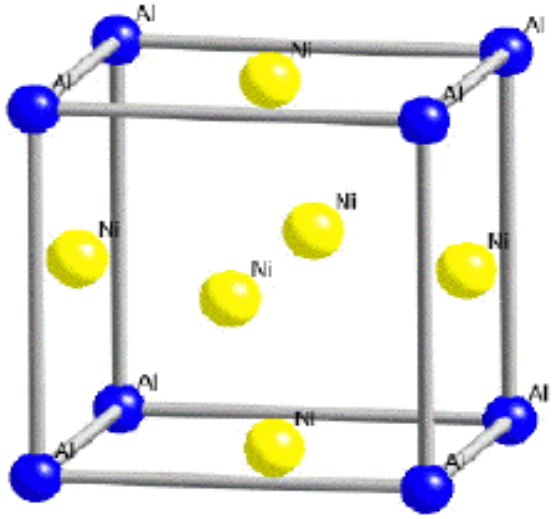


Figure 2.2 A fcc crystal structure of the γ′ precipitate [Bhadesia, 2003]

The alloy's strength is attained through heat treatment processes, such as solid solution strengthening and precipitation [Hertzberg, 1989; Sims *et al.*, 1989]. It is through solid

solution strengthening, where the γ′ is allowed to precipitate in the γ matrix, that high strength can be obtained. The strength of γ′ increases with increasing temperatures and figure 2.3 shows the high strength the γ′ can obtain at high temperatures, when ordinary materials are no longer capable and are most likely to fail. The γ′-phase has a high melting temperature of 1140°C. Once this phase melts, the alloy will not be able to preserve high temperature properties, hence NBSAs are limited to temperatures of only 1100°C.

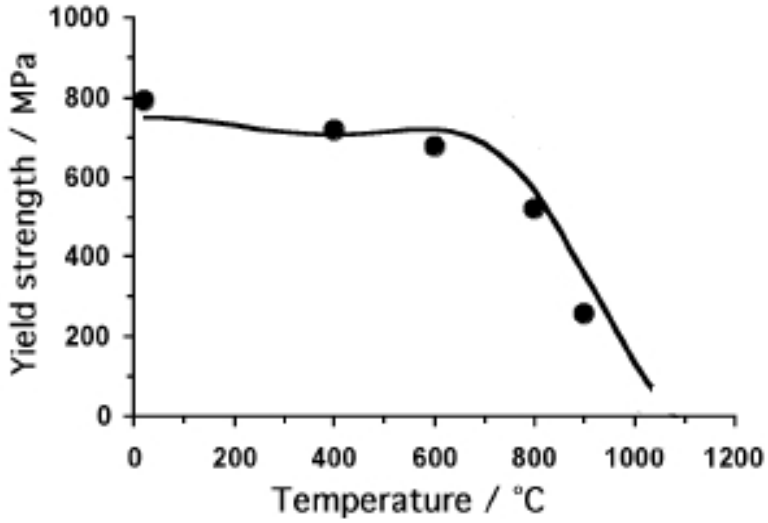


Figure 2.3 Yield strength versus temperature indicates capabilities of the γ′ -phase with increasing temperature [Bhadesia, 2003]

Parameters that are designed and controlled during the development of NBSAs are particle size, morphology, volume fraction of the γ′-phase and the sign of the lattice misfit. Low misfits (~0-1%) reduce creep rates [Bradley, 1979], while high volume fractions (~70%) improves strain coherency [Sims *et al.*, 1972; Hertzberg, 1989; Bowman, 2000].

Microstructural properties of NBSAs are easily influenced by different processing techniques and different alloying elements. These processes were aimed at improving strength and increasing working temperatures.

2.3 CHEMICAL COMPOSITION AND THE EFFECT OF ALLOYING ELEMENTS

A wide range of NBSAs has been produced since the alloys were first introduced. The most common NBSAs commercial names that are used today are given in table 2.1 together with their nominal chemical compositions.

Table 2.1 Nominal chemical composition of commercial NBSAs [Bhadesia, 2003]

Alloy	Ni	Cr	Co	Mo	W	Ta	Nb	Al	Ti	Fe	C	B	Zr	Re	Hf
CMSX-4	Bal	5.7	1	0.42	5.2	5.6		5.2	0.74					3	0.1
IN-718	Bal	18.6		3.1			5	0.4	0.9	18.5	0.04				
Mar-M200	Bal	9	10		12		1	5	2		0.15	0.015	0.05		
Nimonic 80A	Bal	19.5	1.1					1.3	2.5		0.06				
IN-738LC	Bal	16	8.5	1.7	2.9	1.7		3.4	3.4		0.11		0.05		

From table 2.1, it can be noted that NBSAs are highly alloyed materials. This is specifically to increase the strengthening effects [Bradley, 1979; Bradford, 2002]. Chemical compositions of NBSAs were modified by increasing the amount of Al, Ti and refractory elements [Chen and Little, 1997; Pomeroy, 2005]. High solubilities of Al and Ti are achieved by lowering the Cr content in the alloy. Originally, NBSAs had a high Cr content of 20 wt %. Over the years, the composition has decreased drastically and now only 5 wt % Cr is added in single crystal alloys [Pomeroy, 2005]. Cr has been claimed to be most effective alloying element in increasing corrosion resistance [Bradley, 1979;

Stringer, 1987; Gurrappa, 2003; Sidhu *et al.*, 2004; Singh *et al*., 2004; Pomeroy, 2005;], giving good oxidation and hot corrosion resistance, provided that temperatures do not exceed 950ºC, above which Cr form volatile CrO_3 instead of Cr_2O_3 [Elliot, 1990; Bradford, 2002]. The low Cr content has affected the corrosion properties of NBSAs and caused the alloys to be more susceptible to high temperature corrosion [Stringer, 1987; Bhadesia, 2003].

Al additions were intended to aid in the formation of Al_2O_3, which is thermodynamically more stable than Cr_2O_3 [Elliot, 1990]. Al, together with Cr, Zr and Hf are used as surface stabilizers, forming a protective scale on the substrate which prohibits the underlying metal from interacting with the environment. Carbide formers such as W, Mo, Nb, Ta, Ti, Cr and V restrict the grain boundary sliding and migration in the polycrystalline alloys by lowering the diffusion coefficient of the alloy [Hertzberg, 1989]. However, carbon in large quantities can have detrimental effects by forming carbides, which are said to provide sites for hot corrosion initiation [Gurrappa, 2003]. The effect of increased Ru in the fourth generation superalloys was to improve phase stability and creep resistance of high temperature materials.

Additions of refractory elements are beneficial in improving strength of the alloys [Pomeroy, 2005]. However, their influence in hot corrosion properties is detrimental, as they make the alloy susceptible to hot corrosion attacks [Deb *et al.,* 1996]. A summary of some alloying elements is presented in table 2.2.

Table 2.2 Effects of various alloying elements in NBSAs [Bradley, 1979; Hertzberg, 1989; Elliot, 1990]

Elements	Effects
Chromium	Oxidation resistance, carbide former ($M_{23}C_6$ and M_7C_3)
Molybdenum, Titanium, Tungsten	Solid solution strengtheners, carbide former (M_6C and MC)
Aluminum, Titanium	Formation of γ' [Ni_3 (Al, Ti)] hardening precipitate, titanium forms MC type carbide as well
Cobalt	Raises the solvus temperature of γ'
Boron, Zirconium	Increases rupture strength, boron also forms borides when present in large enough amounts
Carbon	Formation of various carbides such as MC, M_6C, $M_{23}C_6$, M_7C_3
Columbium	Formation of Ni_3Cb hardening precipitate, carbide former (MC)
Tantalum	Solid-solution strengthener, carbide former (MC)
Silicon	Improves resiliency of the scale. Silica forms a glassy surface that is extremely protective and resistant to carburising and sulfidising atmospheres
Rare earth elements	More resilient scale, delaying oxidation and hot corrosion

2.4 PROCESSING TECHNIQUES OF NBSAs

Gradual temperature increases of ± 400°C were obtained over a period of 70 years in the gas turbine industry. As already mentioned, these temperatures were to improve the performance of engines of aircrafts. Figure 2.4 gives a schematic presentation of successful processes that led to the evolution of NBSAs, with 40% of material development contributing towards increased temperatures and 60% attributed by advanced cooling concepts and the use of coatings.

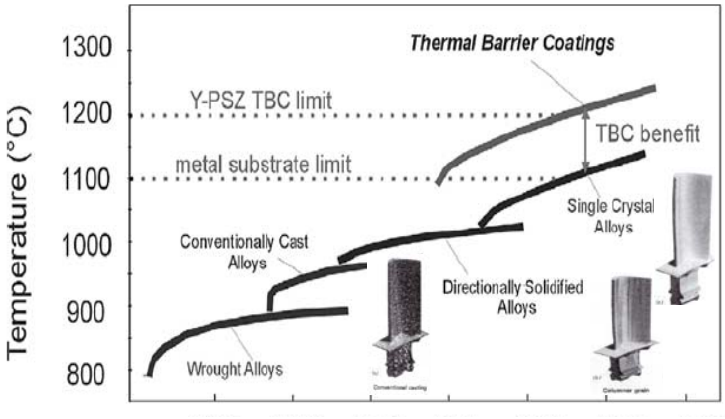


Figure 2.4 Processing techniques developed to increase working temperatures in gas turbines [Schultz *et al.*, 2003]

Vacuum melting was introduced in the 1950's. It was through the vacuum melting process where elimination of oxygen and nitrogen from the alloy melt were made possible. This effectively resulted in the formation of improved microstructures of higher purity [Sims *et al.*, 1972; Hertzberg, 1989]. The practice of casting in air or under controlled inert environments was replaced in 1956, when vacuum investment castings were put in place. This technique was used to reduce levels of dissolved gases in the melt, control grain size and improve mechanical properties [Sims *et al.*, 1972]. Powder metallurgy methods were used to produce components that were difficult to make through conventional casting methods such as turbine disc rotors.

Granular fracture, creep and thermal fatigue were improved by casting directionally solidified alloys (DSAs). DSAs were designed such that the grains were aligned parallel to the growth axis. Studies conducted on a directionally solidified superalloy IN-738LC and findings were compared to a conventional cast alloy. The findings showed that mechanical properties of the directionally solidified alloy were significantly improved over conventional alloys [Kermanpur *et al*., 2000].

Single crystals are a modification of directionally solidified casts. These alloys obtain their strength through the elimination of grain boundaries, and further prevent premature failure that would have occurred when grain boundaries were present. Single crystal alloys have the capability to carry tensile stresses of over 100 MPa at 80% of the alloy's melting temperature [McLean *et al.*, 1999]. Moreover, single crystals alloys have higher melting points and improved creep properties [Bowman, 2000; Bhadesia, 2003]. Today high pressure blades are made out of single crystal alloys.

2.4.1 Coatings and blade cooling in gas turbines

A wide range of coatings based on overlays, diffusion and thermal barriers coatings (TBCs) were developed for components subjected to harsh environments in high temperature applications, including the aerospace, land base and power industry [Chen *et al*., 2003; Formanek *et al*., 2005]. The development of coatings was influenced by constant demands for higher turbine entry temperatures [Gurrappa, 2003]. Since their introduction, coatings have dominated gas turbine applications, allowing for temperature increases of up to 200°C [Siebert *et al.,* 1999; Pomeroy, 2005]. Moreover, coatings extend the life of the components and preserve mechanical properties of the underlying substrate, while simultaneously protecting the substrate from degradation mechanisms such as erosion, wear and hot corrosion [Gurrappa, 2001; Sharafat *et al.,* 2002].

Coatings have shown reliability and good performance under corrosive environments encountered in gas turbines due to the formation of a slow-growing, stable, dense and adherent oxide scale [Mévrel, 1989; Brandl *et al.,* 1998; Gurrappa, 2001; Sidhu and Prakash, 2003; Wang *et al.,* 2004; Zheng *et al*., 2006]. An α-alumina compound is

preferred as the external scale because it is effective as a diffusion barrier, minimising the diffusion effect of substrate elements [Müller and Neuschütz, 2003; Saltykov *et al*., 2004], with high thermal stability at high temperatures [Zheng *et al*., 2006] and low solubility in molten salts [Chen *et al*., 2003].

Yttria-stabilised zirconia (YSZ) TBCs have shown outstanding performance as a result of low thermal conductivity and high thermal expansion coefficient [Gurrappa and Rao, 2006]. These coatings find their applications in the aerospace industry, protecting blades, vanes, gas turbine shrouds and combustion cams [Sharafat *et al.,* 2002] in gas turbine engines. The thickness of coatings affects the performance of coatings. An optimum thickness of 300μm on TBC coatings performed well when exposed to 90%Na_2SO_4-5%NaCl-5%V_2O_5 salt [Gurrappa and Rao, 2006].

Overlay coatings (MCrAlY) are used as a bond coat for TBCs to provide a rough surface for mechanical bonding of ceramic tops and to mininise outward diffusion of substrate elements [Gurrappa, 2001], or are used as standalone coatings. Overlay coatings are preferred in most demanding applications, because of their excellent diffusional and environmental stability [Fritscher *et al.,* 1995] and are common in aircraft engines [Stringer, 1987]. High Cr content makes them desirable for protection against type II hot corrosion.

Simple diffusion coatings, such as Ni-aluminide, are used as protective coatings to protect NBSAs against degradation. Recently, the Pt-modified coatings have dominated the industry due to the alloy's excellent corrosion resistance, especially against type I hot

corrosion [Mévrel, 1989; Purvis and Warnes, 2001]. Addition of reactive elements such as yttrium, promotes selective oxidation of the protective scale and improved oxide scale adherence [Brandl *et al.,* 1998].

The newly developed coatings, called smart coatings, were developed to overcome the problem of different corrosion forms that occur due to different temperature gradients. Unlike other high temperature coatings, smart coatings are enriched with Al and Cr and these coatings have the capability to resist both the type I and type II hot corrosion [Nicholls *et al*., 2002].

Surface engineering techniques are important in selecting a suitable coating in high temperature applications. Feasibility and cost are the determining factors in selecting a suitable process [Shultz *et al.,* 2003]. According to studies by Sidhu *et al.* (2006) a cheaper process, namely the high velocity oxy-fuel (HVOF) is now commercially viable in depositing overlay coatings and improving properties of superalloys. Physical vapour deposition (PVD) is cheap and commonly used for TBCs. However, electron beam physical vapour deposition (EB-PVD) has shown better performance over PVD [Gurrappa and Rao, 2006]. Rapid remelting and solidification of MCrAlY before EB-PVD enhances oxidation resistance of the coating, while simultaneously improving the quality of the thermally grown oxide [Dragos *et al.,* 2005]. Remelting the plasma sprayed coatings using a laser reduces porosity and homogenise the microstructure [Sidhu and Prakash, 2006]. A comprehensive summary on the development of coatings is presented by Goward (1998) and discusses the background and other areas of research conducted in surface engineering.

Incorporating cooling by design to ceramic coatings applied to high temperature components in gas turbines can reduce the inlet temperatures by up to 100°C across a coating thickness of 125-200μm [Wing, 2000; Pomeroy, 2005]. On the other hand, large quantities of air required in cooling schemes lowers the overall efficiency in gas turbines [Ashby and Jones, 1988].

2.5 HIGH TEMPERATURE MECHANICAL PROPERTIES

Aerospace engine components are subjected to extreme temperature variations, high loadings and wear. High temperature materials should have good mechanical and chemical integrity. Thus these materials should inherently possess mechanical properties such as creep strength, high melting points and moduli of elasticity, thermal fatigue strength, thermal expansion, thermal conductivity, thermal shock, phase instability, low diffusivity, erosion, wear and surface stability [Sims *et al*.,1972; Ashby and Jones, 1988; Schweitzer, 1998]. These are discussed in more detail in the next section.

2.5.1 Creep resistance

Creep is a time dependant, permanent deformation that develops in an inter-crystalline manner and takes precedence at high temperatures. Creep characteristics are affected by the melting temperature of an alloy, the elastic modulus and grain size. The greater the elastic modulus and larger grain size, the better is the material's resistance to creep. Smaller grain size permits more grain boundary sliding, which results in higher creep rates. Creep resistance of NBSAs is enhanced by solid solution alloying and by the addition of dispersed phases that are insoluble in the matrix [Callister, 1999].

2.5.2 Good tensile strength

Generally, the strength of a material decreases with an increase in temperature, making alloys hot workable. NBSAs, however, retain their strength because of the presence of the intermetallic precipitate (γ') whose strength increases with increasing temperatures [Bradley, 1979]. Most alloying elements, especially refractory elements, were added to improve the strength of superalloys [Bhadesia, 2003]. Typical high temperature strength values of NBSAs are given in table 2.3.

Table 2.3 Properties and applications of NBSAs at 870°C [Hale, 2000]

Alloy	Condition	Ultimate Tensile Strength (MPa)	Yield Strength (MPa)	Elongation in 50mm (%)	Typical applications
Astroloy	Wrought	770	690	25	Forgings for high temperature
HastelloyX	Wrought	255	180	50	Jet engine sheet parts
IN-100	Cast	885	695	6	Jet engine blades and wheels
IN-102	Wrought	215	200	110	Superheater and jet engine part
Inconel 718	Wrought	340	330	88	Jet engine and rocket parts
MAR-M-200	Cast	840	760	4	Integrally cast turbine wheels
Rene'41	Wrought	620	550	19	Jet engine parts
Udimet 700	Wrought	690	635	27	Jet engine parts
Waspaloy	Wrought	525	515	35	Jet engine parts

2.5.3 Thermal expansion

Metals expand and contract upon heating and during thermal cycling that leads to thermal and fatigue stresses. Therefore during design, low thermal expansion coefficients are desired [Sims *et al.*, 1972].

2.5.4 Thermal conductivity

Thermal conductivity governs the rate at which heat is dissipated. High thermal conductivities are desired to allow for the dissipation of heat, minimizing temperature gradients and simultaneously reducing thermal stresses [Sims *et al.*, 1972].

2.5.5 Low density

Density plays an important role in design considerations of rotating components, because centrifugal stresses are diminished when the density is low [Sims *et al.,* 1972; Callister, 1999]. Typical densities of superalloys range between 38-45 g/cm^3. Light alloys such as composites, ceramics and intermetallics are desired to improve performance and reduce the total weight of the aircraft [Elliot, 1990].

2.5.6 Surface stability

Surface stability can become the limiting service factor as the alloy can undergo two types of reactions: oxidation and hot corrosion, which cause materials to deteriorate [Sims *et al.,* 1972]. Therefore high temperature materials need to be resistant to both oxidation and hot corrosion, which dominates at high temperatures and where there is a high concentration of impurities. These properties are a reason why some of the

developed alloys will not reach the commercialisation stage [Gurrappa and Rao, 2006; Pint *et al*., 2006;].

2.5.6.1 Oxidation

Gas turbines operate under oxidizing environments and good oxidation resistance is attained when a tenacious stable oxide layer is formed on the alloy surface. Oxide scale is controlled by both thermodynamic and kinetic factors. Stable oxides have a large negative value for the Gibbs free energy and are summarised in the Ellingham diagram in figure 2.5.

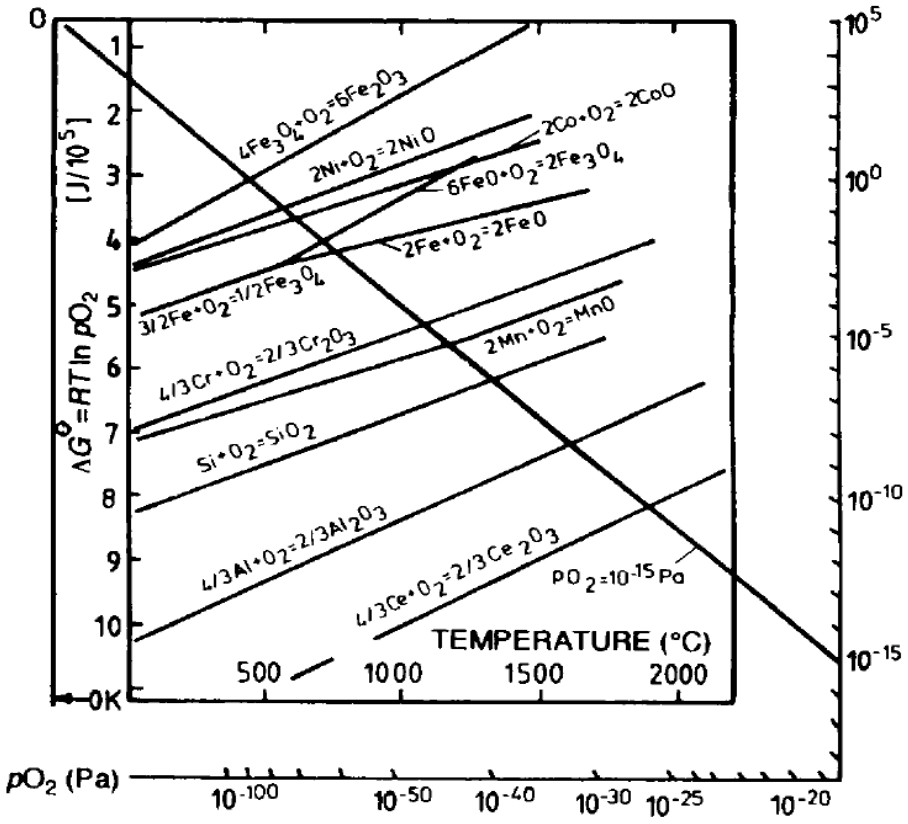


Figure 2.5 Ellingham diagram of oxides plotted against partial pressures [Gaskel, 1981]

The three main protective oxide scales, Al_2O_3, SiO_2, and Cr_2O_3 are preferred to protect superalloys from degradation, since they have low reaction rates at high temperatures. Table 2.4 gives the reaction rates of the three oxides at 1200 ºC. However, Cr_2O_3 is limited to temperatures below 950 ºC, above which Cr_2O_3 forms volatile CrO_3 [Chatterjee *et al*., 2001].

Table 2.4 Kinetics of Cr, Al, and Si oxides at 1200 ºC

Oxide	Low flow dry air /O_2 reaction rate at 1200 ºC (g^2/cm^4s)
Cr_2O_3	10^{-9} to 10^{-10}
Al_2O_3	10^{-11} to 10^{-12}
SiO_2	10^{-12} to 10^{-13}

2.5.6.2 Hot corrosion

Hot corrosion is a common problem encountered in various high temperature industrial applications such as recovery boilers in the pulp and paper industry, internal combustion engines, gas turbines in the aerospace industry and fluidised bed reactors [Sidhu *et al*., 2005]. Hot corrosion can be defined as a catastrophic failure resulting from an accelerated oxidation reaction in the presence of combustion gases or molten sulphate salts [Eliaz *et al.*, 2002; Shirvani *et al.*, 2003]. Hot corrosion studies are the focus of this research study. Since conditions encountered in the gas turbine environment are highly corrosive, resistance to oxidation and hot corrosion plays a significant role in selecting a material for high temperature applications [Hertzberg, 1989; Gurrappa and Rao, 2006].

During combustion, a gaseous reducing atmosphere is created due to the presence of gases such as SO_2 and SO_3. These gases lead to a phenomenon called sulphidation.

However, other phenomena such as nitridation, carburisation and chlorination can also take place, depending on the environment.

Deposits could lead to a phenomenon commonly known as hot corrosion. It has been generally accepted that sodium sulphate is a prerequisite to hot corrosion [Lee and Lin, 2002], whereby molten oxyanion salt act as the source of sulphur [Stringer, 1987]. Na_2SO_4 is thermodynamically stable at high temperatures and forms according to the reaction given below.

$$2NaCl + SO_2 + O_2 \rightarrow Na_2SO_4 + Cl_2 \qquad (2.2)$$

The salts act as fluxes, removing the protective scale. Impurities such as vanadium from the fuel and sulphur from air aggravate the conditions, making the environment more corrosive.

Research studies have shown that the reaction between Na_2SO_4 with other compounds such as K_2SO_4, NaCl and V_2O_5 form eutectics that have a lower melting point and are more corrosive that the Na_2SO_4 salt [Deb *et al.,* 1996;Gitanjaly *et al.,* 2002; Tsaur *et al.,* 2005]. Figure 2.6 shows the phase diagram of Na_2SO_4-V_2O_5 and indicates the different eutectic reactions taking place at temperatures below the melting point of both Na_2SO_4 and V_2O_5. Hot corrosion of 310 stainless steel was severe when the alloy was exposed to a melts at 628ºC [Tsaur *et al.,* 2005].

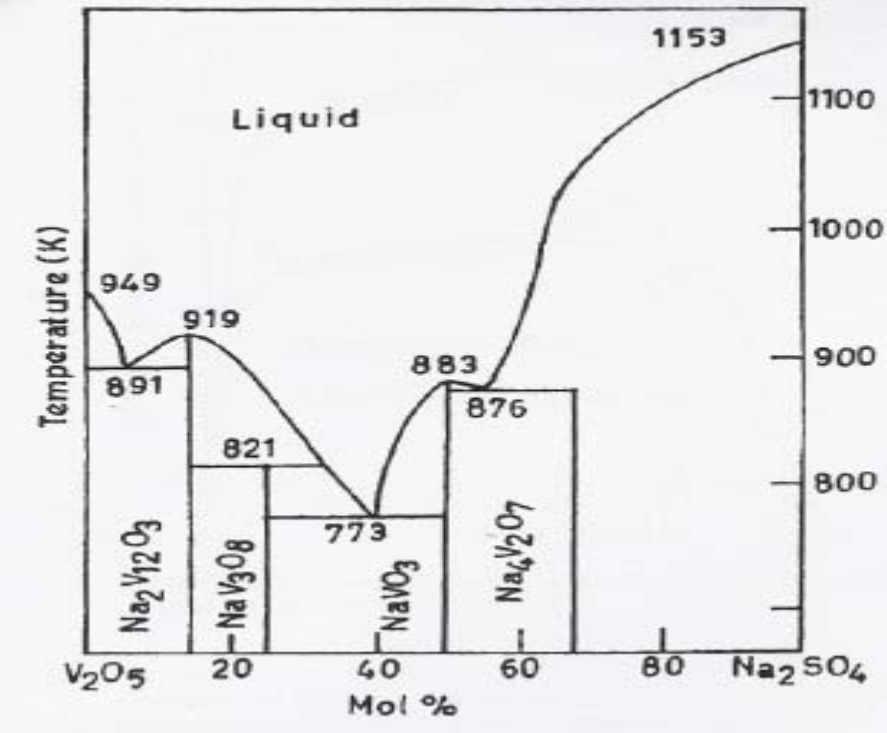


Figure 2.6 Equilibrium phase diagram for Na_2SO_4-V_2O_5 [Gitanjaly *et al.*, 2002]

With intended increased operating temperatures, it is becoming difficult to design alloys that have both high temperature strength and corrosion resistance [Dragos *et al.,* 2005]. Surface engineering plays an important role in the gas turbine industry in protecting the metal from degradation and today virtually all superalloys are coated because of inadequate hot corrosion resistance of the alloys. However, coatings are also limited at high temperatures by factors such as substrate compatibility, porosity of coatings, adhesion and the effect of environmental factors, which includes thermal cycling, erosion, wear and corrosion resistance [Dragos *et al.,* 2005; Pint *et al*., 2006].

Other high temperature processes encountered in the chemical and petrochemical industries cause the gas turbines to undergo different modes of corrosion in the temperature range from 480 to 1090ºC and these are summarised in table 2.5.

Table 2.5 High temperature processes with respective corrosion mode [Elliot, 1990]

Process/components	Temperatures (ºC)	Type of corrosion
Chemical/petrochemical		
Ethylene steam cracking furnace tube	to 1000	Carburization; Oxidation
Steam reforming tubes	to 1000	Oxidation; Carburization
Vinyl chloride crackers	to 650	Halide gas
Hydrocracking heaters, reactors	to 550	H_2S and H_2
Petroleum coke calcining recuperators	816	Oxidation; Sulphidation
Cat cracking generators	to 800	Oxidation
Flare stack tips	950-1090	Oxidation; Thermal fatigue; Sulphidation
Carbon disulphide furnace tubes	850	Sulphidation: carburization: deposits
Melamine production	450-500	Nitriding
Other processes		
Ti production reactor vessel	900	Oxidation; Chlorination
Nitric acid-catalyst grid	930	Oxidation; Nitriding; Sulphidation
Nuclear reprocessing reactors	750-800	Oxidation; Fluorination
Oil-fired boiler super heaters	850-900	Fuel ash corrosion
Gas turbine blade corrosion	to 950	Sulphate: chlorides: oxidation: ash
Waste incinerators-super heaters	480	Chlorination; Sulphidation; Oxidation
Fiberglass manufacturing recuperator	1090	Oxidation; Sulphidation; Molten salts

Hot corrosion can be classified into two forms, namely type I hot corrosion, also known as high temperature hot corrosion (HTHC) and type II hot corrosion or low temperature hot corrosion (LTHC). Type I hot corrosion is commonly observed at temperatures ranging between 850-950°C, whilst type II hot corrosion occurs at temperature ranging from 650-800°C [Stringer, 1987; Eliaz *et al.,* 2002]. The major distinction between these two forms of corrosion is their degradation morphology [Stringer, 1987]. A typical type I hot corrosion morphology is distinguished by the formation of a non-porous protective

scale, with internal sulphidisation and depletion of Cr. Figure 2.7 shows the typical morphology that forms as a result of type I hot corrosion attack.

Three degradation stages in type I hot corrosion is the incubation, initiation and the propagation stages. HTHC is initiated once the protective oxide layer becomes porous and less protective by allowing molten salt to penetrate the metal.

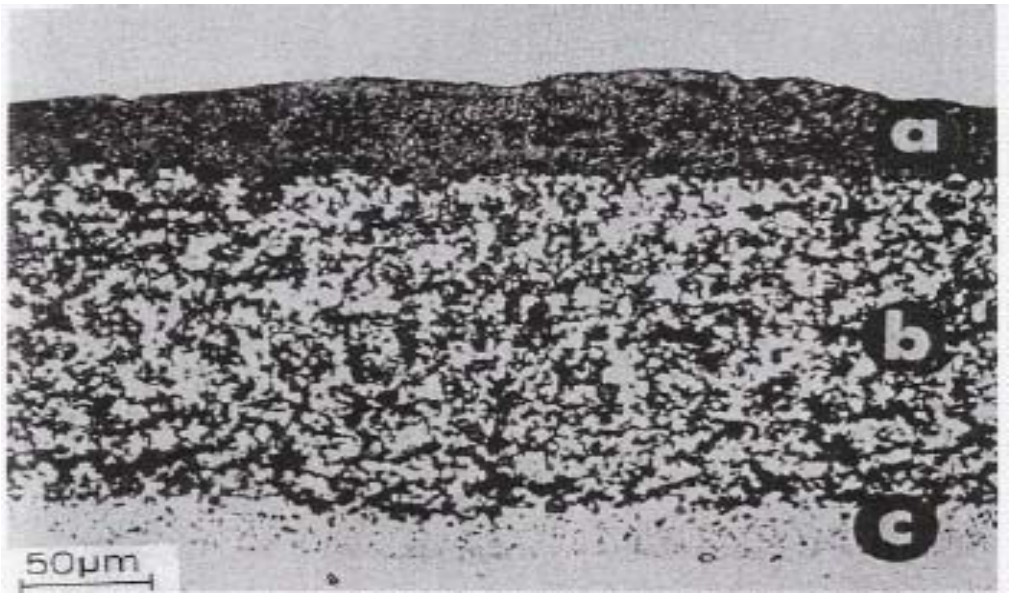


Figure 2.7 Typical microstructure of type I hot corrosion [Stringer, 1987]

The morphology that results in type II hot corrosion is characterised by pitting attack, with no internal sulphidation. High partial pressures of SO_3 are required to sustain LTHC [Khajavi and Shariat, 2004]. A case study by Khajavi and Shariat (2004) showed that another form of corrosion, the transition type corrosion, having characteristics of both type I and type II hot corrosion, was possible. Figure 2.8 gives a schematic presentation of the three forms of hot corrosion. Regardless of the type of corrosion, hot corrosion has

detrimental effects towards the mechanical integrity of superalloys and should be detected at earlier stages.

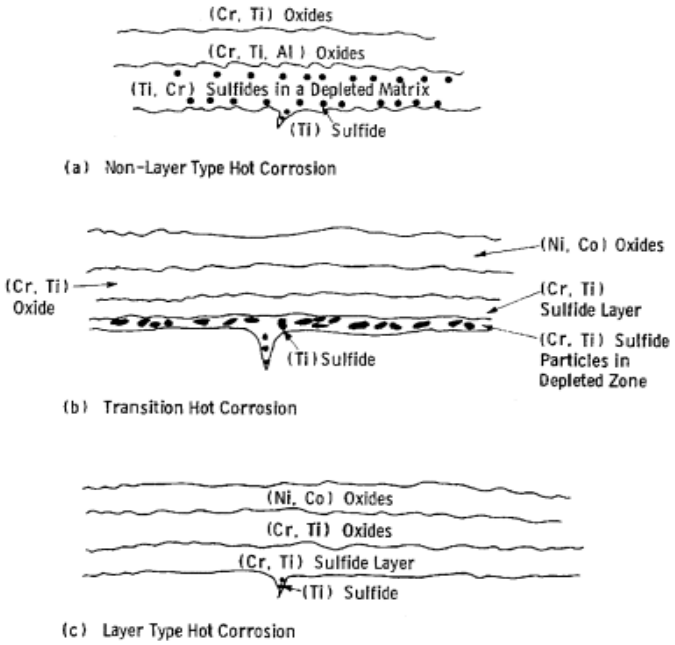


Fig. 8. Schematic characterization of corrosion products found at areas typical of the three different hot corrosion regions.

ı b)

Transition type hot corrosion c) Layered hot corrosion [Viswanathan, 2001]

2.6 FACTORS AFFECTING HOT CORROSION

Hot corrosion is influenced by a number of factors such as alloy composition, thermo-mechanical properties, contaminants composition, flux rate, temperatures, temperature cycles, gas composition, gas velocity and erosion [Prasad *et al.,* 1999], which are discussed in the following sections.

2.6.1 Alloy composition

Elements such as cerium, lanthanum, yttrium, and scandium increase resistance to hot corrosion by improving the adhesion between the alloy and the protective oxide. Silicon,

platinum and hafnium are effective in resisting LTHC while aluminum, titanium and niobium resist HTHC [Sims *et al.*, 1972; Eliaz *et al*., 2002]. Alloys containing up to 25 wt % Cr showed better resistance compared to alloys with low Cr content.

2.6.2 Temperature

The initiation stage is decreased by increasing temperature. Furthermore, the attack becomes less severe at temperatures exceeding 1000ºC. The influence of temperature is very important in hot corrosion since different mechanisms with different initiation stages can take place at different temperatures with many reaction mechanisms being operative [Sims *et al.*, 1972; Eliaz *et al.,* 2002].

2.6.3 Gas composition

The gas composition affects the initiation attack, the rate of attack and the propagation mode [Sims *et al.*, 1972]. Reaction rates in an oxidizing environment are not as severe as the rates in SO_2-SO_3 environment. As already mentioned, SO_3 influences the propagation stage of type II hot corrosion [Sims *et al.*, 1972; Eliaz *et al.,* 2002].

2.6.4 Salt composition and deposition rate

The composition of the deposit affects both the initiation and the propagation stages taking place during hot corrosion. The most detrimental composition contains sodium chloride. The rate of hot corrosion increases with an increase in sodium chloride content [Sims *et al.*, 1972; Eliaz *et al.,* 2002].

2.7 HOT CORROSION MECHANISMS

The two propagation mechanisms proposed are sulphidation-oxidation and the salt fluxing mechanisms for high temperature hot corrosion [Stringer, 1987]. At high temperatures, Na_2SO_4 salt dissociates according to the reaction given in equation 2.3

$$Na_2SO_4 \leftrightarrow Na_2O + SO_3 \qquad (2.3)$$

The dissociation could either be acidic or basic. Na_2O contributes towards the basicity of the salt, while SO_3 gas forms the acidic component in the salt [Stringer, 1987]. In the presence of molten Na_2SO_4 salt, oxides are dissolved and leads to fluxing of the protective scale. Solubilities of different metal oxides were calculated at 1200 K in molten Na_2SO_4 salt and are presented in figure 2.9 [Rapp, 2002].

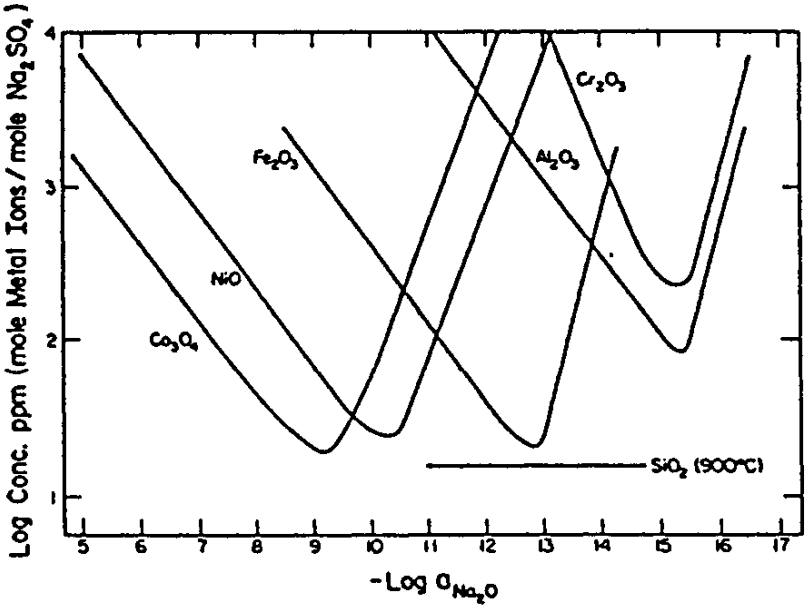


Figure 2.9 Calculated solubilities of metal oxides at 1200 K in molten Na_2SO_4 salt [Rapp, 2002]

Metal oxides have an amphoteric behaviour, with the left arm of the curve representing basic dissolution and the right curve representing acidic dissolution of the oxide. Acidic and basic reactions proposed by Cutler (1987) are presented in the equations below.

Acidic fluxing:

$$Al_2O_3 + 3Na_2SO_4 \rightarrow Al_2(SO_4)_3 + 3Na_2O$$
$$Cr_2O_3 + 3Na_2SO_4 \rightarrow Cr_2(SO_4)_3 + 3Na_2O$$
$$NiO + Na_2SO_4 \rightarrow NiSO_4 + Na_2O$$
$$Co_3O_4 + 3Na_2SO_4 \rightarrow 3CoSO_4 + 3Na_2O + \tfrac{1}{2}O_2$$

Basic fluxing:

$$Al_2O_3 + Na_2O \rightarrow 2NaAlO_2$$
$$Cr_2O_3 + 2Na_2O + \tfrac{3}{2}O_2 \rightarrow 2Na_2CrO_4$$
$$2NiO + Na_2O + \tfrac{1}{2}O_2 \rightarrow 2NaNiO_2$$
$$Co_3O_4 + \tfrac{3}{4}Na_2O + \tfrac{1}{4}O_2 \rightarrow 3NaCoO_3$$

Hot corrosion due to basic fluxing occur in alloys with high Al and Cr contents (e.g. IN 738LC), while acidic fluxing occurs in alloys with high concentrations of refractory alloying elements [Eliaz *et al.*, 2002; Sidhu *et al.,* 2005]. Acidic fluxing is more aggressive compared to basic fluxing and is self-sustaining [Sidhu *et al.,* 2005].

2.8 LABORATORY TESTS USED TO STUDY HOT CORROSION

Four main tests are used to evaluate corrosion behavior of high temperature materials. The crucible test is usually used as a ranking tool because of the aggressive nature of the test. Samples are either partially or completely immersed in molten salts at high temperatures.

Burner-rigs are used to closely simulate the environment in gas turbines. High pressures and high velocities are attainable when using this test. Figure 2.10 shows a simple configuration of the test.

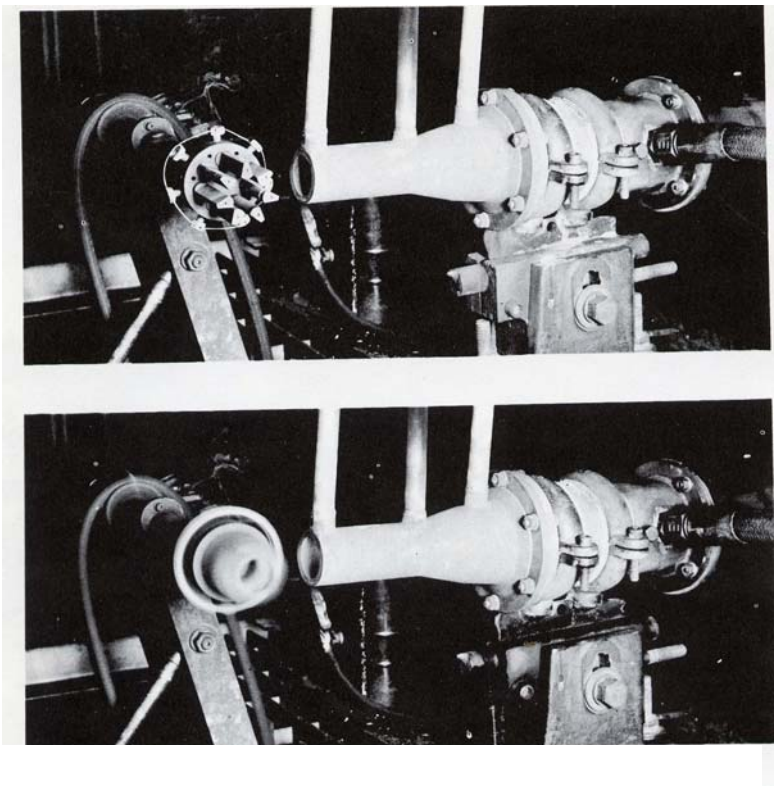


Figure 2.10 Burner rig test configuration showing a sample under the test [Bradley, 1979]

Electrochemical studies at high temperatures can be employed to study high temperature corrosion since the reactions are electrochemical in nature. The environment is similar to that of the crucible test, whereby molten salts are used as conductive media.

3.1 INTRODUCTION

Evolution of NBSAs was largely influenced by the improvement of metallurgical processes and materials. Future trends are towards developing innovative high temperature materials that will be able to have a positive economic and commercial potential in the gas turbine industry. These materials are to operate and withstand temperatures as high as 1300 ºC [Cornish *et al.,* 2004]. Understanding how various alloying elements influence failure mechanisms and microstructure are important and critical in developing new alloys with enhanced capabilities.

The major reason for developing better performing high temperature alloys is influenced by the fact that the currently used alloys have reached their limit. Some of the materials that emerged as suitable replacement candidates were materials such as ceramics, intermetallics, refractory metals and the Platinum Group Metals (PGMs). The advantages and disadvantages of these materials are discussed below.

3.1.1 Ceramics

Ceramics are traditionally known for their high melting points, high moduli of elasticity, low densities, and creep resistance [Ashby and Jones, 1988], making ceramics ideal candidates for high temperature applications. This is illustrated in table 3.1, where properties of NBSAs are compared to some of those of the ceramic materials.

Table 3.1 Properties of ceramics material compared to Nimonic, a nickel based superalloy [Ashby and Jones, 1988]

Metal	Density	Melting temperature	Modulus	Expansion coefficient	Thermal conductivity	Fracture Toughness
Al_2O_3	3	2320	360	6.9	7	5
Si_3N_4	3.1	2173	310	3.1	16	5
SiC	3.2	3000	420	4.3	60	3.5
Nimonic	**8**	**1600**	**200**	**12.5**	**12**	**100**

A commonly found application of ceramics in high temperatures is as thermal barrier coatings for gas turbines. Ceramics are limited by poor ductility at room temperatures. Studies by Levine *et al.* (2002) indicated that ceramic materials were unstable when exposed to gas turbine environments (water vapour) and therefore not suitable for the application.

3.1.2 Intermetallics

Interesting properties of intermetallics are their capability to retain strength at high temperatures, when metals are no longer capable of doing so. The strength of intermetallics increases with increasing temperature, making intermetallics desirable for high temperature applications. Intermetallics, like ceramics, have high melting points, low densities, good oxidation, diffusional creep resistance and high temperature strength [Wolff and Hill, 2000; Singh *et al.,* 2005]. One of the successful intermetallic alloys, IC-6, was said to be able to operate at relatively low temperatures (1050-1150°C) [Huo *et al.,* 1999]. Intermetallics have not been able to get to the commercialisation stage, because of the material's brittle failure at room temperature [Wolff and Hill, 2000; Lee and Lin, 2002].

3.1.3 Refractory metals

Metals such as Nb, Mo, W, etc. have drawn interest as possible replacement alloys because of their inherent high melting temperatures [2469ºC, 2623ºC and 3020ºC, respectively]. Positive results in developing refractory materials have been reported by other researchers [Schneibel, 2001]. The main disadvantage of refractory metals is their susceptibility to oxidising environments, when refractory oxides form volatile materials that lead to catastrophic attacks at high temperatures. Poor fabricability and poor resistance to creep at high temperatures are other serious limitations [Yamabe-Matarai *et al*, 1996; Cornish *et al.,* 2003].

3.1.4 Composites

Of the materials discussed thus far, composites emerge as prominent materials in aerospace industry [Sidhu *et al.,* 2005]. General Electric has embarked on using composites for both the fan cases and fan blades of gas turbine. This was due to the advantageous properties they possess at increased temperatures. Composites are lightweight, with high melting points and high strength. Furthermore, additions of carbon nanotubes improve strength and stiffness of composites. It has been suggested that future gas turbines will comprise of carbon composites to reduce weight in gas turbines [Miller, 1996]

3.1.5 Platinum group metals-(PGMs)

Attention towards the development of platinum group metals [Pt, Ir, Rh] was driven by the elements' higher melting points and excellent corrosion properties that allowed for numerous applications in the form of Pt-based alloys (e.g Pt-Rh alloys). The development of Pt-based superalloys at Mintek was based on replicating the strengthening mechanism of NBSAs, since

both alloys have similar fcc crystal structures. The Ir and Rh-based alloys exhibited good high temperature strength, with the highest strength of 200MPa at 1800ºC recorded for Ir-based alloys [Yamabe-Mitarai *et al.,* 1996]. However, these alloys were limited by their brittleness. Ductility of Ir-based superalloys was addressed by adding various alloying elements [Yamabe-Mitarai and Aoki, 2002].

3.2 MICROSTRUCTURE AND THE EFFECT OF ALLOYING ELEMENTS IN THE INVESTIGATED ALLOYS

Studies by Hill (2001) have indicated that Pt-based superalloys with a similar microstructure to NBSAs could be developed. Alloy compositions were determined after an extensive study of the binary and ternary phase diagrams. Figure 3.1 shows the Pt-Al phase diagram, from where the Pt_3Al phase was derived.

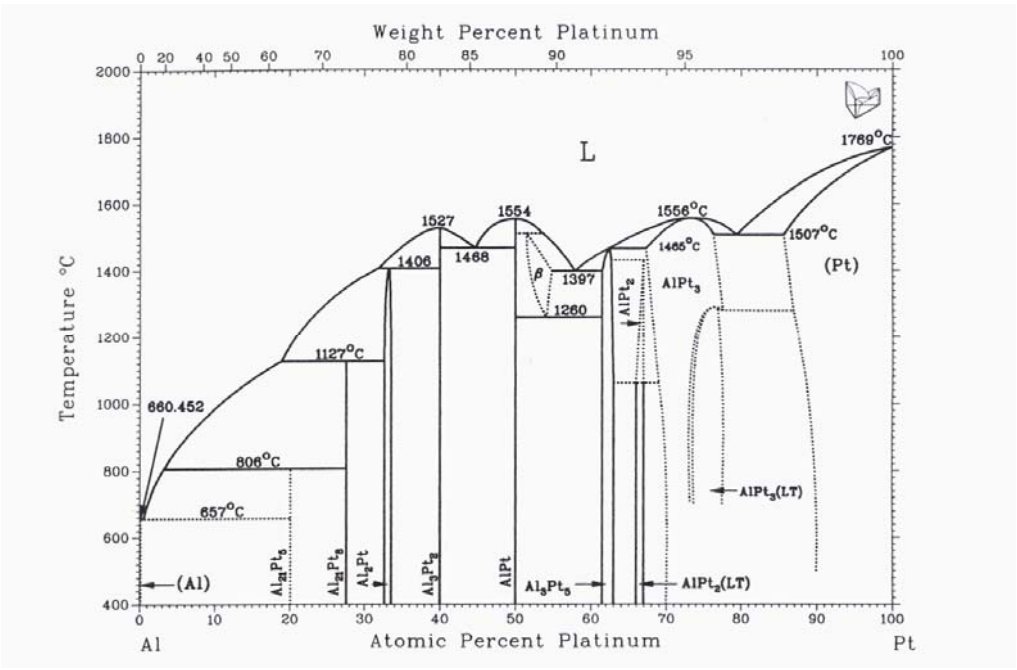


Figure 3.1 Binary phase diagram of Pt-Al system [Massalski *et al*., 1986]

The best alloys developed were based on Pt-Al-Cr, Pt-Al-Ru and the Pt-Al-Co systems. Pt-based superalloys form the ordered $L1_2$ phase at high temperatures and a secondary phase (tetragonal DO_{24}) at low temperatures. Cr was added as an alloying element to stabilise the Pt_3Al-$L1_2$ phase and improve mechanical properties of the alloy [Süss *et al*., 2001]. Ru acts as a solid solution strengthener in alloys RS2 (Pt-Al-Ru) and RS3 (Pt-Al-Ru-Cr) [Hill *et al.,* 2001]. In addition, alloying with Ru increased the volume fraction of the γ′. Al additions were mainly used to form the precipitate phase. Moreover, oxidation studies indicated that Al was beneficial by forming a protective oxide scale [Süss *et al*., 2001] which improved the oxidation resistance of the alloys. Addition of Co in alloys P420 (Pt-Al-6Co) and P421 (Pt-Al-12Co) enhances the formability of the alloys and slightly reduced the density of Pt-based superalloys [Chown *et al.,* 2004].

Alloy RS3 was considered the optimum alloy, because it formed cuboidal precipitates, with no primary phase and showed good oxidation properties [Süss *et al.,* 2003]. The comparison between the NBSA and the optimum Pt-alloy is shown in figure 3.2.

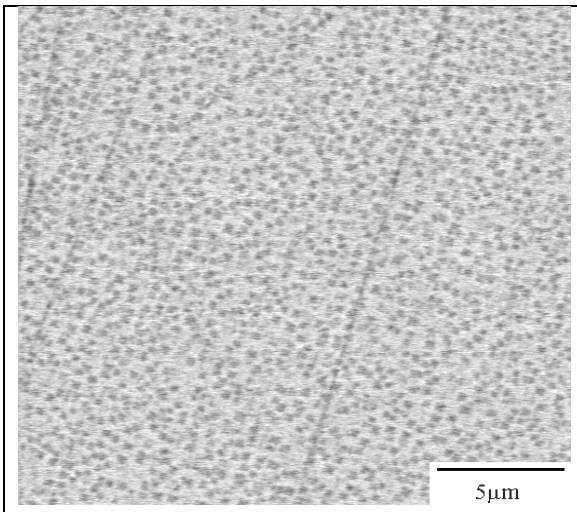


Figure 3.2 (a) **Pt-based superalloy**: SEM-BSE of optimum $Pt_{84}Al_{11}Ru_2Cr_3$ alloy



Figure 3.2 (b) **NBSA**: Cuboidal γ' precipitates of MAR-M200 alloy [Hertzberg, 1989]

Pt-based superalloys have a negative low, lattice misfit below 1%. Misfit calculations based on equation 3.1 for the ternary alloys investigated by Hill *et al*. (2001) are presented in table 3.2, where a_γ is the lattice parameter of the Pt phase and a_γ' is the lattice parameter of the ~Pt_3Al phase.

$$\text{Misfit} \approx \frac{(a_\gamma' - a_\gamma)}{a_\gamma} \qquad (3.1)$$

Table 3.2 Misfit calculations of the developed Pt-based superalloys [Hill *et al*., 2001]

Alloy	Lattice misfit (%)	
	Room temperature	800°C
$Pt_{86}Al_{10}Ti_4$	-0.72	-0.72
$Pt_{86}Al_{10}Cr_4$[2]	-0.72	-0.72
$Pt_{86}Al_{10}Ru_4$[3]	-1.2	-0.97
$Pt_{86}Al_{10}Ta_4$	-0.67	-0.72
$Pt_{86}Al_{10}Ir_4$	-1.2	-1.2

[2,b] Investigated alloys selected for the current study

However, volume fractions of the γ′-phase are below the desired 70-80% level observed in NBSAs [Cornish *et al.,* 2002]. Further investigations aimed at improving the volume fraction of Pt-based superalloys showed that an addition of Ni, to a limit, increases the volume fraction [Hüller *et al.,* 2005] of the γ′-phase.

3.3 MECHANICAL PROPERTIES OF Pt-BASED SUPERALLOYS

Good high temperature properties are a key to designing a successful high temperature alloy. The creep strength should exceed 170 MPa at a creep rate of 2×10^{-8} s^{-1} at a temperature of 1200 °C, with stress level above 25 J/g and a fracture toughness of 20 MPa as the minimum critical components. In terms of corrosion properties, the oxidation rate should be less than 0.25 μm/hr at 1315 °C [Schneibel, 2001].

Creep and compression tests performed on Pt-alloys suggested that the alloys had better properties over an ODS Fe-based superalloy (PM2000), as depicted in figures 3.3 and 3.4. $Pt_{86}Al_{10}Cr_4$ (RS1) had high rupture strength of approximately 835 MPa with good ductility [Süss *et al.,* 2004]. The compressive strength of Pt-Al-X (Where X is Ru or Re) was found to be higher than that of Mar-M247 above 1150ºC [Hill *et al.,* 2001] and also has a reasonable hardness. The hardness test results of the evaluated alloys are given in table 3.3

Table 3.3 Hardness results of the five Pt-based superalloys used in the investigation

Alloys	Hardness (HV_{10})
RS1 ($Pt_{86}Al_{10}Cr_4$)[4]	317
RS2 ($Pt_{86}Al_{10}Ru_4$)[5]	278
RS3 ($Pt_{84}Al_{11}Cr_3Ru_2$)[6]	360
P420 ($Pt_{79}Al_{15}Co_6$)	383
P421 ($Pt_{73}Al_{15}Co_{12}$)	286

It is anticipated that other properties, such as fracture toughness and impact and fatigue resistance, are to be competitive at high temperatures [Cornish *et al.,* 2004]

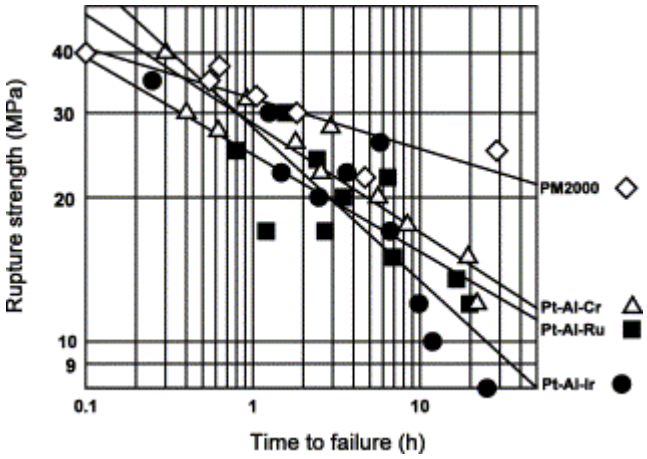


Figure 3.3 Stress rupture strength of an ODS alloy (PM2000) and ternary Pt-based superalloys at 1300 °C in air [Süss *et al*., 2002]

[4, d, e] Reference: Süss *et al*., 2004

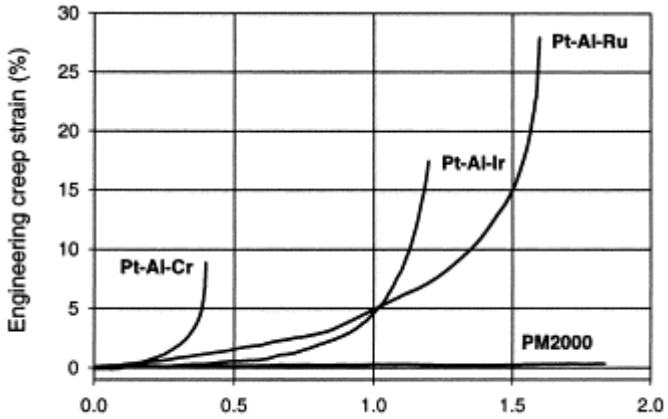


Figure 3.4 Stress rupture strength of an ODS alloy (PM2000) and ternary Pt-based superalloys at 1300 °C and 30 MPa [Süss *et al.*, 2002]

Pt-based superalloys still have poor mechanical properties and do not meet the requirement of the gas turbine industry [Schneibel, 2001]. However, these properties could still be improved by adding suitable alloying elements. Corrosion properties are another one of the main reasons to further develop Pt-based superalloys. Oxidation studies showed that the ternary alloy exhibited improved corrosion resistance and followed parabolic oxidation behaviour with no internal oxidation. Al played a major role, forming a protective scale that hinders further reactions [Süss *et al.,* 2003]. Figure 3.5 shows the difference in oxidation behaviour between Ni and Pt and it was noted that Pt-based superalloys are likely to perform better in corrosive environments compared to Ni.

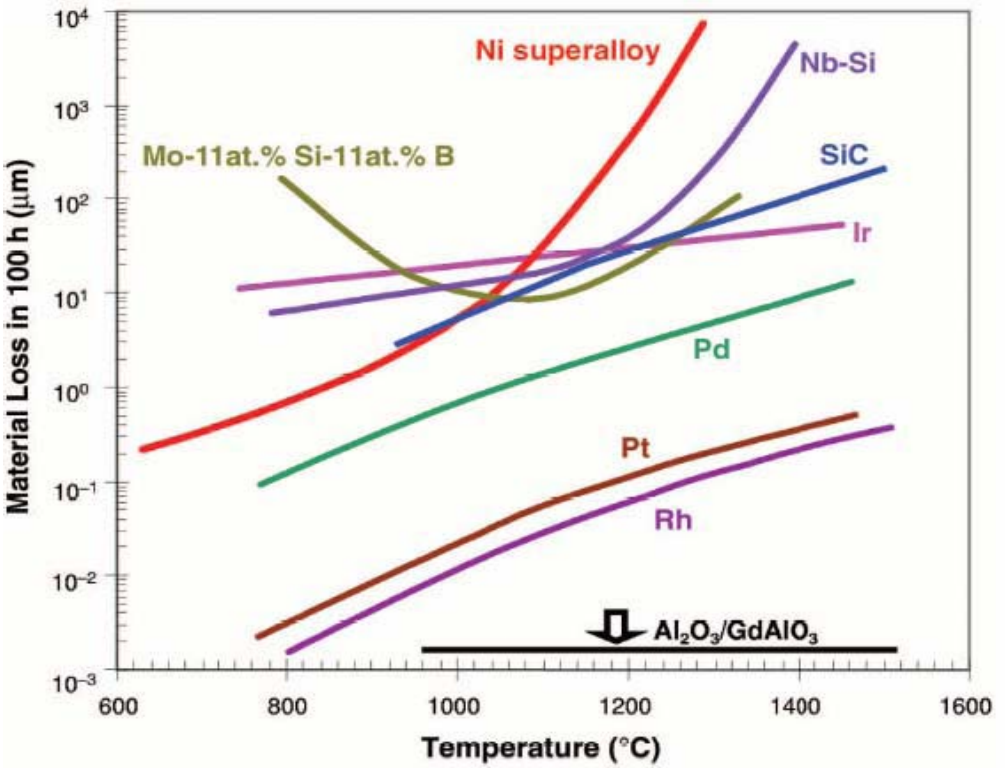


Figure 3.5 Oxidation resistant material used for high temperature applications [Cornish *et al.*, 2003]

Pt and Pt-alloys are known for their inertness and resistance to environmental interactions. Pt-alloys exhibited good oxidation resistance. The conditions encountered in the gas turbine environments such as sulphur from fuel, combustion gases and impurities in the air, their individual or combined action could largely affect the behaviour as a result of hot corrosion. To complete the material selection process of the developed Pt-based superalloys, hot corrosion behaviour of the alloys was evaluated and will be discussed in the next chapter.

4.1 INTRODUCTION

During the development of new high temperature materials for gas turbine blades, vanes and disks, etc., mechanical properties are not the only key properties to be taken into consideration. Creep and corrosion are primary factors that can lead to failure of high temperature materials in gas turbines. Turbine blades are operated under extreme mechanical and chemical conditions, which affect load carrying ability and can result in subsequent failure. Therefore any high temperature materials designed for a specific application, such as turbine blades, must have adequate resistance against creep and corrosion.

A new suite of materials developed for application in gas turbines is the class of Pt-based superalloys. Extensive research work led to the development of the desired two phase microstructure. Mechanical properties, including oxidation tests, were investigated. However, hot corrosion properties remained outstanding. The emphasis of this current research work was to evaluate corrosion behaviour of Pt-based superalloys as a criterion for the material selection process and to identify the best performing alloys for commercial application in the gas turbine industry. In the evaluation process, Pt-based superalloys were ranked and compared to commonly used NBSAs. Weight loss methods were employed to evaluate and assess corrosion behaviour of the proposed Pt-based superalloys in corrosive environments at high temperatures.

High temperature corrosion becomes significant with increasing temperatures. Moreover, traces of impurities commonly found in fuels or ingested air, such as Na, S, V, etc. impact

negatively on corrosion properties, forming solid deposits such as Na_2SO_4. Na_2SO_4, NaCl and other sulphate salts are corrosive in nature when they are in their molten state and lead to a process called hot corrosion. Hot corrosion is accelerated oxidation degradation of high temperature materials in the presence of fused salts. Hot corrosion attacks affect mechanical integrity of alloys, reducing component life. As already mentioned in previous chapters, there are two types of hot corrosion. This study focuses on type I hot corrosion since it is commonly found in aircraft, as opposed to type II hot corrosion.

Gaseous deposits, even in low concentrations, can be detrimental towards mechanical behaviour of high temperature alloys. Effluent gases such as SO_x, CO_2, unburned hydrocarbons and NO_x could lead to processes such as oxidation, nitridation, carburisation and sulphidation. Another area of this study focuses on the effect of sulphur on the behaviour of the developed high temperature materials.

4.2 INVESTIGATED MATERIALS

Five Pt-based superalloys button samples of approximately 2 g were prepared by weighing out masses of elements in their purest form (99,9%) equivalent to the chemical compositions of the alloys. These elements were arc-melted under an argon atmosphere. The alloys were turned several times to have homogeneity in the alloys. Corrosion behaviour of four ternary and one quaternary Pt-based superalloys, with chemical compositions given in table 4.1, were tested and compared with two single crystal alloys, the coated nickel based superalloy, CMSX-4 and an uncoated alloy.

Table 4.1 Nominal chemical composition of selected Pt-based alloys (at %) investigated

Alloy	Pt	Al	Cr	Ru	Co
RS1	86	10	4		
RS2	86	10		4	
RS3	84	11	3	2	
P420	79	15			6
P421	73	15			12

The nominal chemical composition of the benchmark alloy, CMSX-4, is given in table 4.2. A thin aluminide coating of approximately 1μm thickness was applied on one of the benchmark alloys as depicted in figure 4.1. The coated alloy was prepared and supplied by CSIR.

Table 4.2 Nominal chemical composition of CMSX-4 (wt %)

Alloy	Ni	Cr	Co	Mo	W	Ta	Al	Ti
CMSX-4	Balance	5.7	11	0.42	5.2	5.6	5.2	0.74

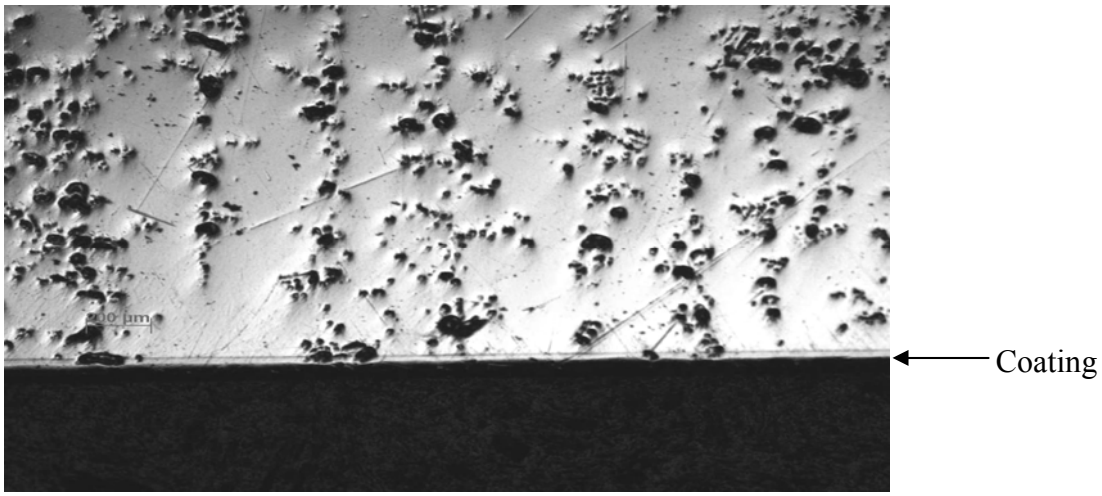


Figure 4.1 Cross section of a coated Ni-based superalloy in as polished condition showing a thin coating applied on the surface of the alloy

4.3 EXPERIMENTAL PROCEDURE

Crucible and sulphidation tests were performed to evaluate the corrosion behaviour of the Pt-based superalloys and NBSAs. In both investigations, weight change methods were employed to assess the performance of the alloys. Experimental procedures are described in the sections below.

4.3.1 Crucible Test

Crucible tests are generally aggressive in nature and used for ranking and studying hot corrosion behaviour of high temperature materials [Sims *et al.,* 1987]. Thin sections of approximately 2 mm thickness disks, were immersed in molten analytical Na_2SO_4 salt inside 20 ml alumina crucibles at 950 °C in static dry air environments. Na_2SO_4 melts at 884 °C, hence the salt was liquid at the operating temperatures. Type I hot corrosion typically occurs between 850-950 °C, so the working temperature was selected because it is the highest temperature at which type I hot corrosion is expected to occur.

Prior to the tests, exposed surfaces of the samples were abraded on silicon carbide paper in successions from 200, 600, up to 1000 μm finish. Samples were rinsed and degreased in acetone and dried.

Cyclic loadings were induced to create a more aggressive environment. Studies were conducted for a total duration of 792 hours with cycles of 72 hours of heating, followed by cooling to room temperature. Samples were cleaned at the end of every cycle by

immersing the samples in boiling distilled water. Boiling distilled water was used to free the samples from the salt melt with no significant effect on mass loss. Clean alloys, free of Na_2SO_4 salt, were weighed and measurements recorded on a Mettler Toledo weighing balance, with a sensitivity of 0.1 mg. Salt was replenished at the end of every cycle with fresh salt. Materials characterisation involved non-destructive tests such as the scanning electron microscopy (SEM) with energy dispersive spectrum (EDS), X-ray diffraction (XRD), Raman spectroscopy, and optical microscopy (OM). Analyses were performed at the end of 540 and 792 hours.

4.3.2 Sulphidisation test

During sulphidation tests, alloys were exposed to a controlled reducing environment. Samples were exposed to a pre-mixed special gas of 0.2% SO_2-N_2 prepared by AFROX. Surface preparation described above in the crucible test was similar for the sulphidation test. The gas was first allowed to flow through oil to remove moisture and then charged into the horizontal, electric tube furnace preheated to 900 °C. The gas leaving the furnace was flown into oil before venting the gas to the atmosphere. The air in the furnace was purged by allowing the mixed gas to flow for approximately 15 minutes at the specified temperature, prior to placing samples in the test chamber.

The test was run for a total of 60 hours with cycles of 5 hours of heating, followed by furnace cooling to room temperature. At the end of each cycle, weight changes were recorded and the samples were placed back into the furnace. Characterisation methods similar to those conducted in the crucible test were employed.

4.4 MATERIALS CHARACTERISATION

The four characterization techniques were employed to study and evaluate corrosion products and the corrosion mechanism that resulted.

4.4.1 Scanning electron microscopy (SEM) with X-ray energy dispersive spectrometry (EDS)

A JEOL 840 scanning electron microscope was used to identify the corrosion morphology and study the cross sectional analysis of the alloys, using a voltage of 20 kV. Quantitative and qualitative analyses were determined from using EDS connected to the SEM unit.

4.4.2 X-Ray diffraction (XRD)

A Phillips-PW1710 XRD was used to identify corrosion products that formed on the surfaces of the seven alloys. Generator settings for the analysis were set at 40 kV and 20 mV with copper K-alpha as the anode. A scan with a step size of 0.02° per minute was run from a starting position of 10° up to 100° (2θ). Expert High Score software was used to identify peaks in each of the spectra.

4.4.3 Raman spectroscopy

Raman spectroscopy is used to identify thin surface films at a high resolution. A laser source was used at room temperature to capture the scan pattern. A light microscope was used to capture the image on the surface of the alloy. Raman spectroscopy (JOBIN-YVON T64000) was used in the investigation to identify thin surface films on the

samples. The spectrum was collected by directing a continuous laser of Ar^+ (514.5nm) on the alloy surface at room temperature. The spectrum covered a scanning range between 250 cm^{-1} and 2500 cm^{-1}.

4.4.4 Optical Microscopy

Optical microscopy was employed to conduct cross sectional analyses of the coating on the benchmark alloy and on the corroded samples. Axiocam microscope installed with the Axio vision 3.1 programs was used to study the cross sections of the corroded sample. Low magnifications of up to 50X were employed.

5. EXPERIMENTAL RESULTS

Results yielded during hot corrosion and sulphidation investigations are presented in the sections below. The results present corrosion kinetics, corrosion morphologies and characterisation for both Pt-based and Ni-based superalloys.

5.1 Hot Corrosion Results

5.1.1 Corrosion kinetics

Weight changes of the investigated alloys during the evaluation of type I hot corrosion in molten Na_2SO_4 salts at 950ºC are presented in figures 5.1-5.4. The corrosion kinetic curves are given by the plots of weight change of specimens against the duration of the test, representing the corrosion behaviour of the alloys. The investigated alloys displayed different corrosion characteristics.

The uncoated alloy was the first to undergo degradation and failed prematurely within the first 11 hours of the experiment. Significant weight changes were observed after the 6^{th} cycle, following linear corrosion kinetics and quickly reaching the propagation stage. The kinetics curve of the uncoated alloy is presented in figure 5.1.

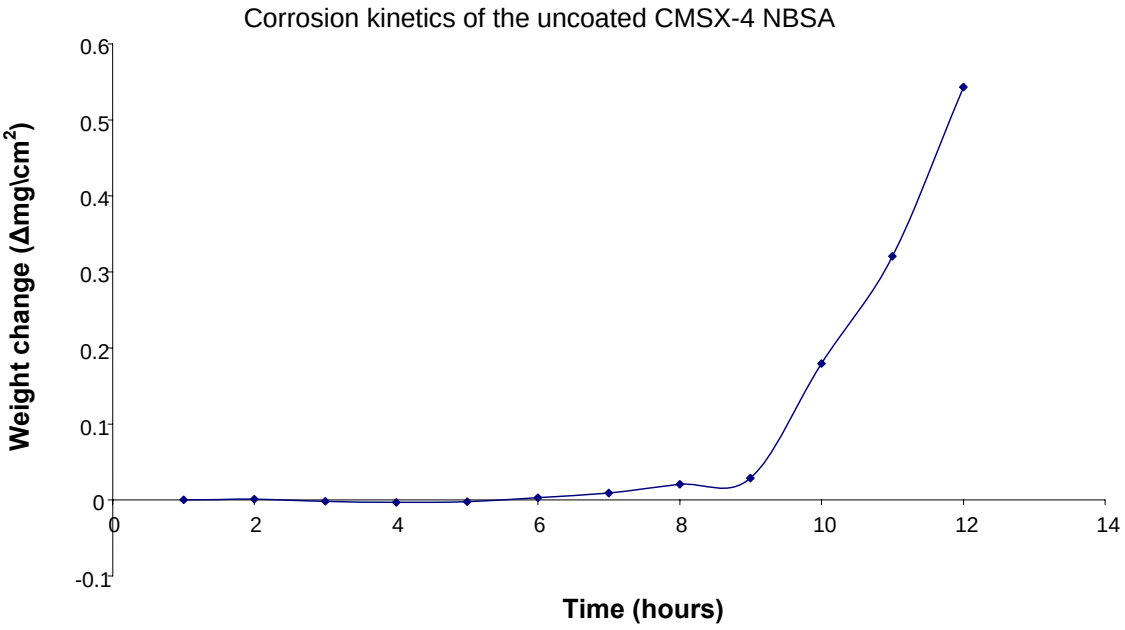


Figure 5.1 Corrosion kinetics of uncoated Ni-based superalloy (CMSX-4) after exposure to molten Na_2SO_4 salt at 950°C

The coated alloy showed better corrosion resistance than the uncoated alloy, following a parabolic rate law as depicted in figure 5.2. No significant changes were observed during the initiation stage. Considerable mass gains were recorded during the propagation stage. The exposure of the alloy was stopped after 540 hours.

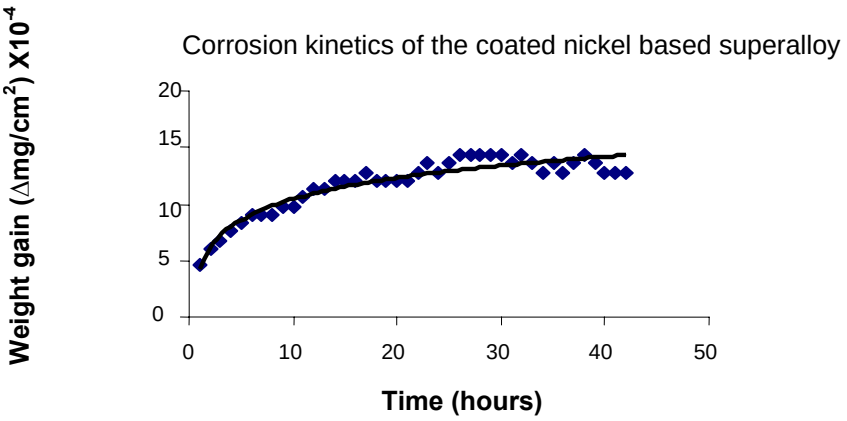


Figure 5.2 Corrosion kinetics of the coated nickel based superalloy after exposing the sample to molten Na_2SO_4 salt at 950°C

Figure 5.3 shows corrosion behaviour of Pt-based superalloys after a total of 792 hours. These alloys exhibited better corrosion resistance than the benchmark alloys, recording the least weight gains in molten salts. Alloy RS1, RS2 and RS3 remained in the propagation stage for a longer period without significant mass changes. Fluctuations in mass change were due to the combined effect of mass gains due to the formation of corrosion products and mass losses as a result of the corrosion products spalling off. Alloy P421 was the least resistant when exposed to the salt for 792 hours.

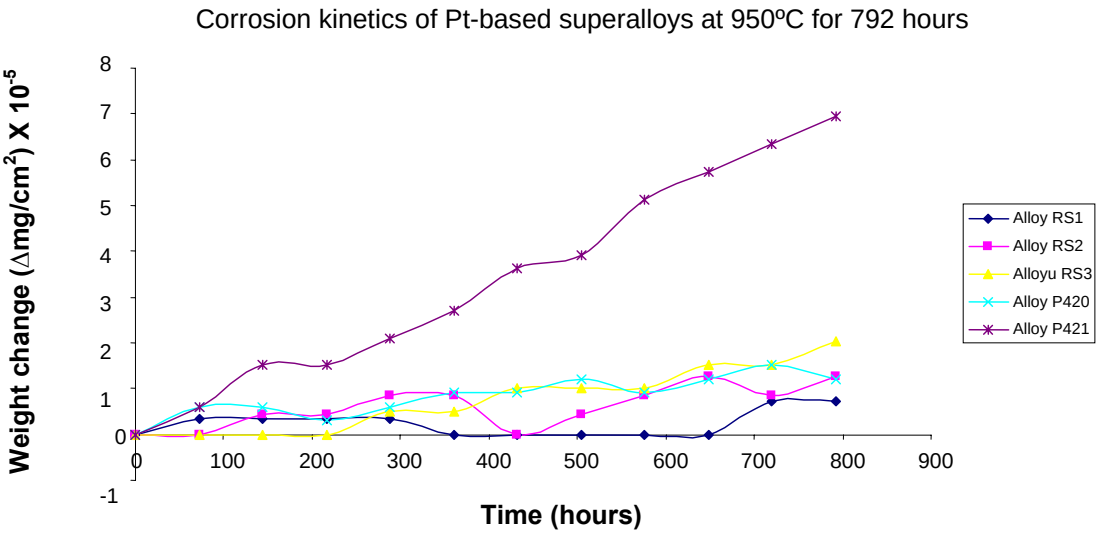


Figure 5.3 Corrosion kinetics of Pt-based superalloys in molten salts at 950°C for duration of 792 hours

Alloy RS1 recorded the least weight gain amongst the Pt-based superalloys. Cumulative weight plots in figure 5.4 summarises the performance of Pt-based superalloys at 950°C for 792 hours. Co-containing alloys exhibited poor corrosion resistance amongst the Pt-based superalloys.

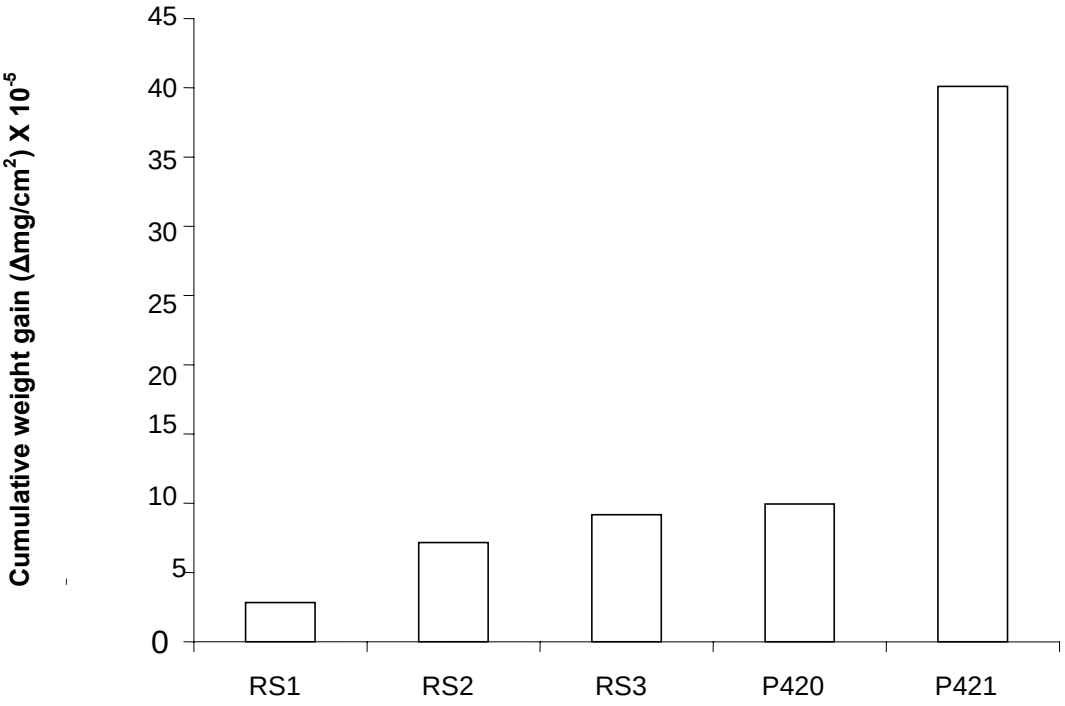


Figure 5.4 Cumulative weight gains of Pt-based superalloys after 792 hours in molten salt

5.1.2 Corrosion morphologies and cross sectional analysis

Figure 5.5 shows the corrosion morphology that resulted on the external surface of the coated alloy. Conglomerates of porous crystal-like particles were formed. The porous scale leads to further attack by allowing penetrations of corrosive species that led to internal attacks.

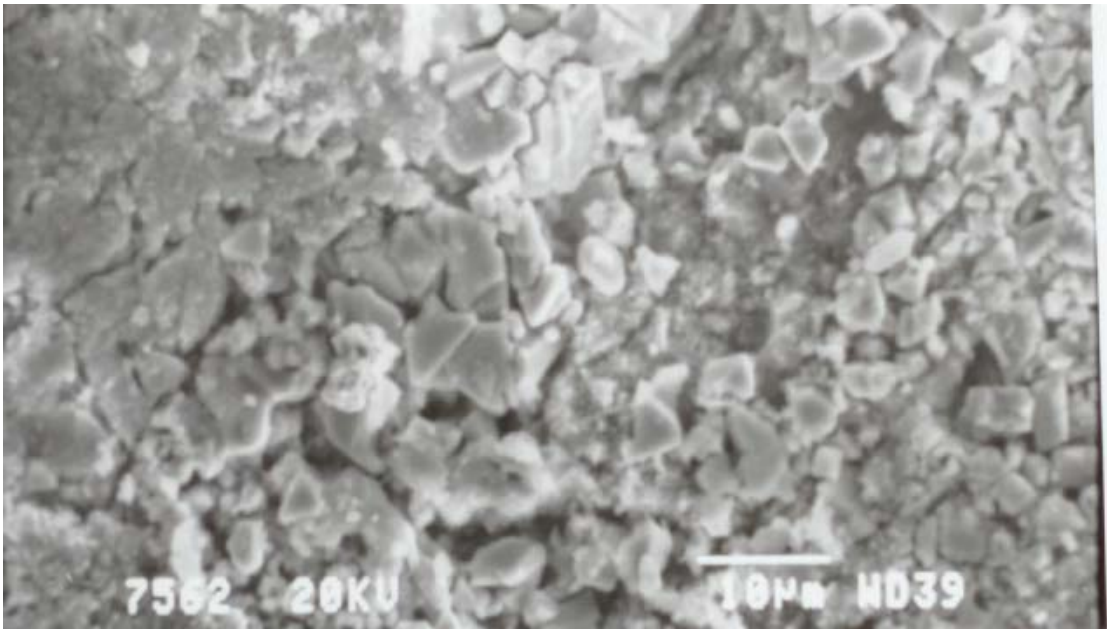


Figure 5.5 Secondary electron micrograph showing corrosion morphology of the coated NBSA that resulted after hot corrosion in molten Na_2SO_4 salt at 950°C

Figure 5.6 shows non-protective scale on the surface of the uncoated alloy. The scale was brittle and spalled off during handling. A crack running across the surface of the alloy was noticed. EDS analysis performed on the surface of the alloy is shown in figure 5.7. Elements detected on the external surface were Ni and alloying elements such as Cr and Co with traces of Na_2SO_4.

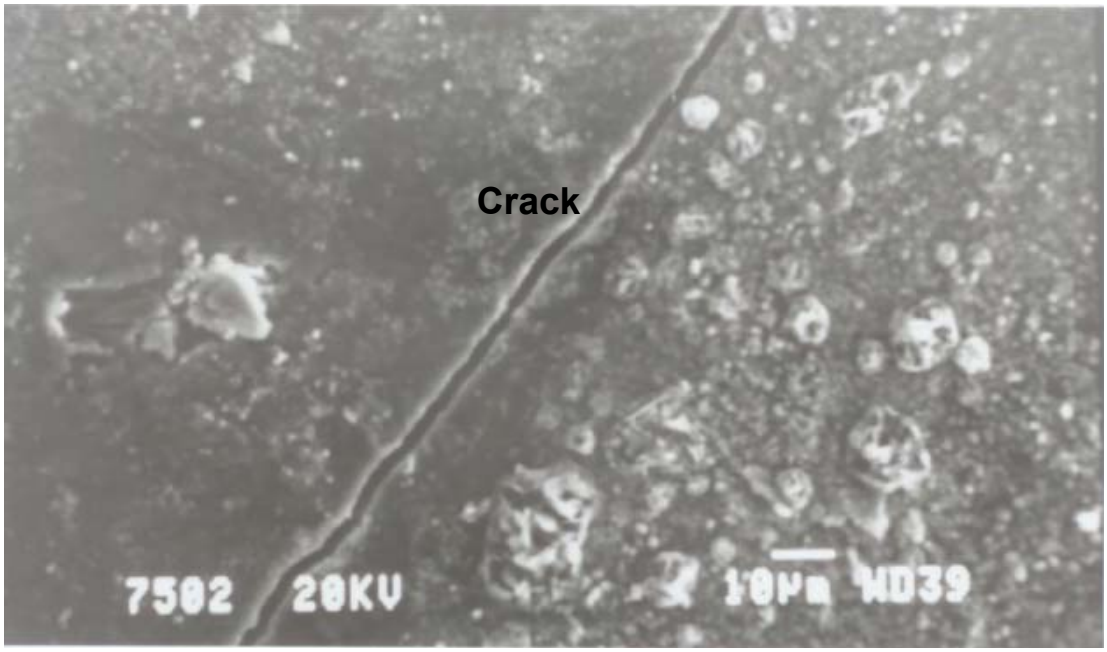


Figure 5.6 Secondary electron image of the corrosion morphology of the uncoated CMSX-4 after hot corrosion at 950°C with a crack running across the surface of the alloy

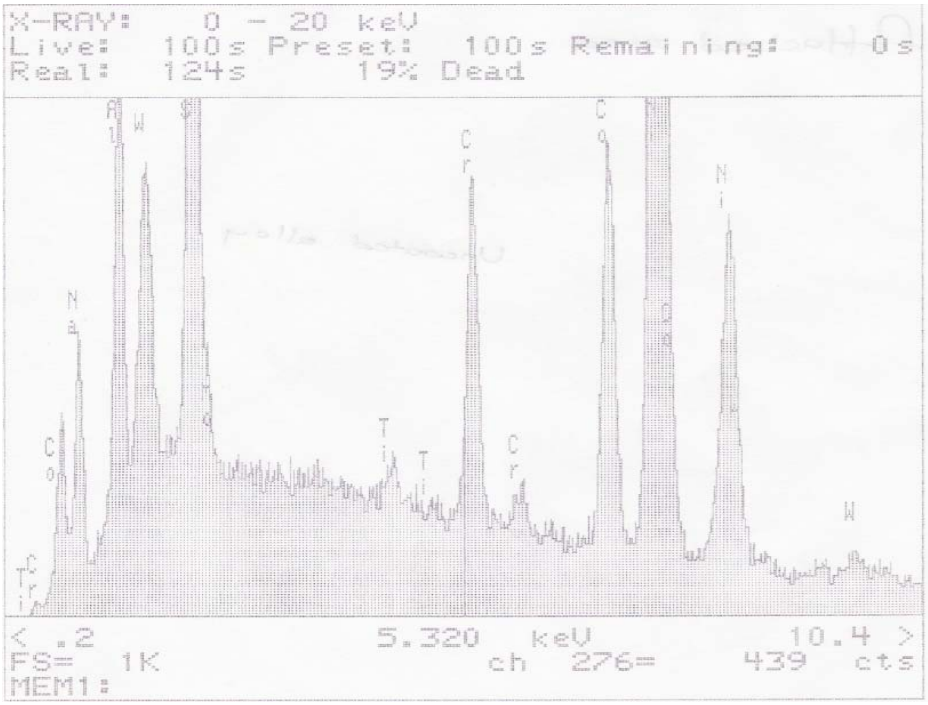


Figure 5.7 EDS analysis performed on the surface of the uncoated alloy that was exposed to molten salt at 950ºC for a period of 792 hours

Corrosion morphologies of Pt-based superalloys were evaluated after 540 hours when the coated alloy failed. The alloys were further exposed to molten salt for a total period of 792 hours. Figures 5.8 and 5.9 show disintegrated scale that formed on the outer surface of alloy P421 [Pt-Al-12Co] after 540 and 792 hours respectively. The alloy suffered serious degradation attacks after being exposed to the salt for a longer period. The alloy formed a porous black corrosion compound that was crystalline in nature. The oxide scale was porous and non-protective.

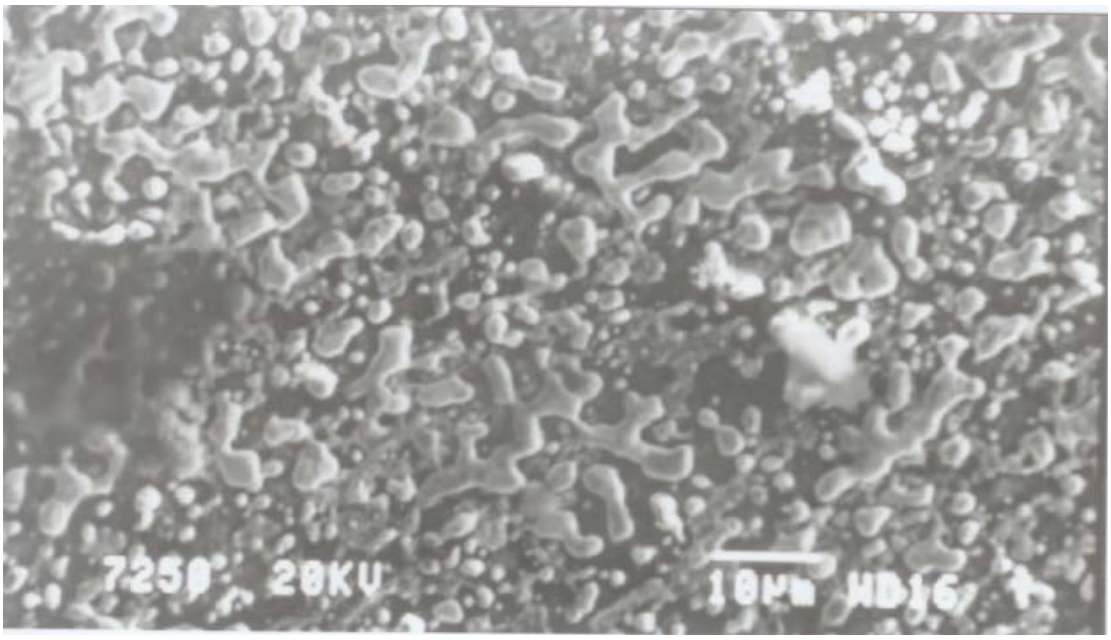


Figure 5.8 Secondary electron image of alloy P421 with non-protective oxide scale after hot corrosion at 950°C after 540 hours

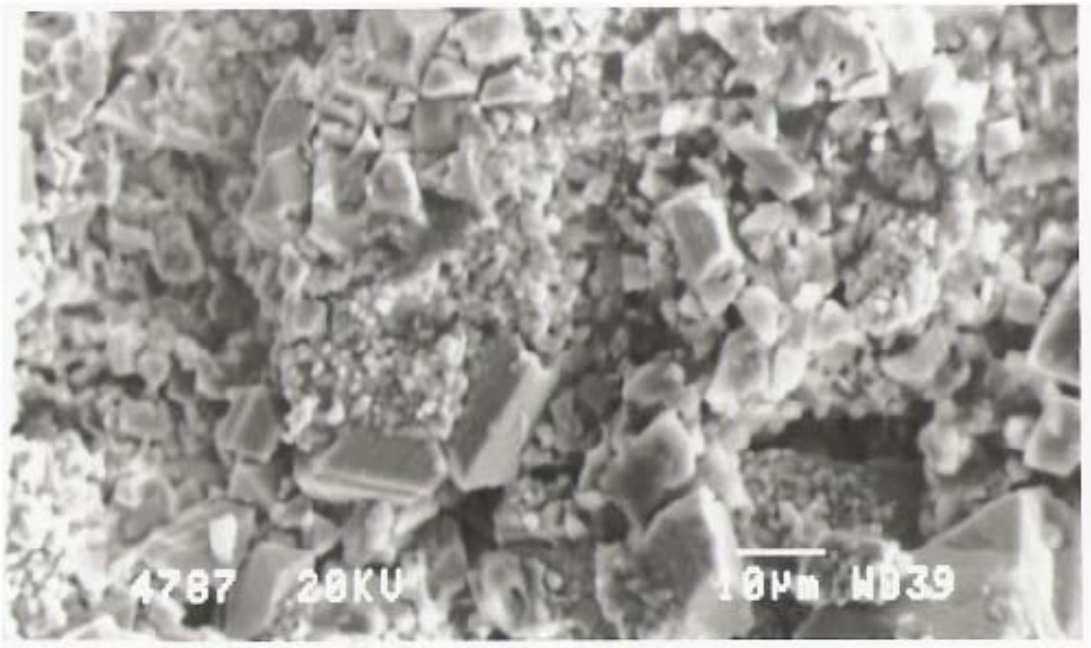


Figure 5.9 Secondary electron image of crystal structured corrosion morphology on alloy P421 after undergoing hot corrosion at 950°C for 792 hours

Figures 5.10 and 5.11 shows the different corrosion morphologies formed on the external surface of alloy P420. Large amounts of the corrosion products precipitated on the surface of alloy P420 after exposing the alloy for a longer period.

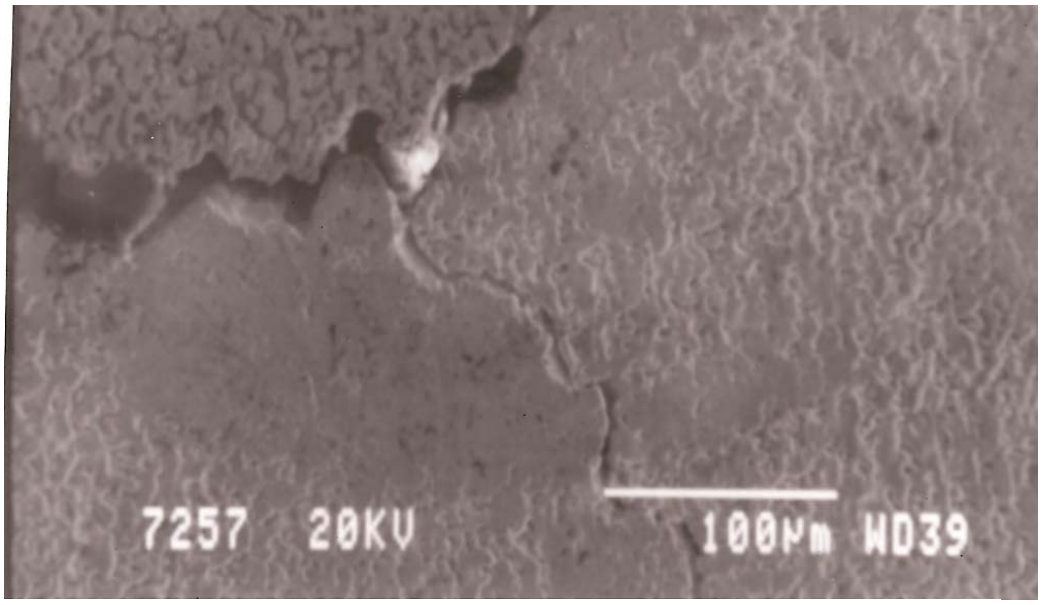


Figure 5.10 Secondary electron image of the surface morphology on alloy P420 after exposure to molten Na_2SO_4 salt for a period of 540 hours

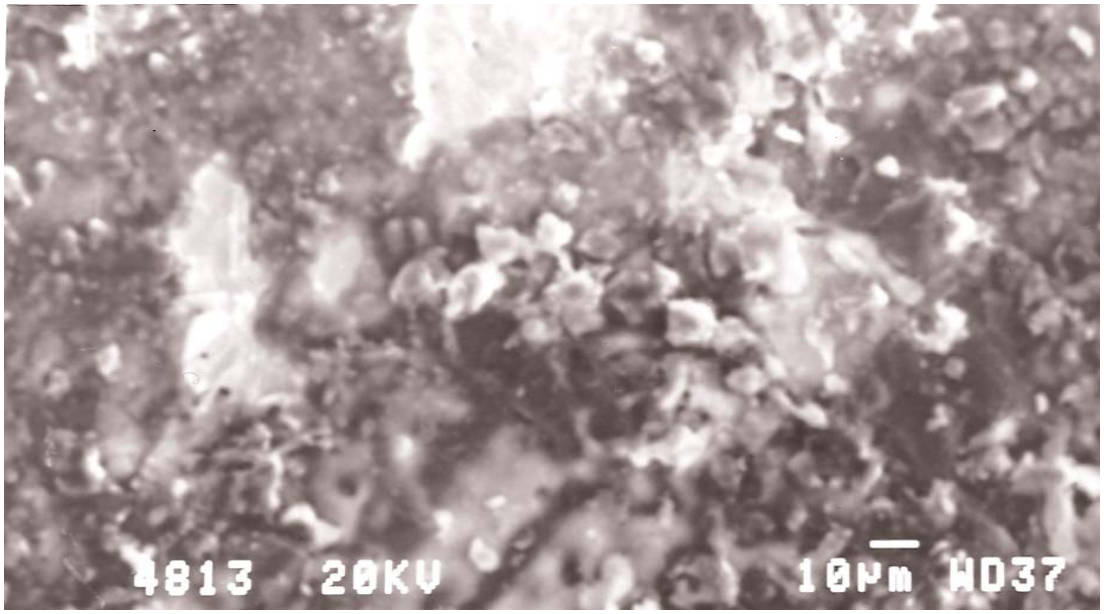


Figure 5.11Secondary electron image of the corrosion morphology of alloy P420 after hot corrosion at 950°C for 792 hours

Kinetics for alloys RS1, RS2 and RS3 were relatively slow compared to the other investigated alloys. The results for better corrosion behaviour could be due to the formation of a less porous and more protective scale compared to the rest of the investigated alloys, thus rendering the alloys more corrosion resistant. Corrosion morphologies of these alloys are presented in figures 5.12-5.17.

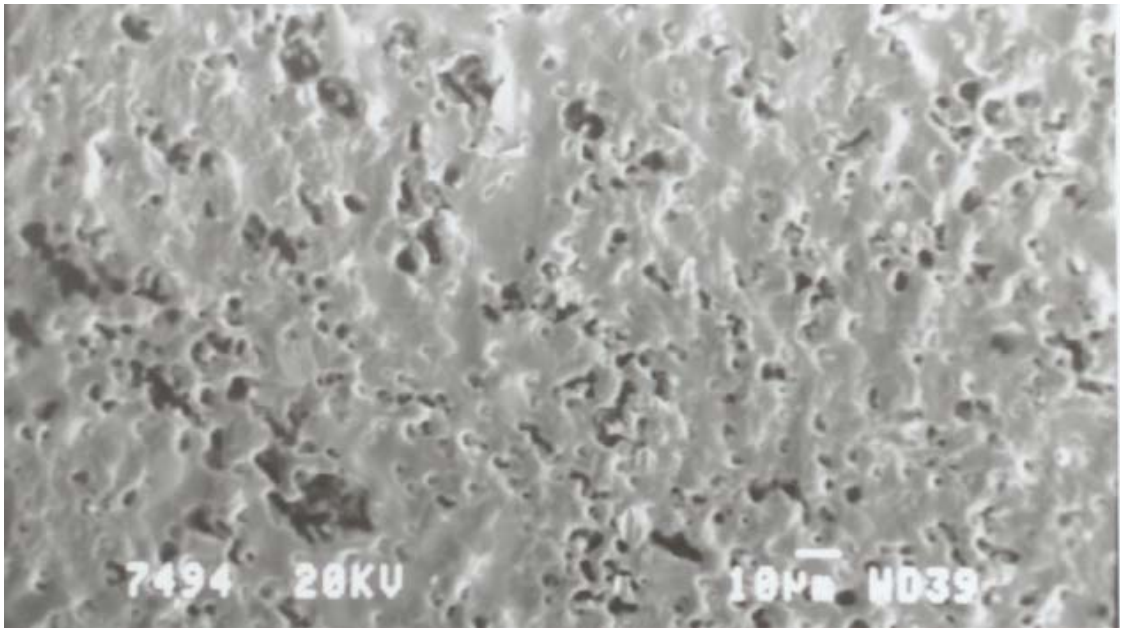


Figure 5.12 Secondary electron images showing a porous oxide scale on the surface of alloy RS1 after hot corrosion in molten salt for 540 hours

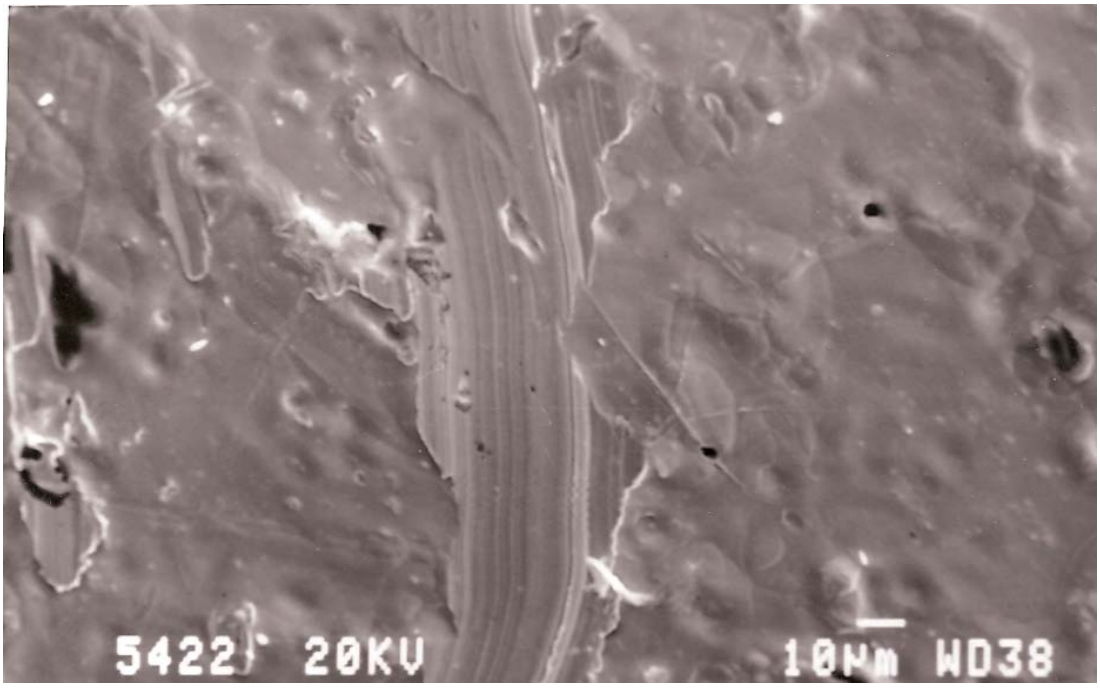


Figure 5.13 Secondary electron images of a porous oxide scale on the surface of alloy RS1 after hot corrosion in molten salt for 792 hours

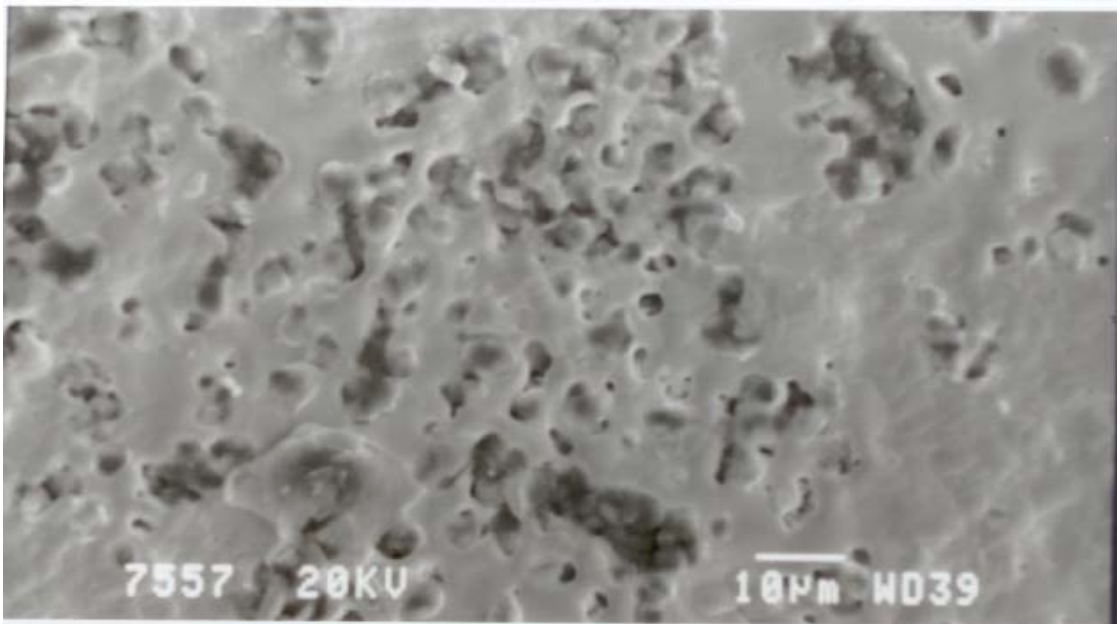


Figure 5.14 Secondary electron image of the corrosion morphology that resulted on the surface of alloy RS2 after at 950°C for 540 hours

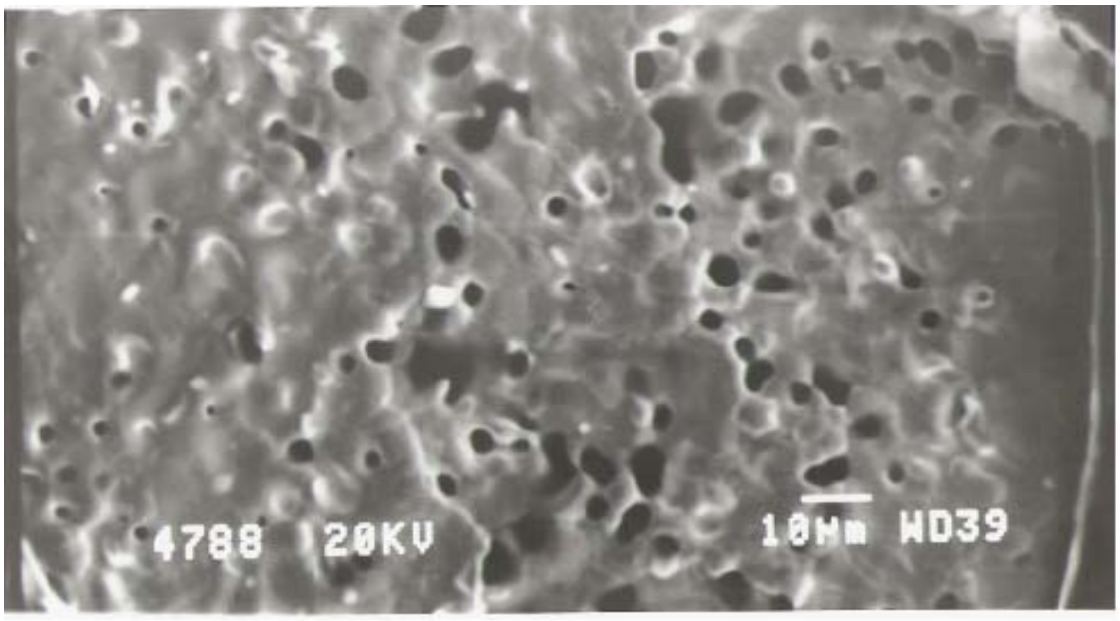


Figure 5.15 Secondary electron image of the corrosion morphology that resulted on the surface of alloy RS2 after at 950°C for 792 hours

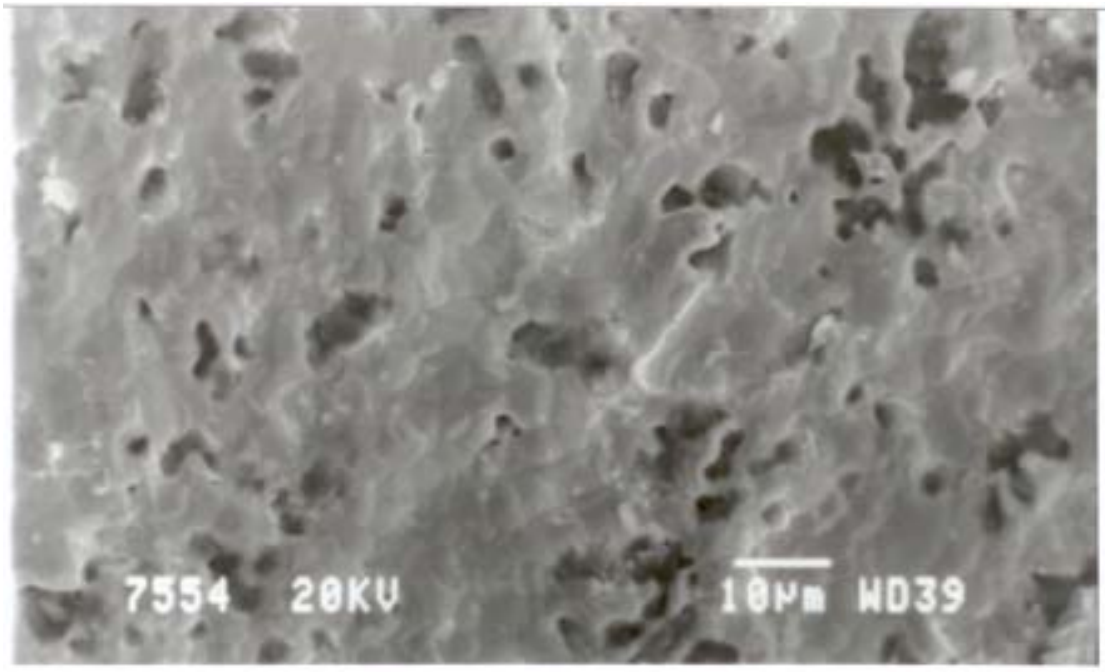


Figure 5.16 Secondary electron image of the corrosion morphology of alloy RS3 after hot corrosion in molten Na_2SO_4 salt at 950°C for duration of 540 hours

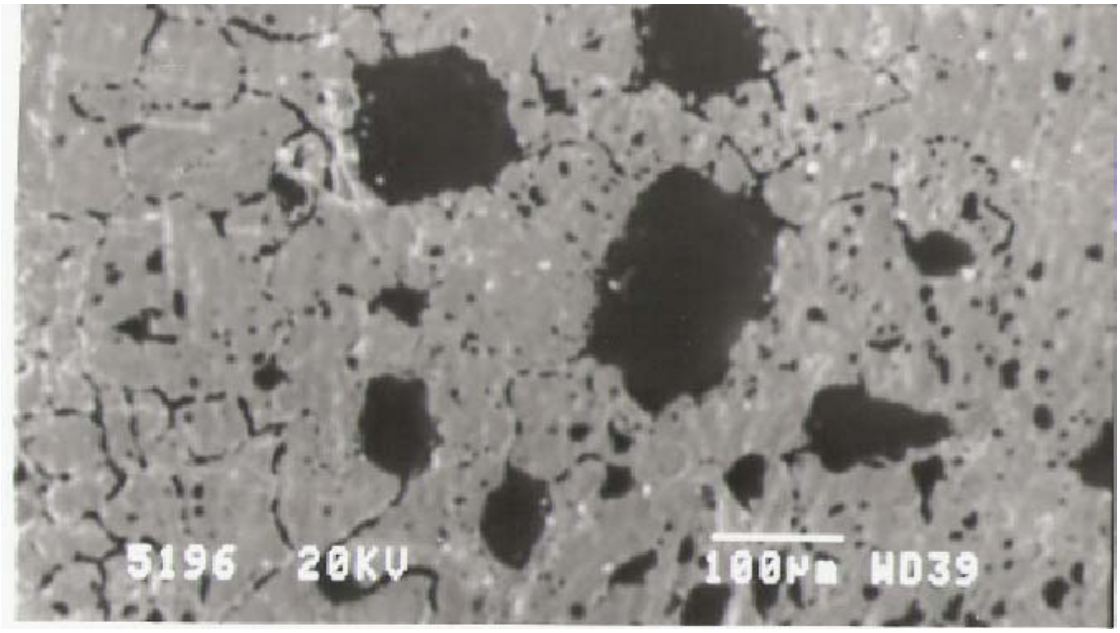


Figure 5.17 Secondary electron image of corrosion morphology of alloy RS3 after hot corrosion in molten Na_2SO_4 salt at 950°C for duration of 792 hours

EDS analysis performed on the surface of alloy RS2 picked up traces of Na_2SO_4 salt on the surface of the alloy. Traces of Ca were impurities found in the bakelite that was used for molding of alloys.

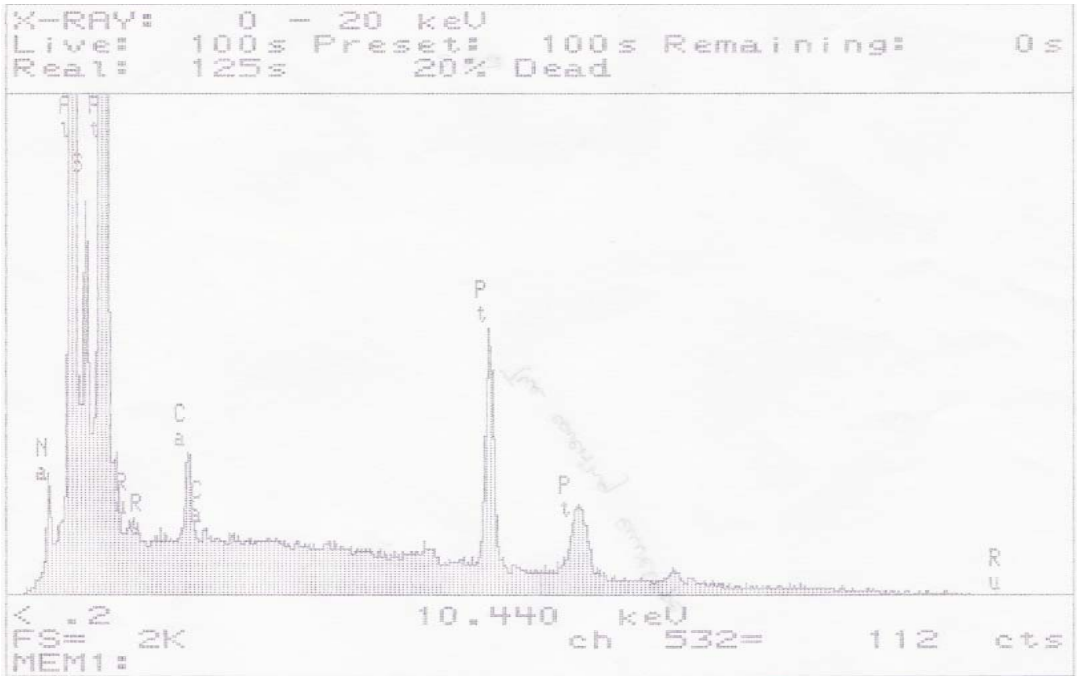


Figure 5.18 SEM scan obtained after performing cross sectional analysis on the surface of the alloy RS2.

The morphology of a typical type I hot corrosion on the uncoated alloy is depicted in figure 5.19. The external scale comprised mostly of NiO. Beneath the oxide scale was a formation of mixed oxides. Sulphides diffused inwards forming stable CrS. The depth of attack on the surface of the uncoated alloy was approximately 160 μm in thickness. EDS analysis performed on the uncoated alloy is presented in figure 5.20.

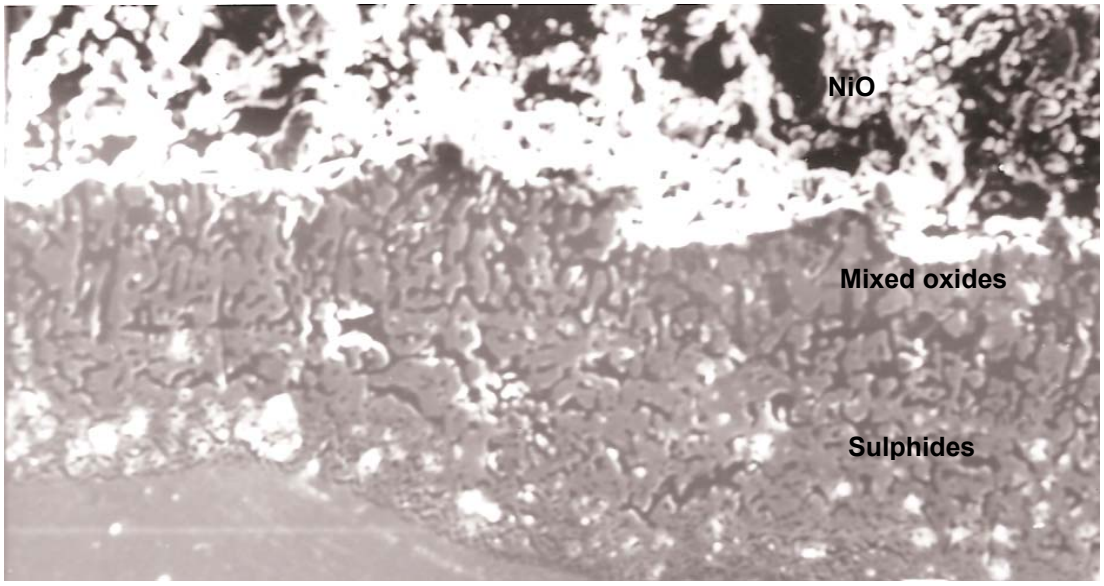


Figure 5.19 Cross sectional morphology of the uncoated alloy after hot corrosion attack in molten Na_2SO_4 salt

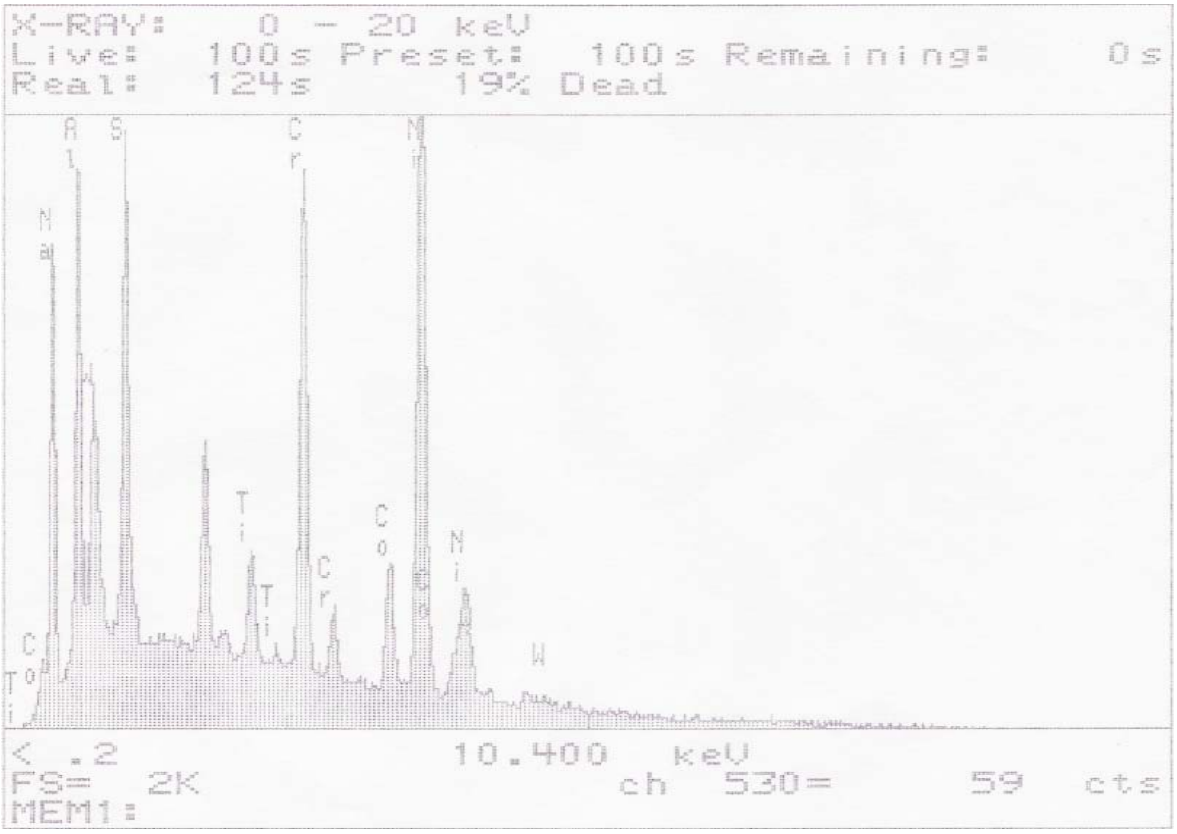


Figure 5.20 SEM scan obtained after performing cross sectional analysis on the surface of the uncoated alloy

Examining transverse sections of the corroded alloys, it was apparent that Pt-based superalloys experienced minimal attack compared to the benchmark alloys. The results are in agreement with corrosion kinetics results obtained. Pt-based superalloys suffered internal oxidation as indicated in figures 5.21-5.23 below. Internal oxidation is undesirable for high temperature materials. However it was noted that alloy RS1 showed better scale adherence compared to alloy RS3.

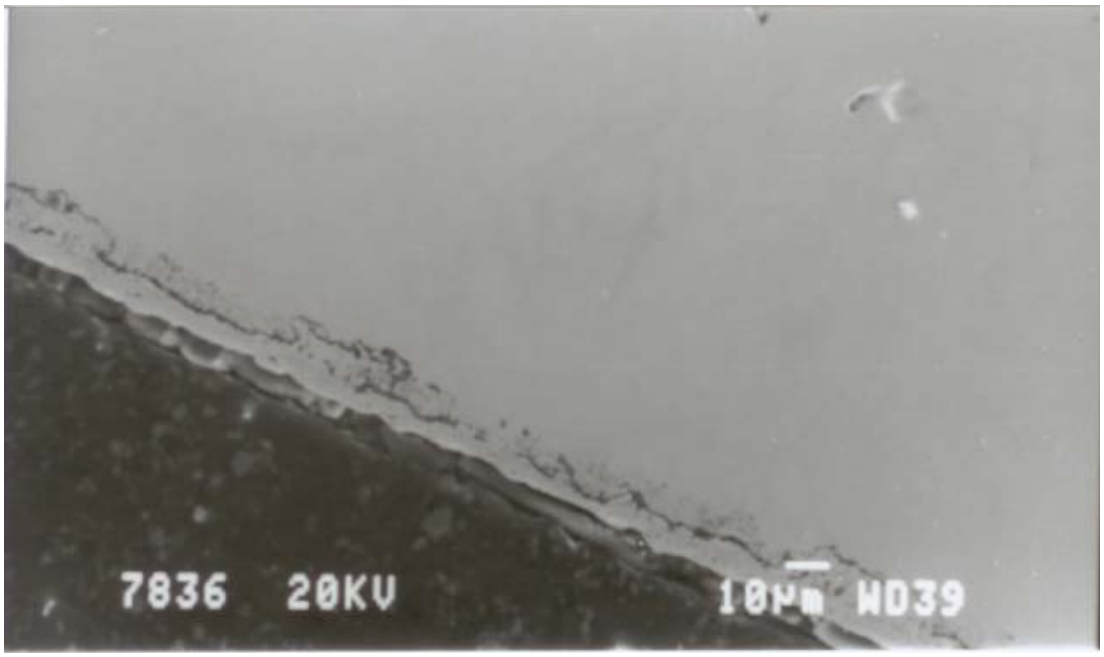


Figure 5.21 Secondary electron micrograph of the cross section of alloy RS1 after hot corrosion test at 950°C

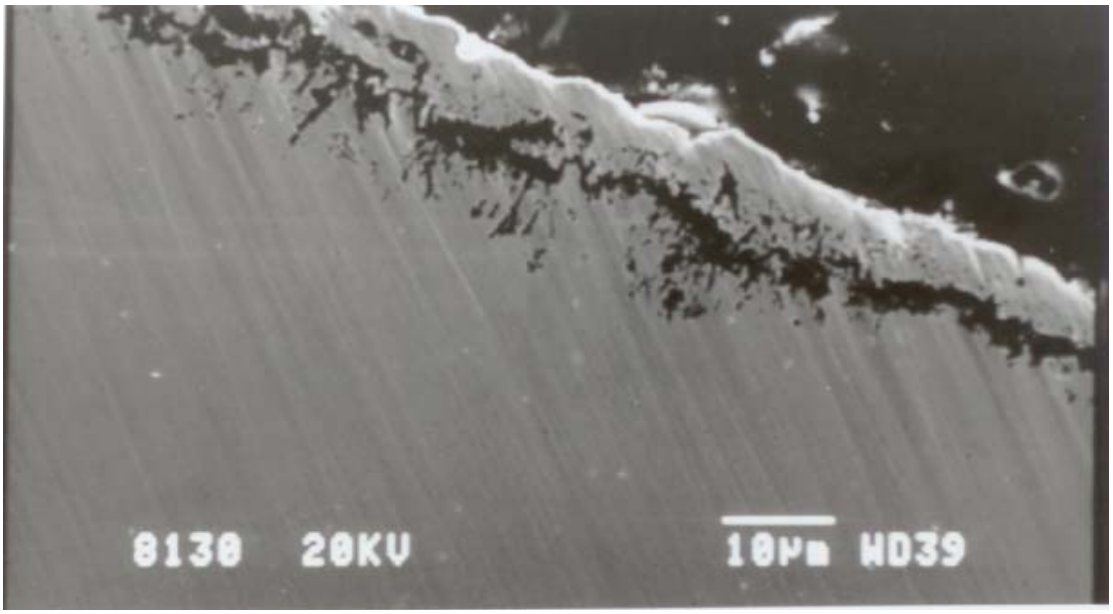


Figure 5.22 Secondary electron micrograph of the cross section of alloy RS2 after hot corrosion test at 950°C

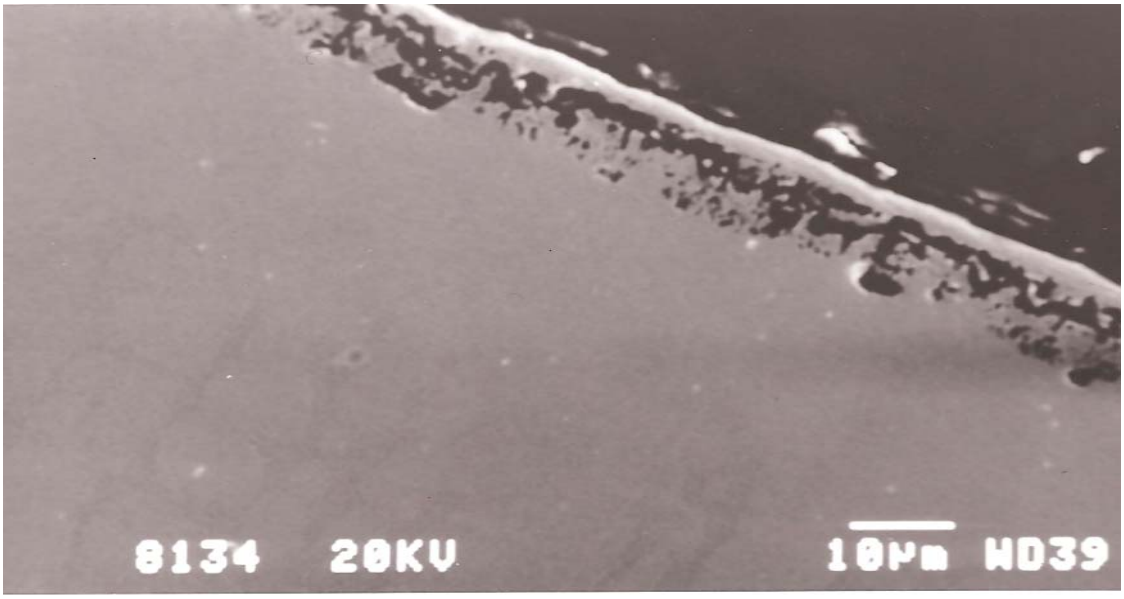


Figure 5.23 Secondary electron micrograph of the cross section of alloy RS3 after hot corrosion test at 950°C

5.1.3 X-ray Diffraction Analysis

Corrosion compounds that formed on the external surfaces of the investigated alloys after hot corrosion were characterized using XRD. The analyses are presented in figures 5.24-5.30, from which it could be deduced that alloys RS1, RS2 and RS3 were able to form alumina. Traces of Na_2SO_4 were detected on the surface, supporting some of the EDS results performed on the surface of the alloys. Oxides further reacted with the salt, forming compounds such as $NaAl(SO_4)_2$ on alloy RS1.

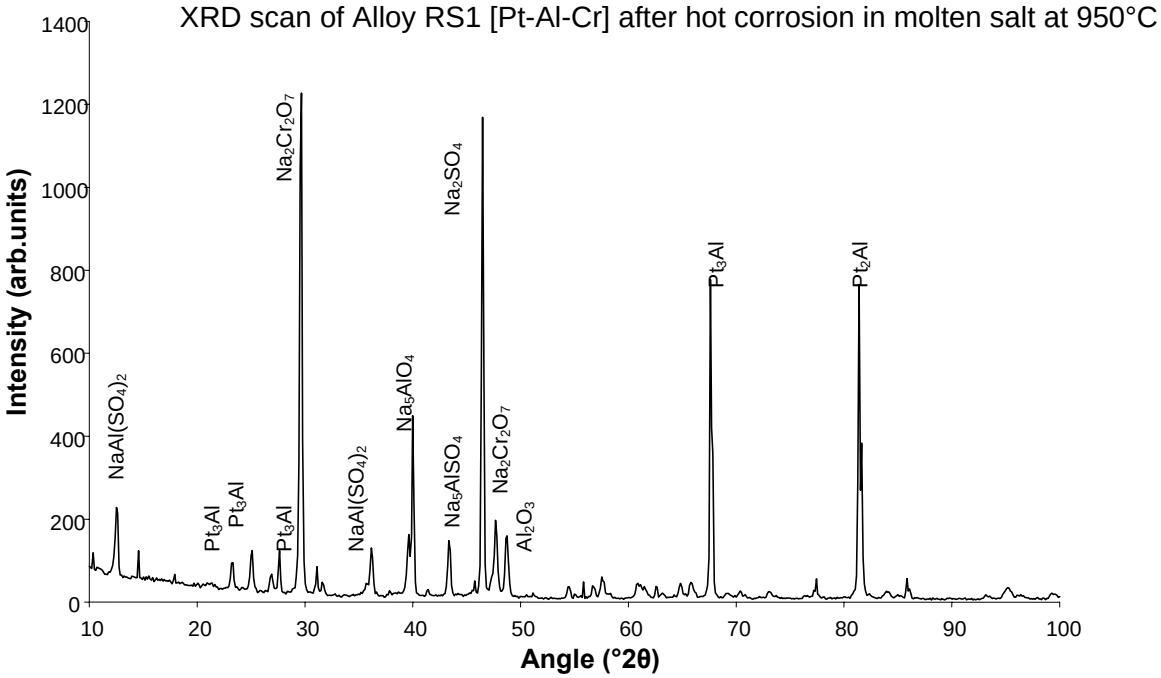


Figure 5.24 X-ray diffraction patterns on the scale of alloy RS1 after hot corrosion

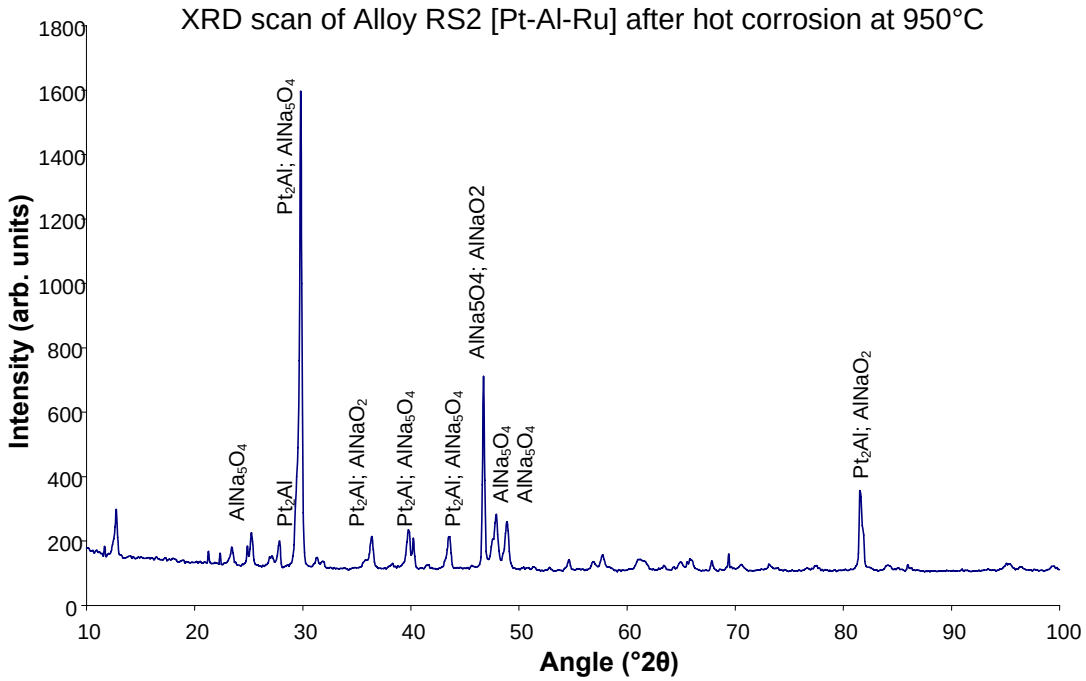


Figure 5.25 X-ray diffraction patterns on the scale of alloy RS2 after hot corrosion

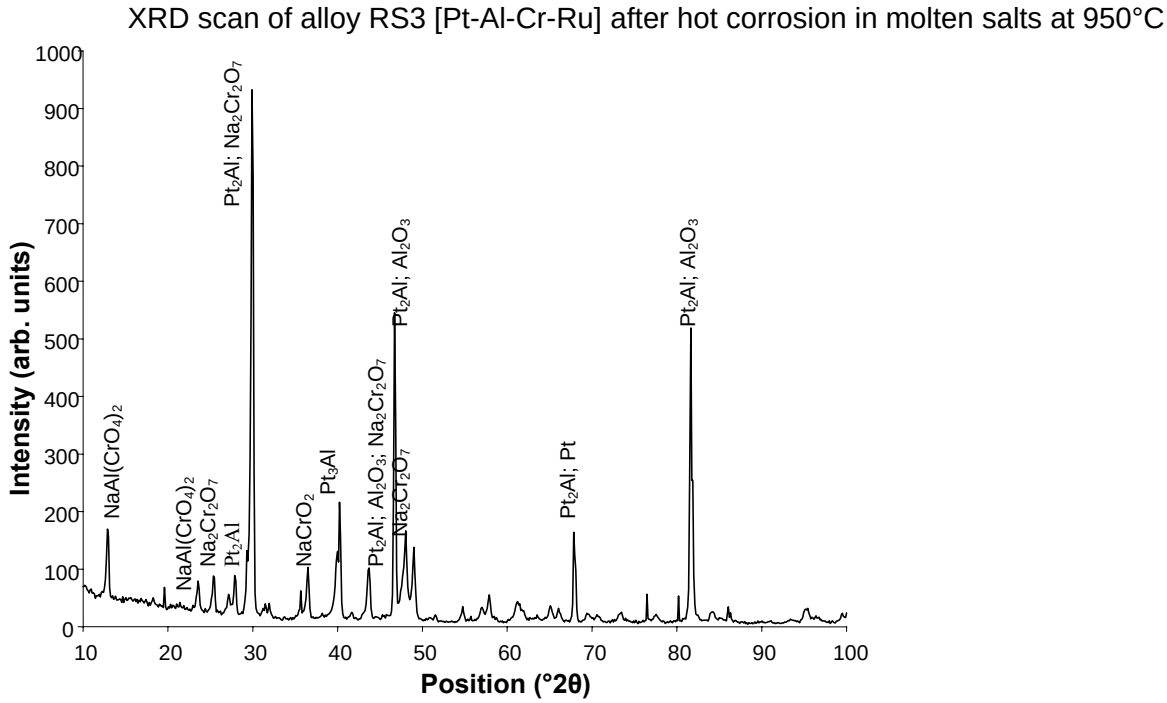


Figure 5.26 X-ray diffraction patterns on the surface of alloy RS3 after hot corrosion

Alloy P420 comprised mostly of the Pt_2Al phase. Co oxides and sulphates formed on the surface of alloy P420. Sulphides were detected on the surface of alloy P420 which led to the formation of deleterious compounds such as PtS which causes embrittlement in Pt-alloys. Outward diffusion of Co led to the formation of $CoSO_4$ detected during the analysis

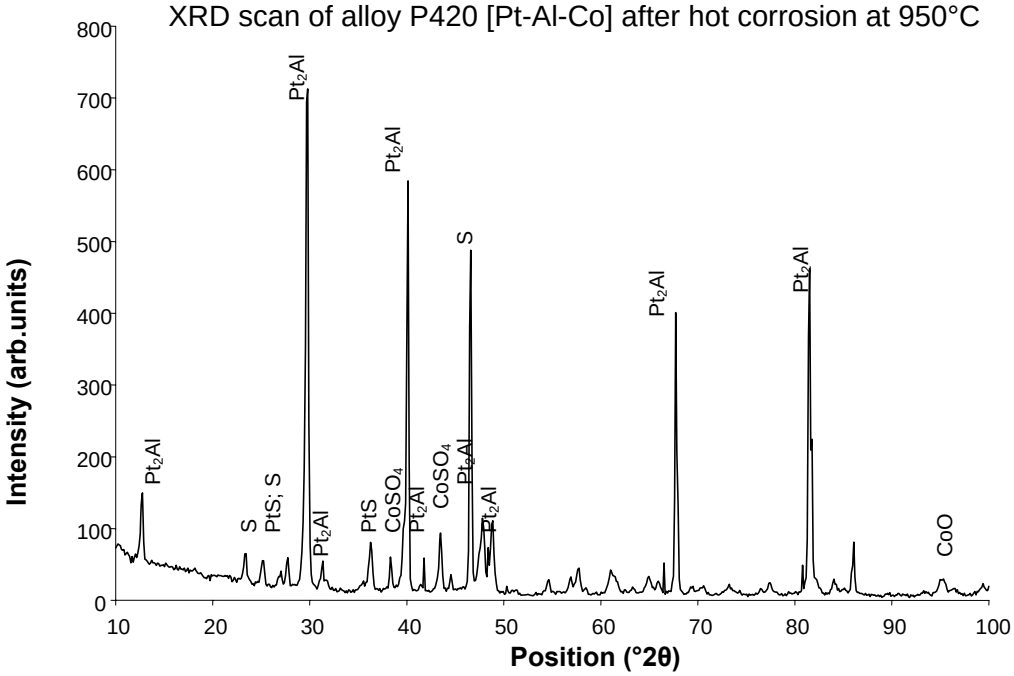


Figure 5.27 X-ray diffraction patterns on alloy P420 after corrosion at 950°C

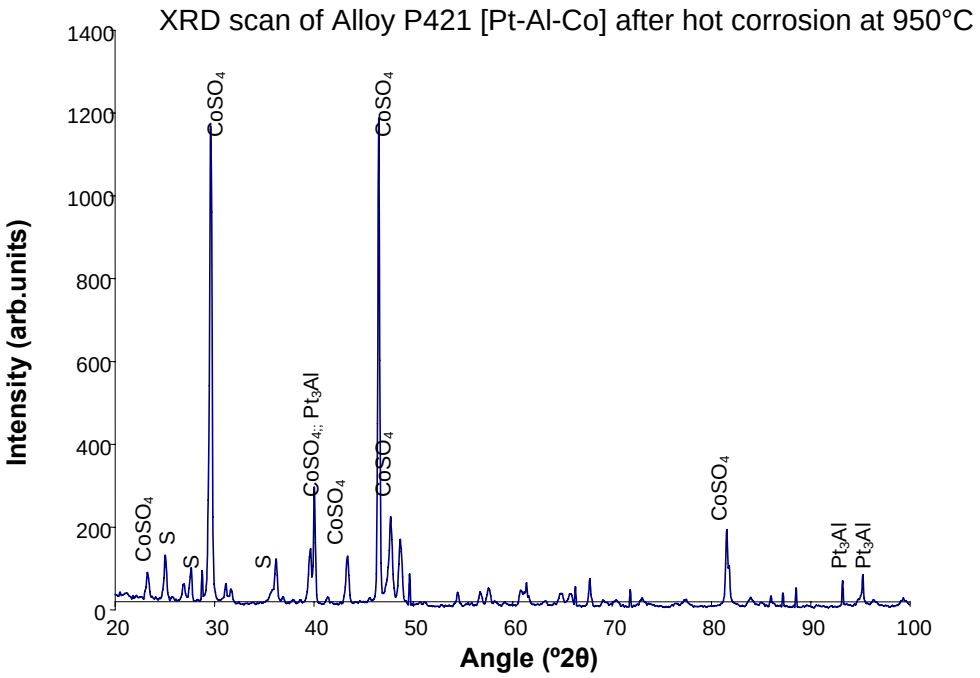


Figure 5.28 X-ray diffraction patterns on the surface of alloy P421 after hot corrosion

The exterior scale on the coated alloy comprised primarily of oxides. The non-protective corrosion compounds in figure 5.29 were identified by XRD as $NiAl_2O_4$, NiO and $NiCr_2O_4$. Since these corrosion products that formed are non-protective, they result in the alloy being susceptible to hot corrosion.

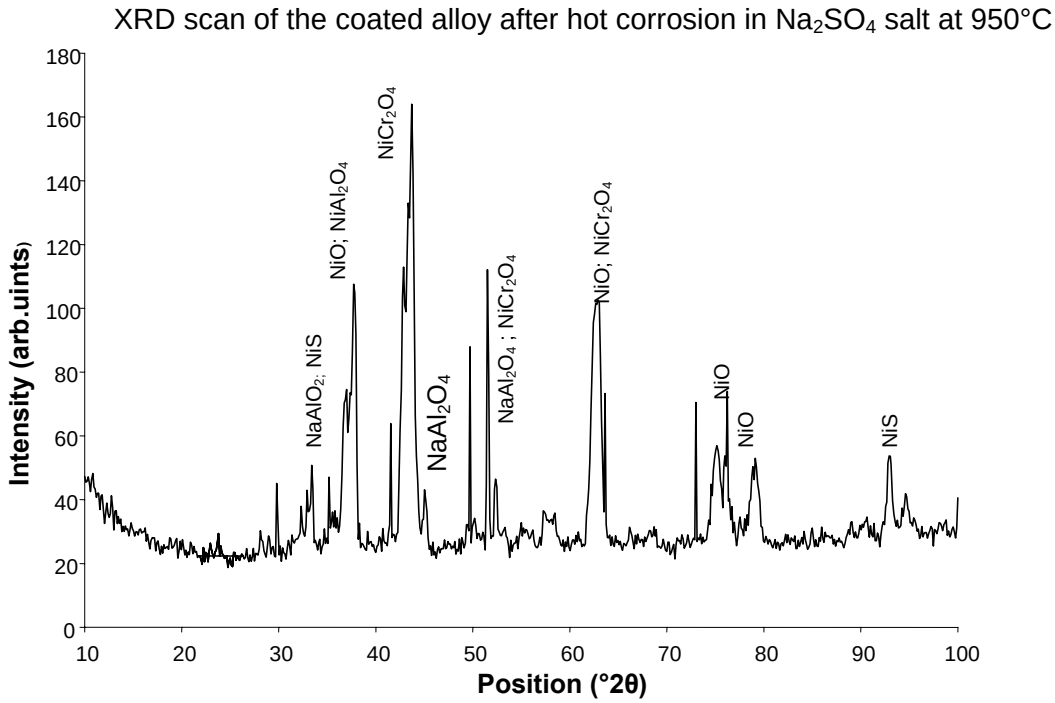


Figure 5.29 X-ray diffraction patterns on the surface of the coated Ni-based superalloys after hot corrosion

NiO was the main corrosion compound that formed on the surface of the uncoated alloy in figure 5.30. The analysis further indicates that MoO_3 also formed. However, MoO_3 volatilizes at temperatures above 800°C

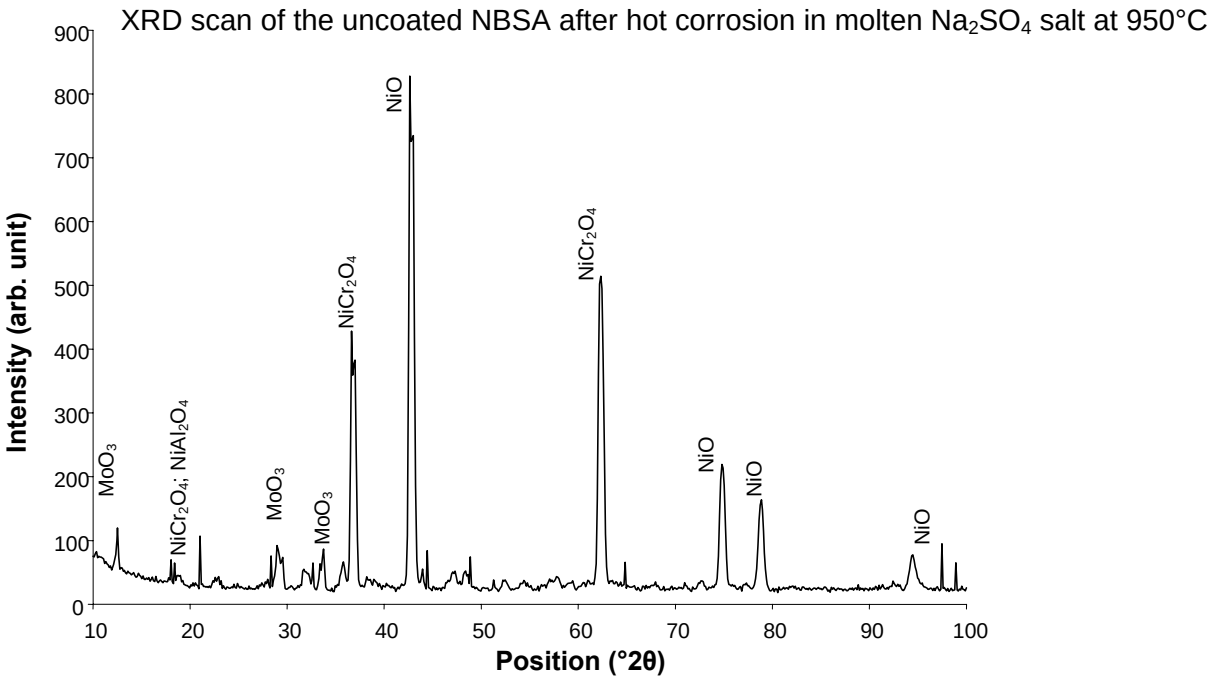


Figure 5.30 X-ray diffraction patterns on the surface of uncoated Ni-based superalloy after hot corrosion

5.1.4 Raman Analysis

Raman spectra were collected over a range of 250-2500 cm^{-1}. Spectra of Pt-based superalloys were plotted on the same set of axis because the spectra for all the samples were similar with a broad band at 1100 cm^{-1}, as shown in figure 5.31. Literature indicates that frequency region for SO_4^{2-} anions formed within the 900-1250 cm^{-1} region. Thus it was suggested that the analysis detected Na_2SO_4 which was due to salt residues [Choi and Lockwood, 2005].

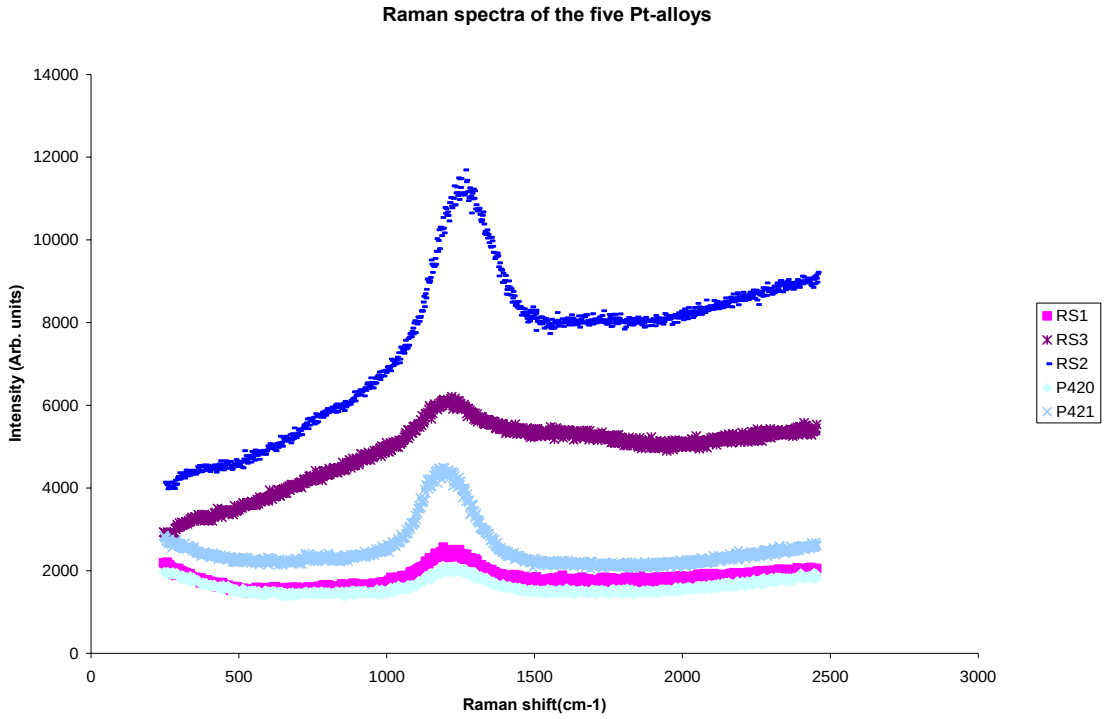


Figure 5.31 Raman spectra obtained from the five Pt-based superalloys after hot corrosion investigations at 950 °C

Raman spectrum on the surface of the uncoated NBSAs shown in figure 5.32 was different from the spectra's observed on Pt-based superalloys. Peak positions are listed in table 5.1. Peaks were matched to NiO, which is in agreement with results obtained from XRD analysis.

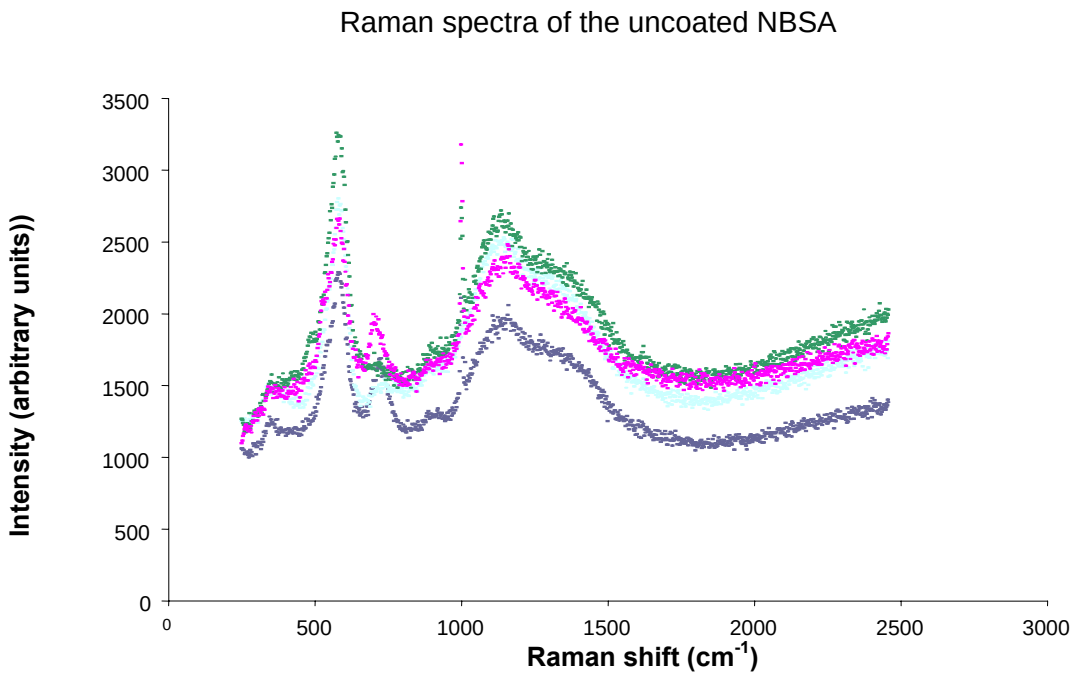


Figure 5.32 Raman spectra obtained from the uncoated CMSX-4 alloy after hot corrosion investigations at 950 °C

Table 5.1 Peak positions in cm^{-1} by Raman spectra on surface of the uncoated NBSA

NiO	This work	Reference [Kim and Wang, 2005]
	1155	1074
	917	910
	727	725
	585	532
	367	400

Figure 5.33 shows the Raman spectra collected on the surface of the coated alloy. Peaks formed at low intensities as compared to the spectrum collected from the uncoated alloy. The peaks were assigned to sulphates.

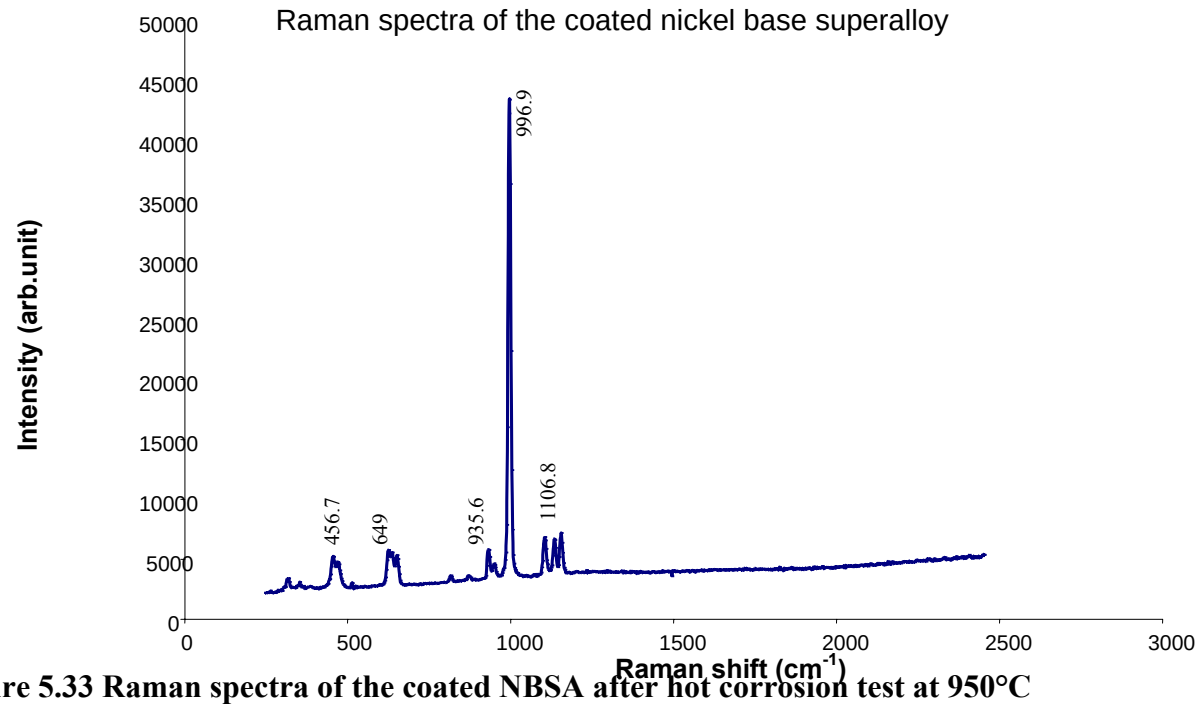


Figure 5.33 Raman spectra of the coated NBSA after hot corrosion test at 950°C

5.2 SULPHIDATION RESULTS

5.2.1 Corrosion kinetics obtained after sulphidation

Figure 5.34 gives the corrosion kinetic curves of the investigated alloys after being exposed to mixed gases at 900ºC for a period of 60 hours. Mass change was the highest for the coated alloy. Rapid mass change was observed on the uncoated alloy, which experienced weight gain during the initial stages of the experiment, followed by a relatively constant behaviour. Minimal mass changes were attributed to the formation of corrosion products that acted as a barrier, making it difficult for elements and the gas to diffuse inwards or outwards.

Noticeably, fluctuations in mass gains were once again observed, especially with alloys P420 and P421. Instability by Co-containing alloys after exposing to corrosive gases indicates poor corrosion resistance of the alloys. Alloy RS1, RS2 and RS3 were reasonably stable with little changes in mass, with alloys RS2 and RS3 recording the lowest mass changes.

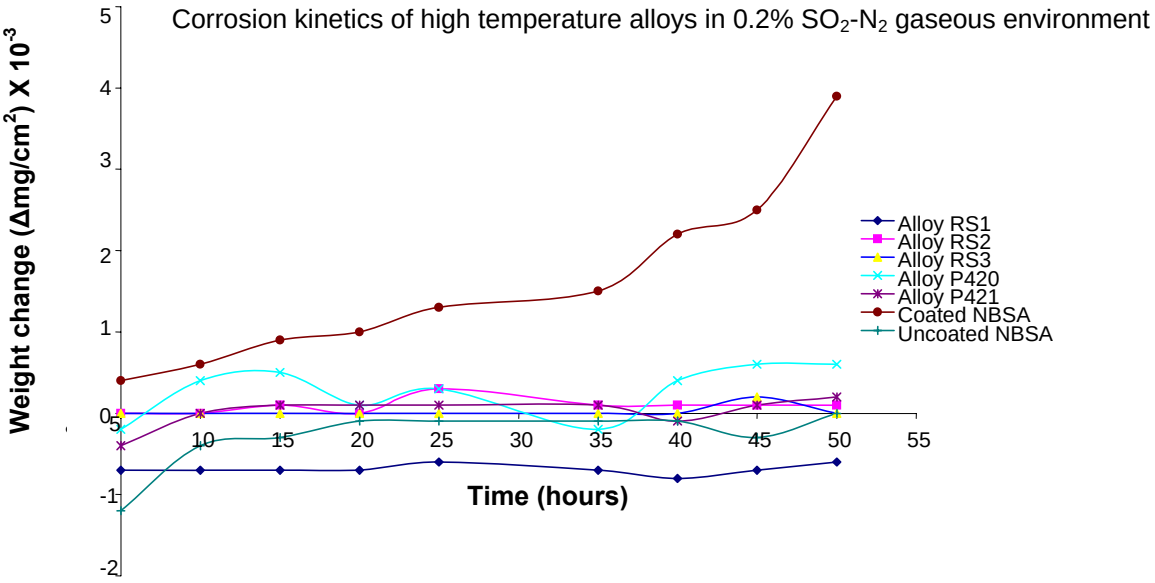


Figure 5.34 Corrosion kinetics of the seven investigated alloys after sulphidation in a 0.2% SO_2-N_2 gaseous environment

5.2.2 SEM analysis with EDS performed on cross sections of the investigated alloys after sulphidation

Cross-sectional examinations of the corroded sections of the investigated alloys were evaluated using the high resolution electron microscope. The attack on the surface of alloy RS1 was not uniform throughout. Figure 5.35 shows the affected corroded area that

was approximately 2µm deep. The same area is shown at higher magnification in figure 5.36, showing internal oxidation. A fine dispersion of precipitates randomly distributed in the alloy is also noticeable in the substrate alloy.

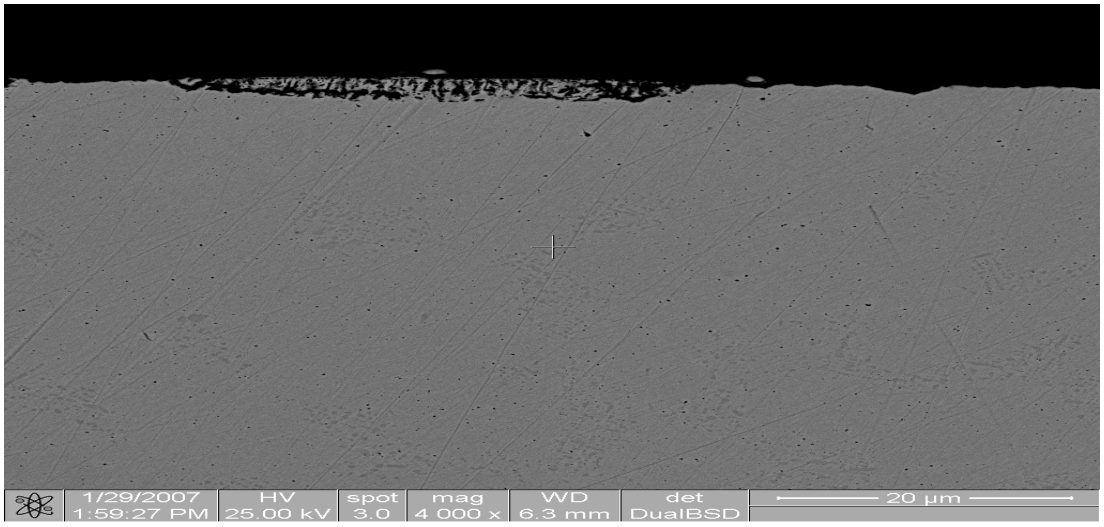


Figure 5.35 SEM image showing cross section of alloy RS1 after the sulphidation test in 0.2%SO_2-N_2 gas at 900ºC

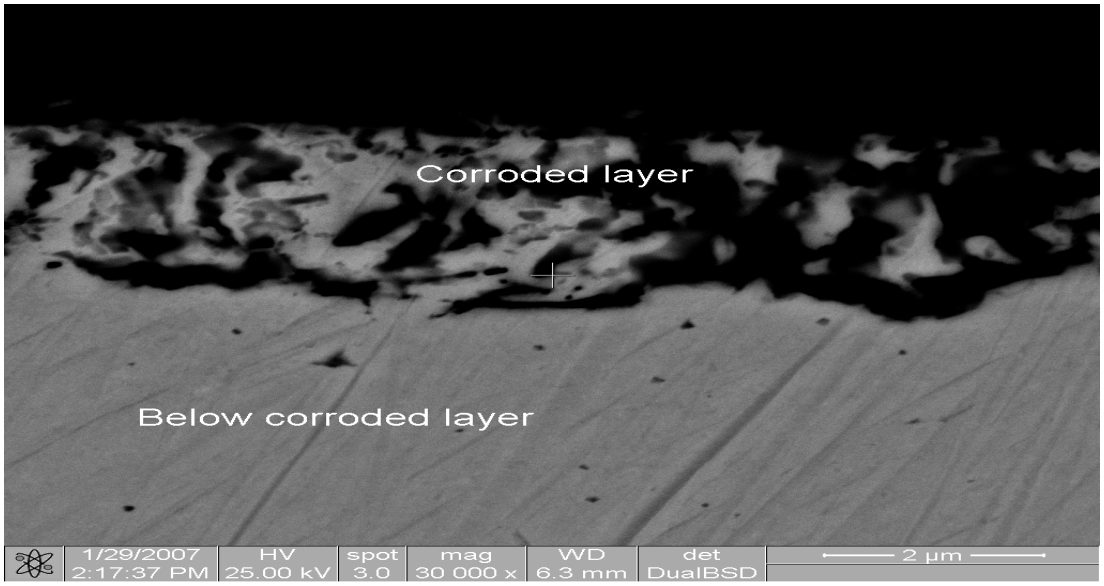


Figure 5.36 Secondary electron images of the cross section of alloy RS1 at 30 000 X magnifications after the sulphidation test, showing the effect and depth of attack by 0.2%SO_2-N_2 gas

No sulphides were detected on the corroded area. However, it was observed that a thin layer of alumina was formed on the external surface of the alloy. The formation of Al_2O_3 scale led to the depletion of the alloying elements that resulted with a Pt-rich area. Cr was in low concentration, and at these working temperatures, it was likely that Cr oxidised, forming volatile compounds. The oxide layer that formed is depicted in figure 5.37 and comprised mostly O_2 and Al. The layer is slow growing and could only be observed at very high magnifications with EDS analysis presented in figure 5.38.

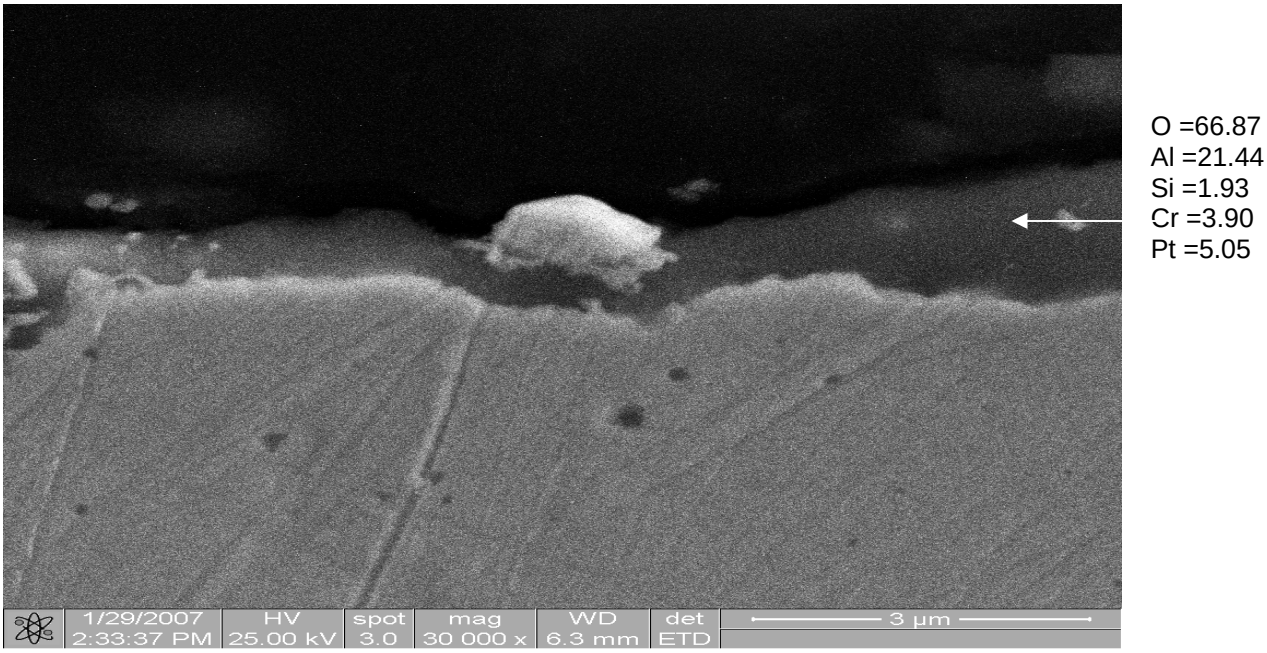


Figure 5.37 SEM image showing the external oxide layer that formed on the surface of alloy RS1

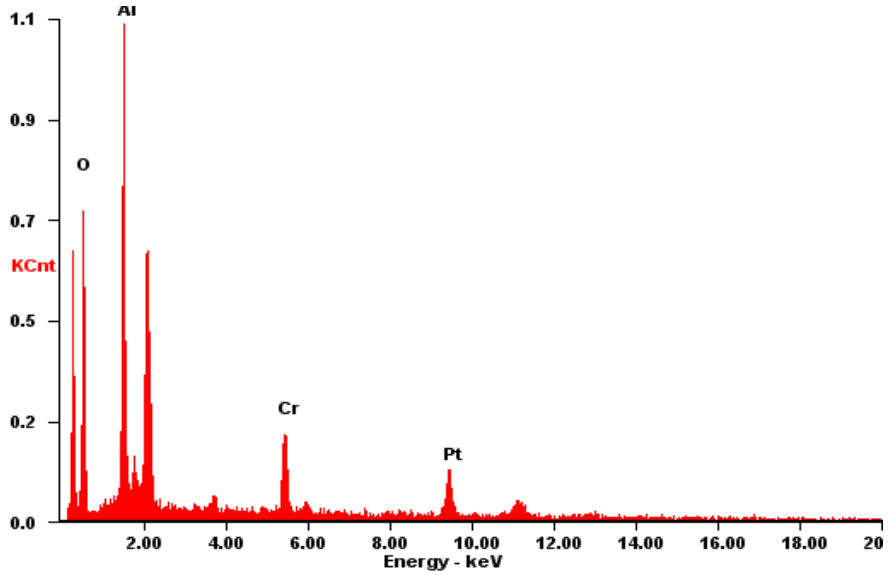


Figure 5.38 EDS analysis performed on the external scale that formed on the surface of alloy RS1 after the sulphidation test in 0.2% SO_2-N_2 environment

Insignificant changes were observed on the external surface of alloy RS2 when the alloy was viewed under the electron microscope. The alloy was unattacked and appeared homogenous and continuous throughout with no internal oxidation. This was exceptional behaviour displayed by a Pt-based superalloy. The cross sectional analysis is shown in figure 5.39.

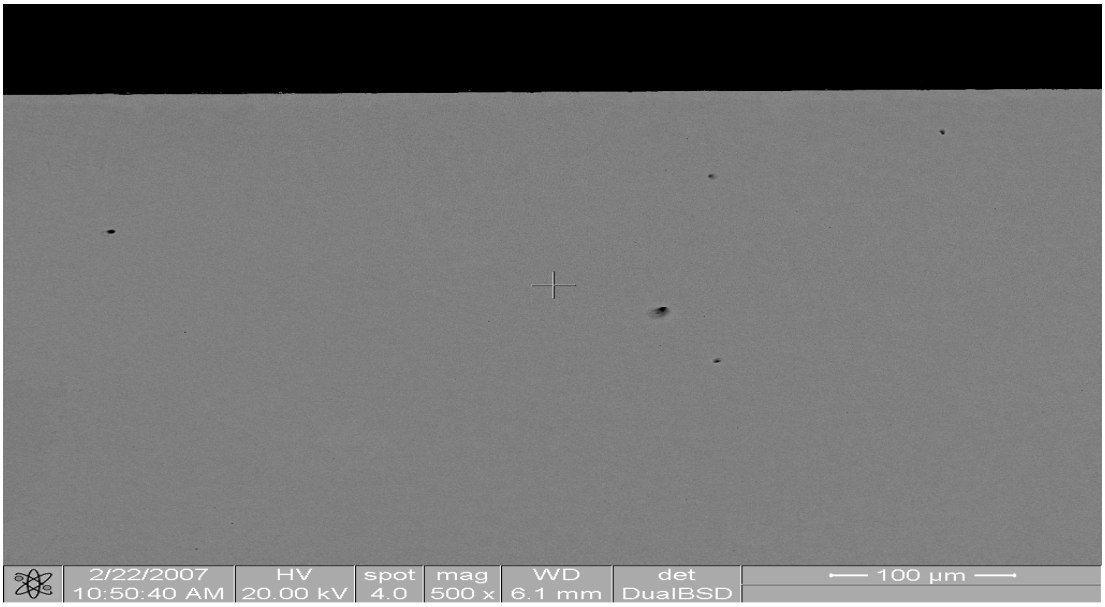


Figure 5.39 Secondary electron images of alloy RS2 after the sulphidation test

Similar to alloy RS1, the alloy was able to form a continuous and tenacious α-Al_2O_3 oxide layer that offered resistance against corrosion from gases, as shown in figure 5.40. The EDS analysis performed on the external oxide scale is shown in figure 5.41.

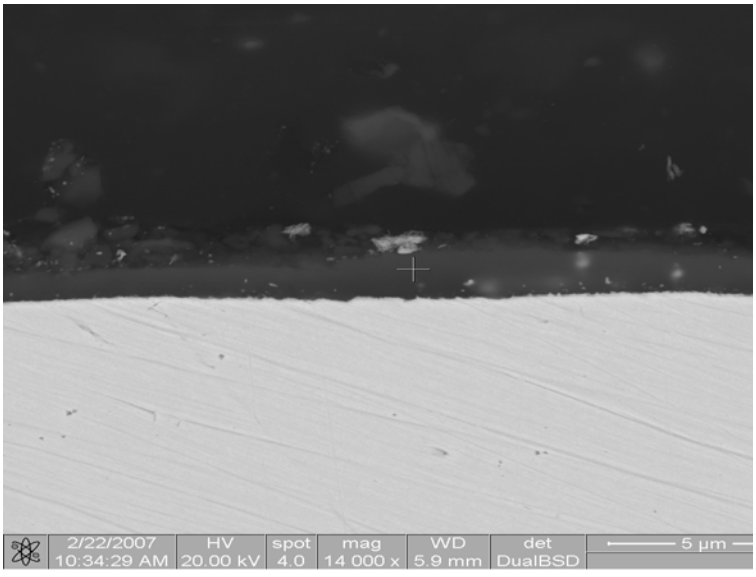


Figure 5.40 Cross section of alloy RS2 at 14000 X magnification with an Al_2O_3 scale forming on the surface of the alloy

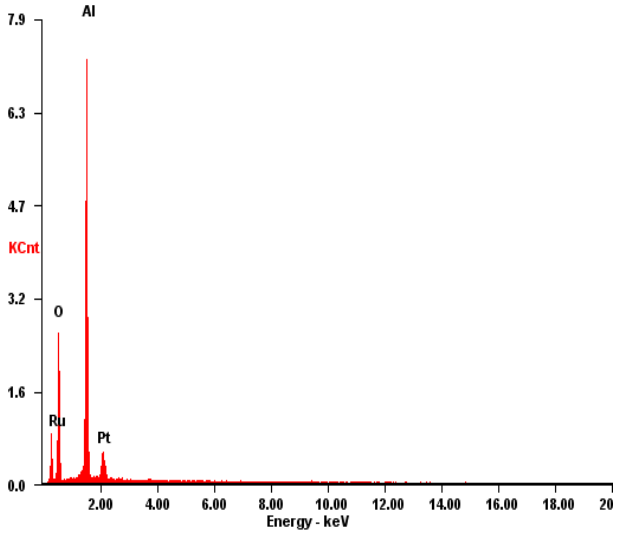


Figure 5.41 EDS analysis performed on the external scale of alloy RS2

Alloy RS3 suffered internal oxidation with possible cracks forming. The depth of attack was approximately 5µm in thickness and is depicted in figure 5.42. The area below the thin oxide scale has lost mechanical integrity. EDS analysis of the oxide scale is given in figure 5.43

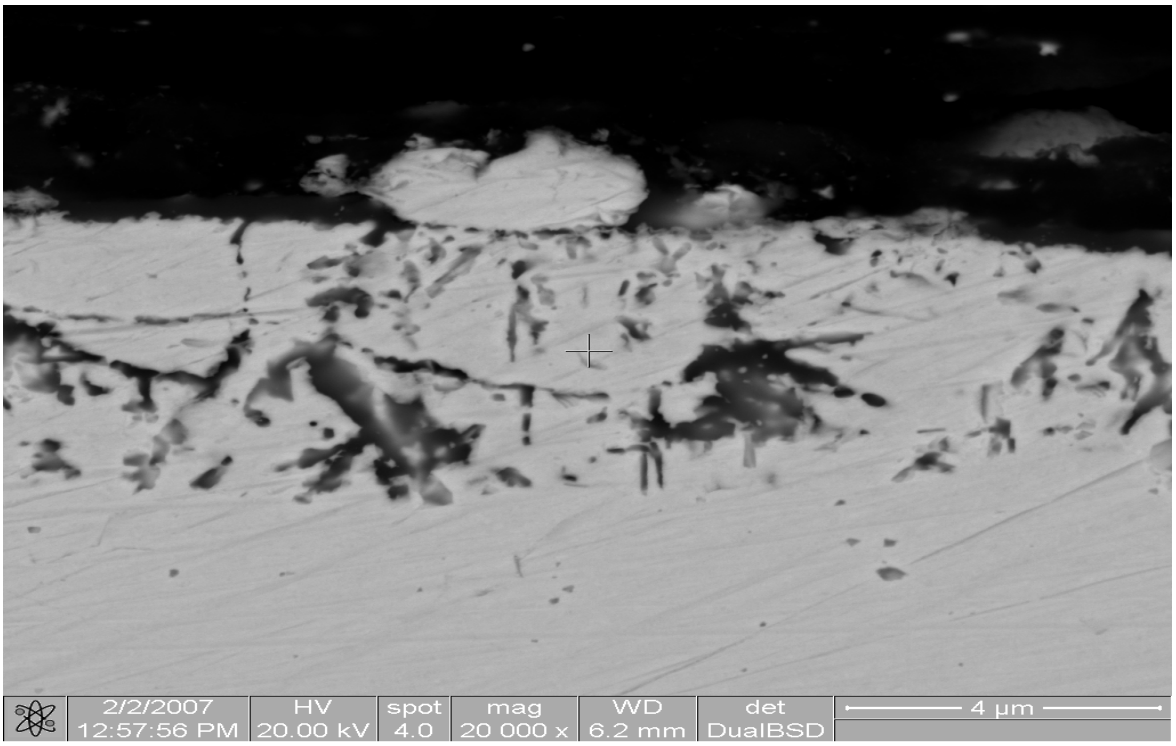


Figure 5.42 Secondary image of cross section of alloy RS3 after sulphidation test

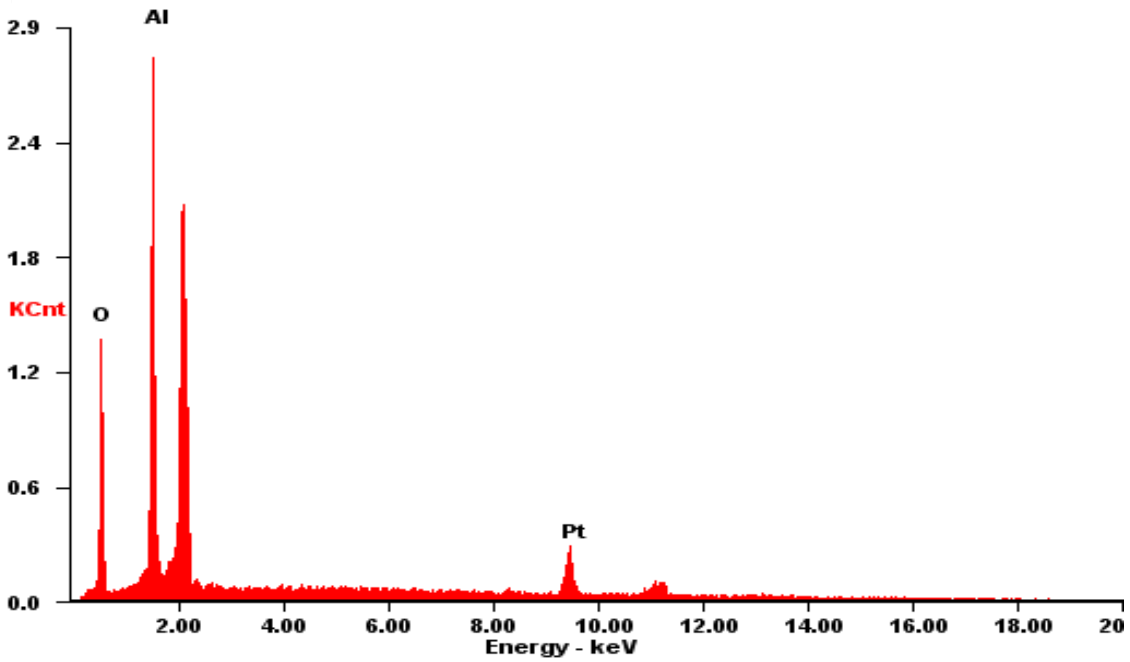


Figure 5.43 EDS analysis performed on the dark area in the corroded section on alloy RS3

Corrosion characteristics of alloys P420 and P421 were nearly similar due to the alloys' similar chemistry. A transverse section of alloy P420 indicated in figure 5.44 shows that the attack was non-uniform across the surface of the alloy. Al_2O_3 that formed was discontinuous.

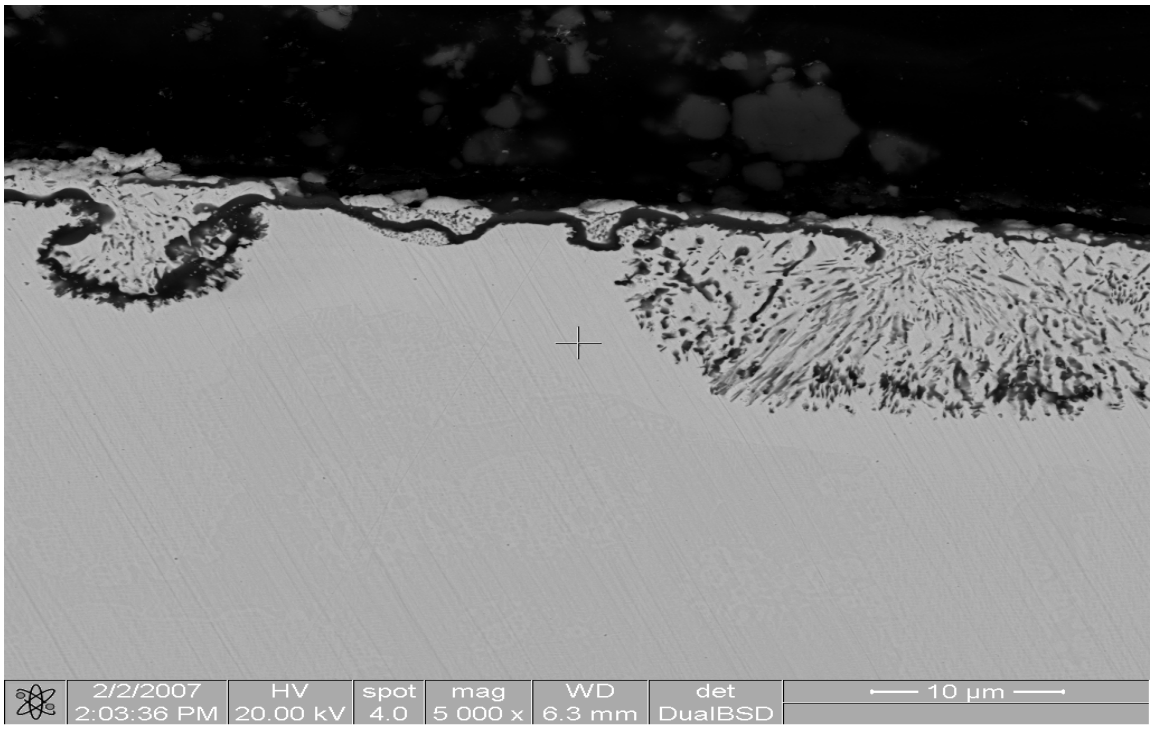


Figure 5.44 Secondary image of alloy P420 after sulphidation test in 0.2% SO_2-N_2 environment

Below the corroded surface is a single phase rich in Pt. The Pt-rich area is depleted of alloying elements, and a dendritic structure formed below the Pt-rich phase as depicted in figure 5.45.

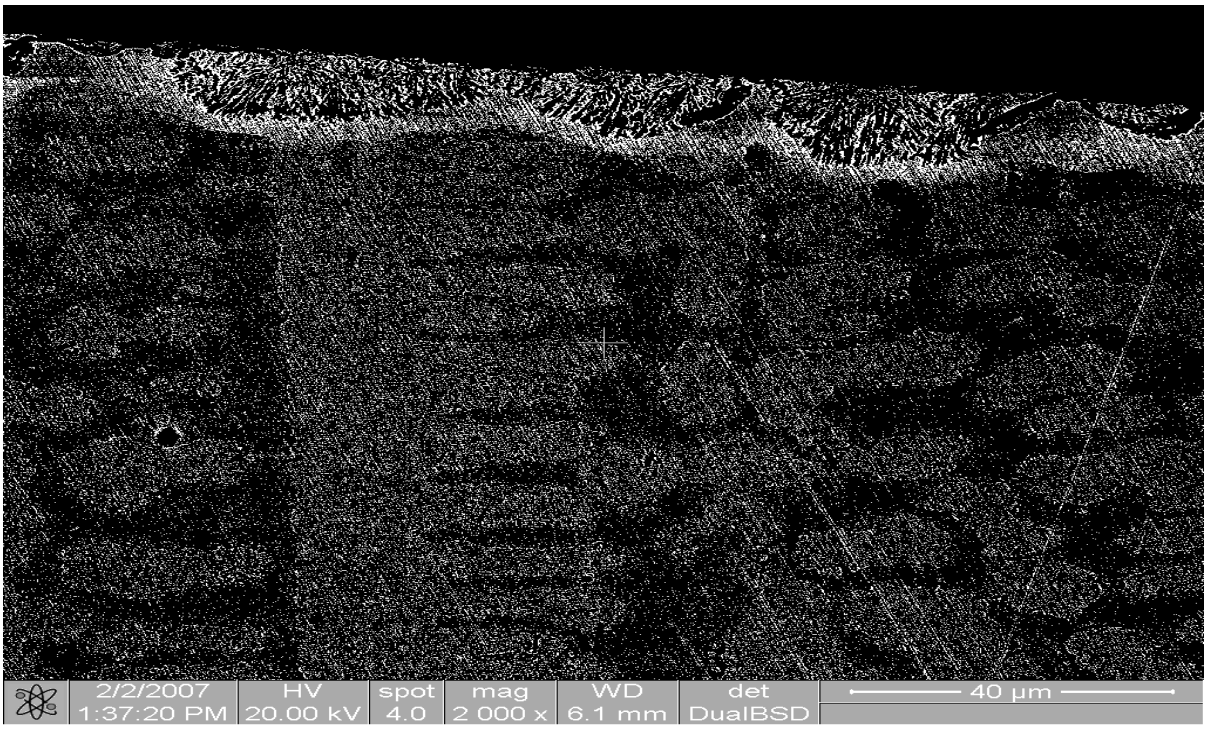


Figure 5.45 Secondary electron image of alloy P420 with the dendritic structure below the corroded area

Co-containing alloys were more susceptible to corrosion attack compared to other Pt-based superalloys. Figures 5.46 and 5.47 are images that were taken across the surface of alloy P421. Similar to alloy P420, an alloy depleted zone rich in Pt was formed. However, the band was thicker that the one observed in alloy P420 as depicted in figure 5.48, suggesting alloy P421 is less resistant to corrosion attacks compared to alloy P420.

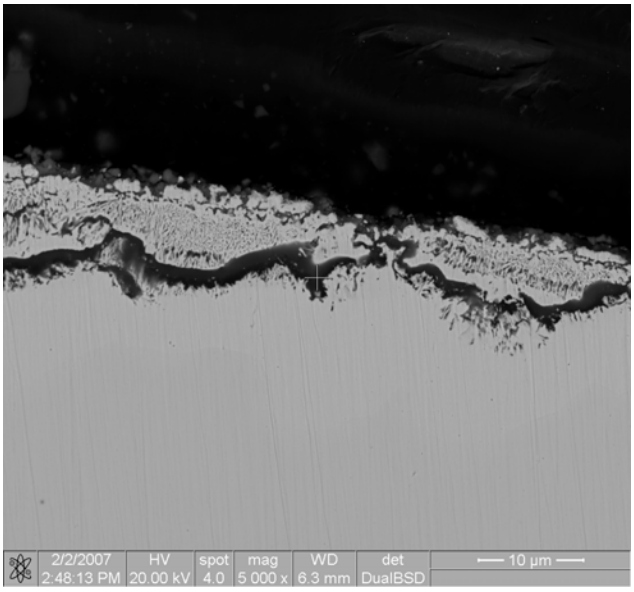


Figure 5.46 Transverse section of corroded alloy P421 after the sulphidation test at 900°C

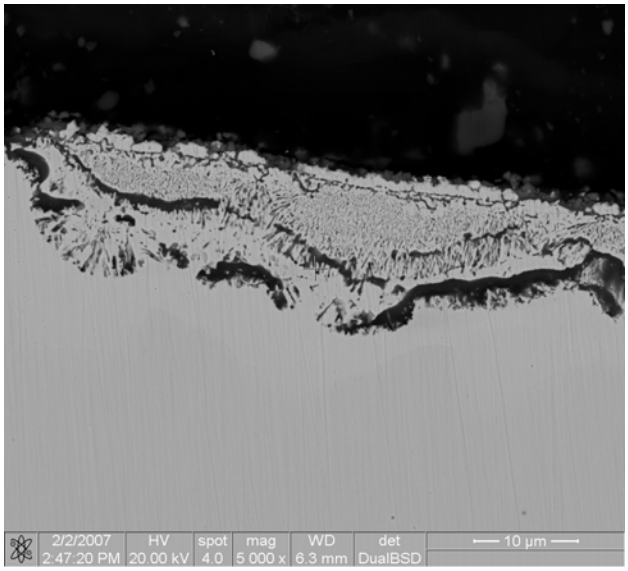


Figure 5.47 Transverse section of alloy P421 across the corroded area of alloy P421 after the sulphidation test

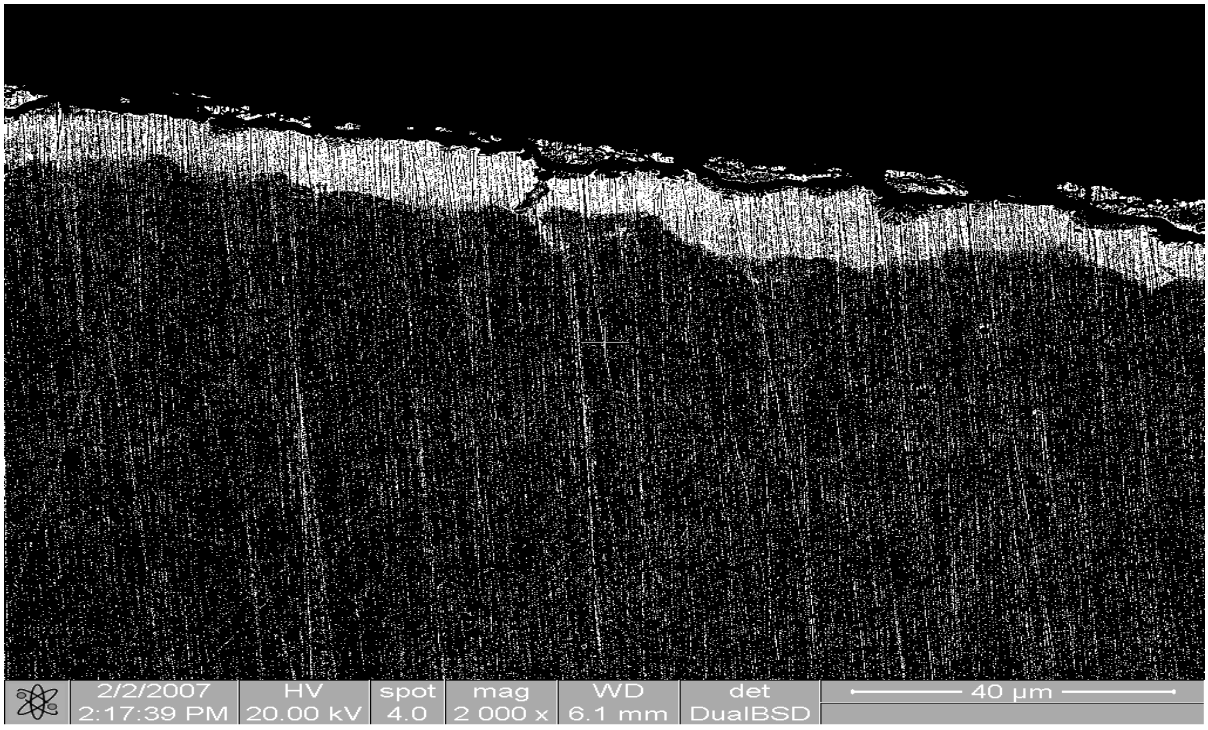


Figure 5.48 Transverse section of alloy P421 showing the Al depleted area after exposing the alloy to a 0.2% SO_2-N_2 environment

Variations across the transverse section of the coated alloy observed in figure 5.49 indicate that there were four different sections that formed. The external area of the coated alloy consisted of a single phase that comprised mainly of Al_2O_3 on its external surface and the EDS performed on the external surface is presented in figure 5.50.

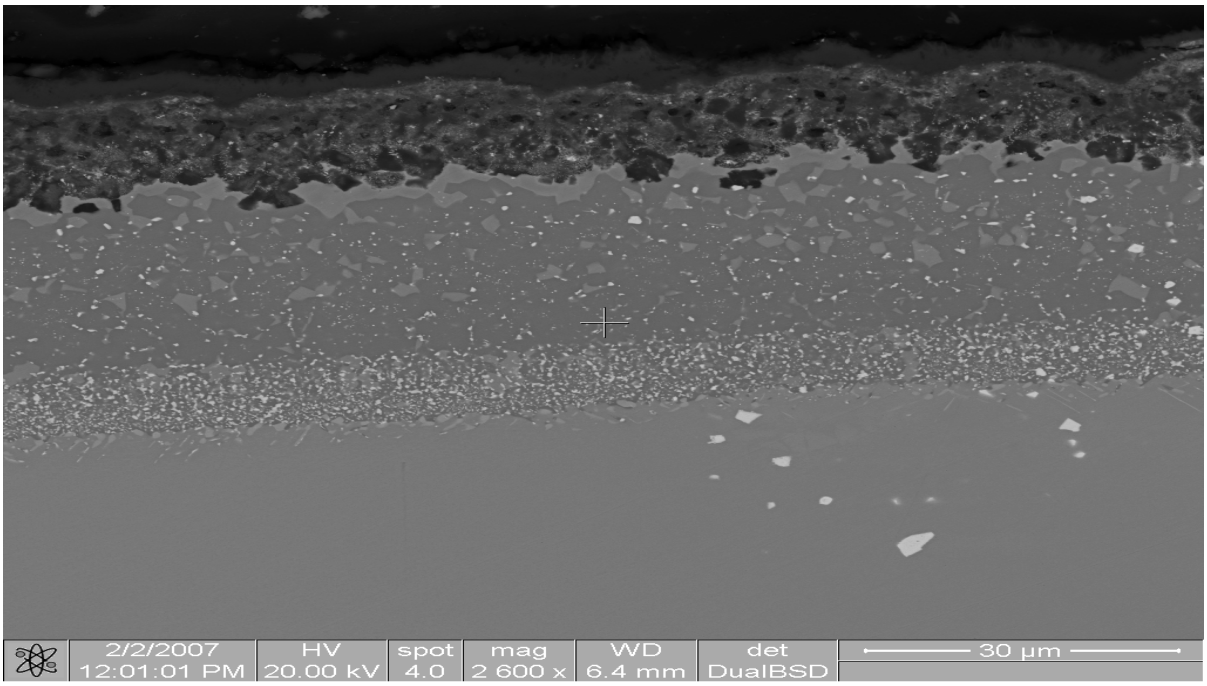


Figure 5.49 Cross section showing the different phases formed when the alloy was exposed to 0.2% SO_2-N_2 atmosphere

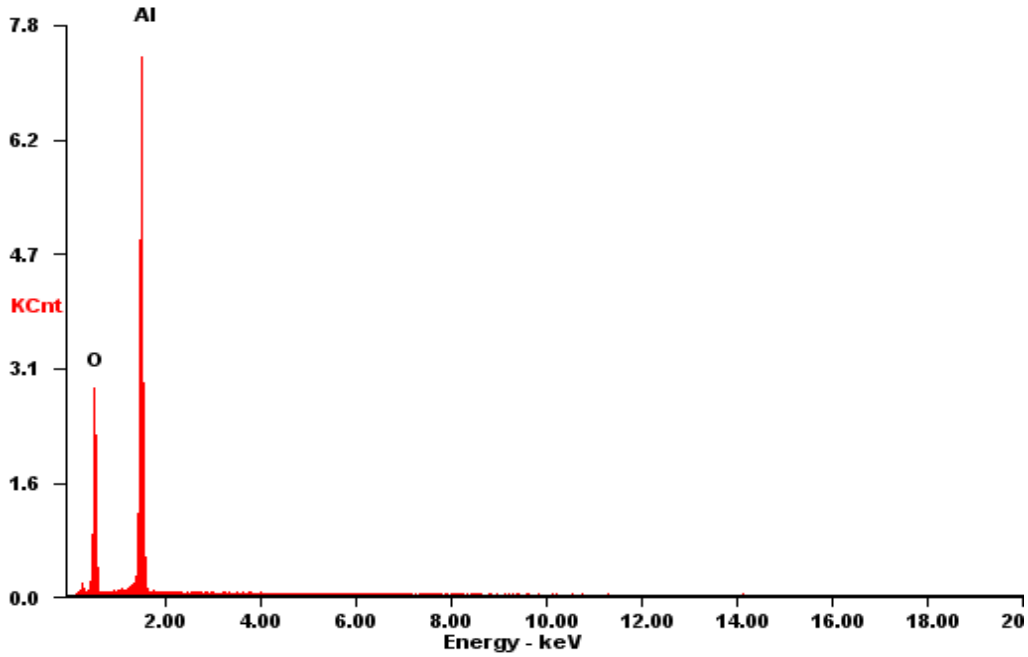


Figure 5.50 EDS analysis performed on the external scale of the coated alloy after sulphidation test

The interdiffusion zone is shown on the micrograph that was taken at high magnification in figure 5.51. Needle-like structures that formed were rich in refractory elements, as determined from EDS performed and given in figure 5.52.

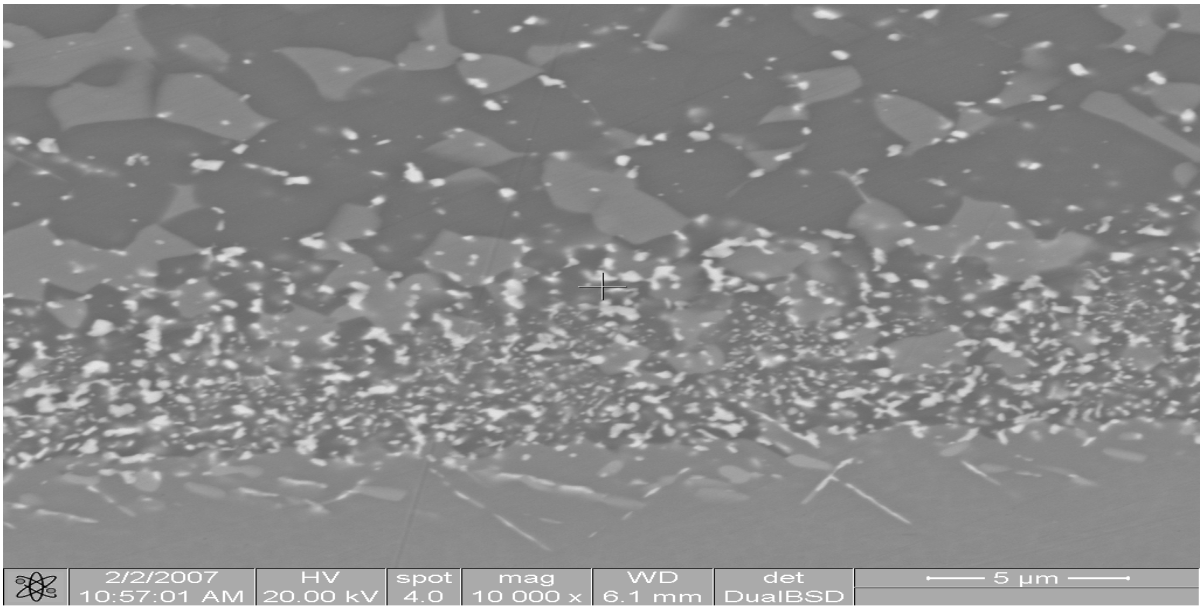


Figure 5.51 Inter-diffusion zone at high magnification of the coated Ni-based superalloy after 60 hours in a 0.2% SO_2-N_2 atmosphere

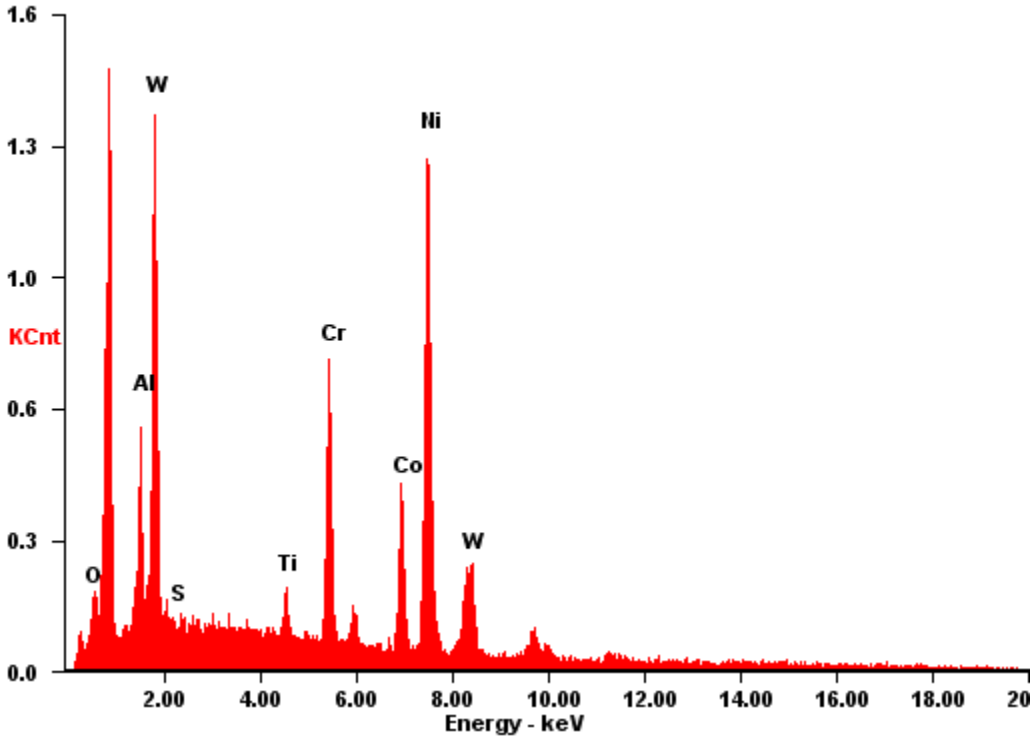


Figure 5.52 EDS analysis performed on the needle-like phases that formed between the substrate and the coating

The effect of sulphur on corrosion behaviour of these alloys was the main focus of the study. It was noted that only the area below the alumina scale was affected by sulphur, where Cr_xS_y and Ni_xS_y compounds formed below the Al_2O_3 scale. Further analysis indicated that there were no traces of S deeper into the substrate. Figure 5.53 shows the EDS analysis performed below the Al_2O_3 scale where sulphidation took place.

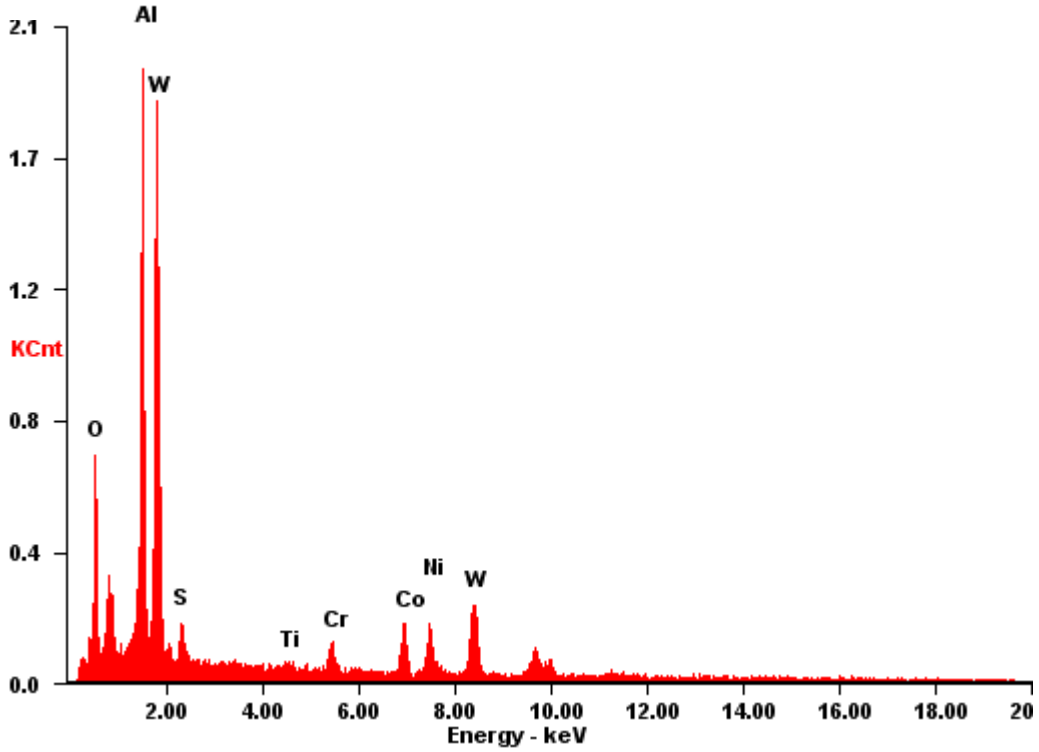


Figure 5.53 EDS analysis performed on the coated alloy in the area below the Al_2O_3 scale

Three distinct areas that were observed during the analysis indicated that instead of alumina, the alloy formed a non-protective columnar structure of NiO. Below the NiO scale was a greyish area rich in Cr, followed by a light phase rich in Ta as shown in figure 5.54.

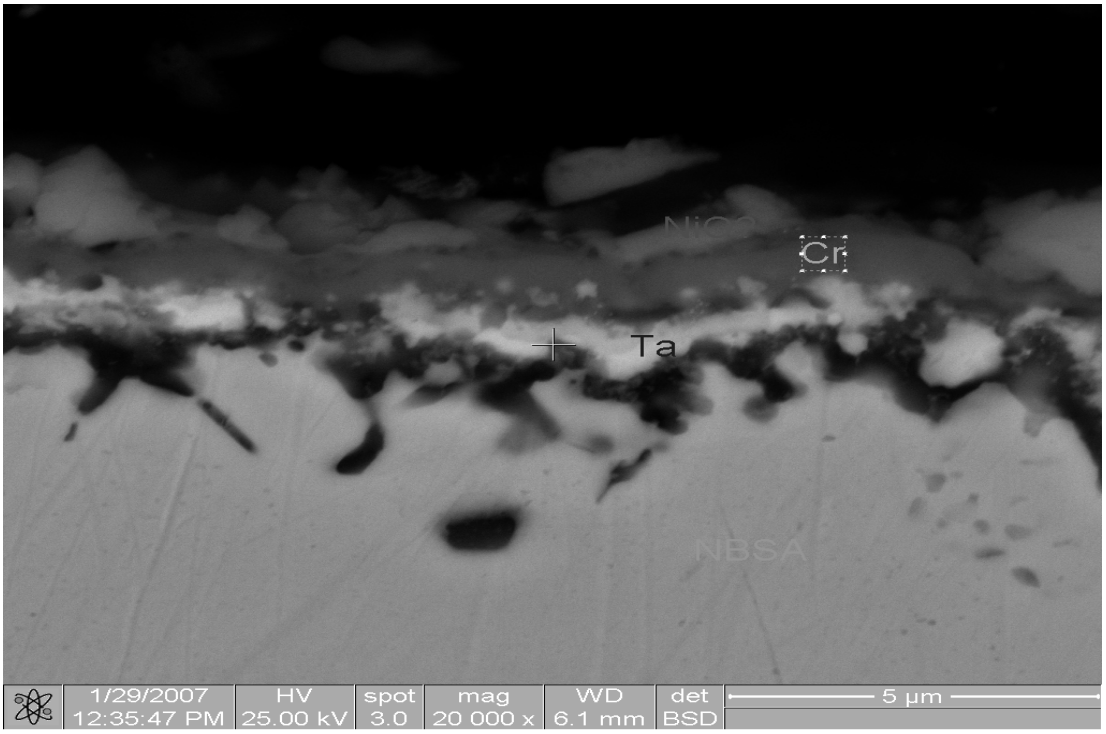


Figure 5.54 Secondary image of the cross section of the uncoated Ni-based superalloy after sulphidation test

5.2.3 X-ray Radiation Diffraction Analysis after Sulphidation

X-ray diffraction patterns obtained from the external surfaces of the investigated alloys before and after conducting the corrosion test in mixed gases containing 0.2% SO_2-N_2 for a period of 60 hours, are presented in figures 5.55-5.61.

A comparative study of two spectra of the coated alloy before and after sulphidation test indicated changes that occurred after the test. β-NiAl phase reacted to form oxides and possible sulphides were formed.

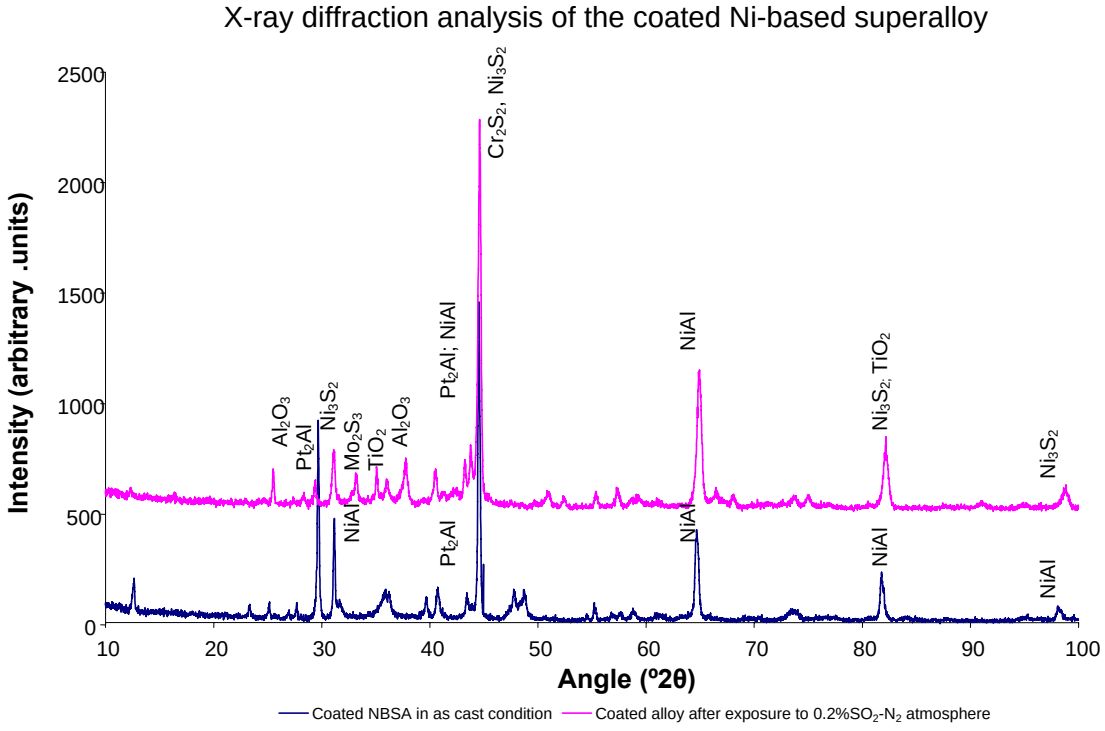


Figure 5.55 XRD spectrum performed on the coated Ni-based superalloy before and after corrosion in controlled atmosphere constituting of 0.2% SO_2-N_2 at 900ºC for a period of 60 hours

The major phase that formed on the external surface of the uncoated alloy was NiO. The uncoated alloy suffered serious internal sulphidation forming sulphides such as Cr_3S_4, according to XRD analysis. The XRD spectra obtained from the surface of the uncoated alloy is presented in figure 5.56.

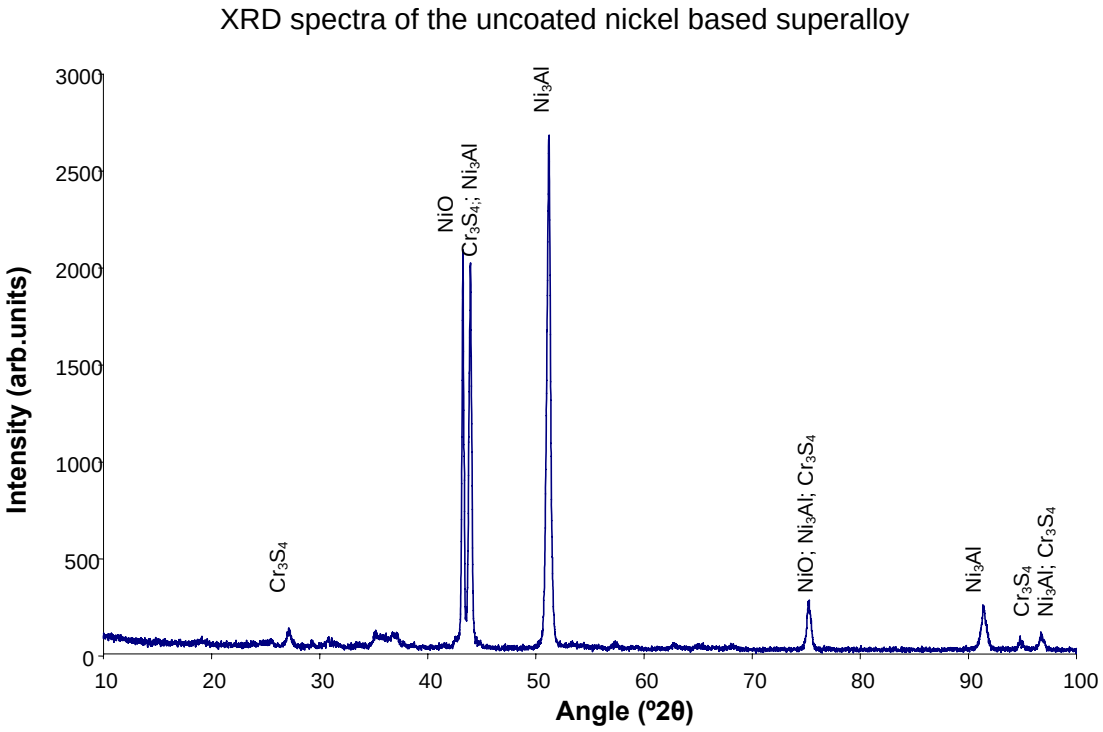


Figure 5.56 XRD pattern on the uncoated Ni-based superalloy after exposure to 0.2%SO_2-N_2 atmosphere

No significant changes were observed on the spectra of alloys RS1, RS2 and RS3 as indicated in figures 5.57; 5.58 and 5.59. Slight intensity increases were observed, and these were due to the formation of Al_2O_3 scale.

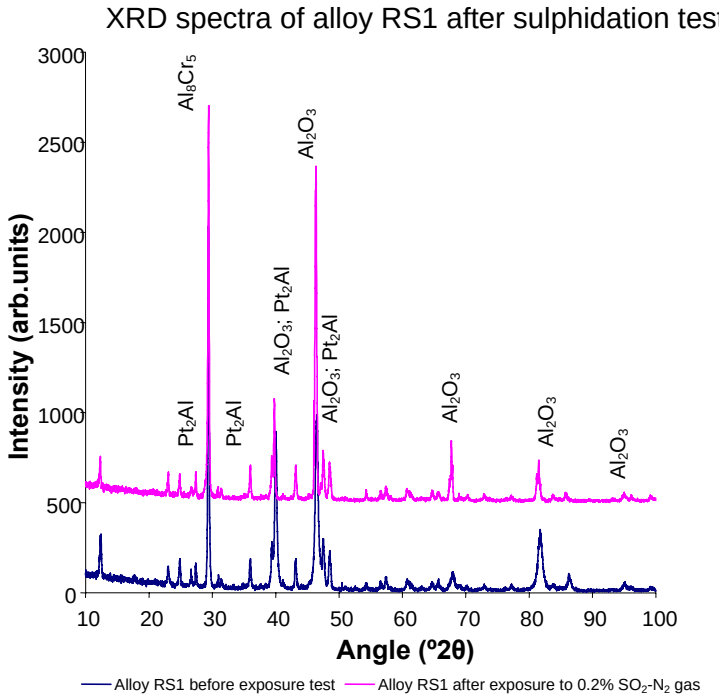


Figure 5.57 XRD spectra performed on the external surface of alloy RS1 before and after exposure to 0.2% SO_2-N_2 atmosphere at 900ºC for a period of 60 hours

Spectra on the surface of alloy RS2 show considerable increase in the intensity of the major peaks of the alloy after the sulphidation test, as depicted in figure 5.58.

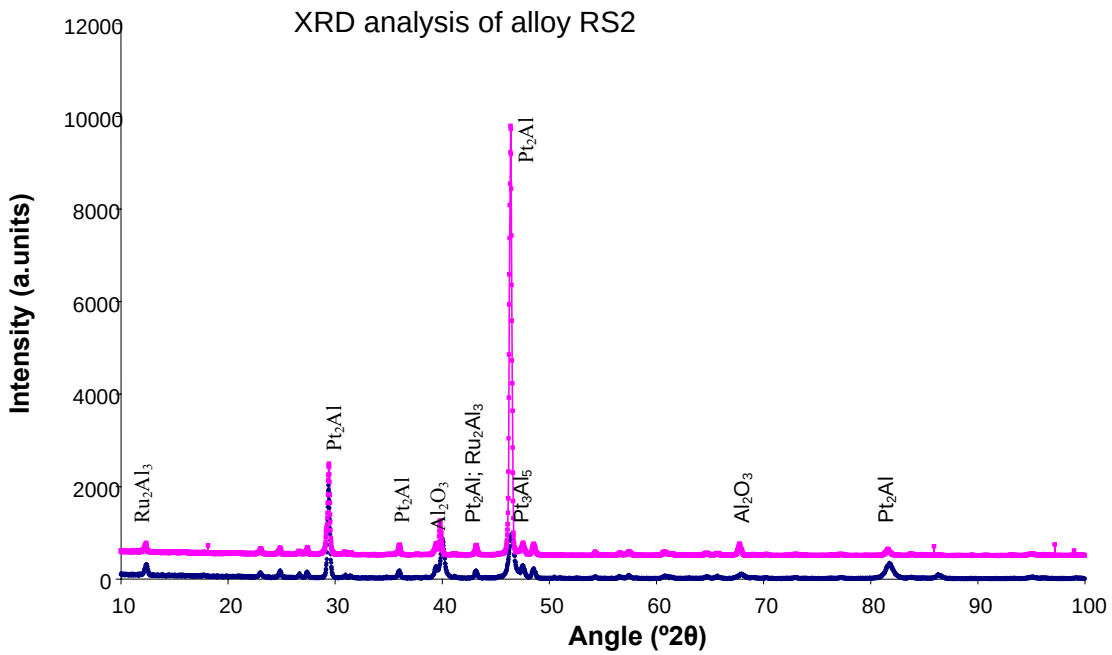


Figure 5.58 XRD spectrum performed on the external surface of alloy RS2 [Pt-Al-Ru] before and after exposure to 0.2% SO_2-N_2 atmosphere at 900ºC for a period of 60 hours

Figure 5.59 represents XRD spectra obtained on the surface of alloy RS3. According to the analysis, some of the corrosion products that were detected were Al_2O_3 and the Pt_2Al phase.

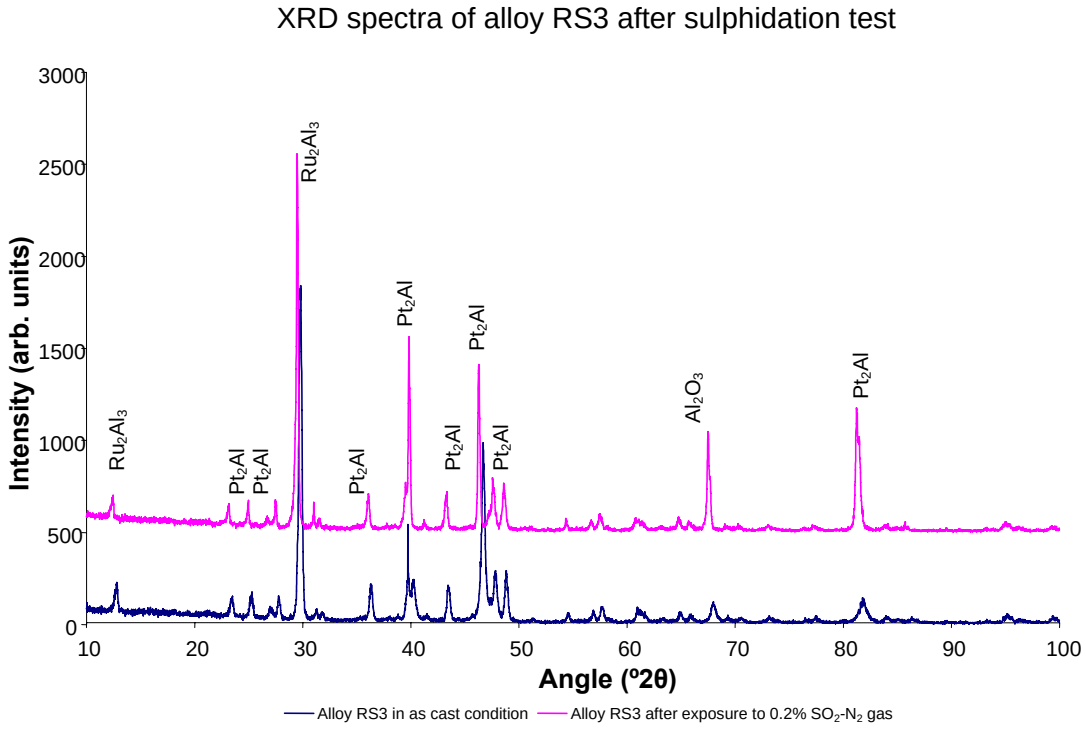


Figure 5.59 XRD spectrum performed on the external surface of alloy RS3 [Pt-Al-Cr-Ru] before and after exposure to a 0.2% SO_2-N_2 atmosphere at 900ºC for a period of 60 hours

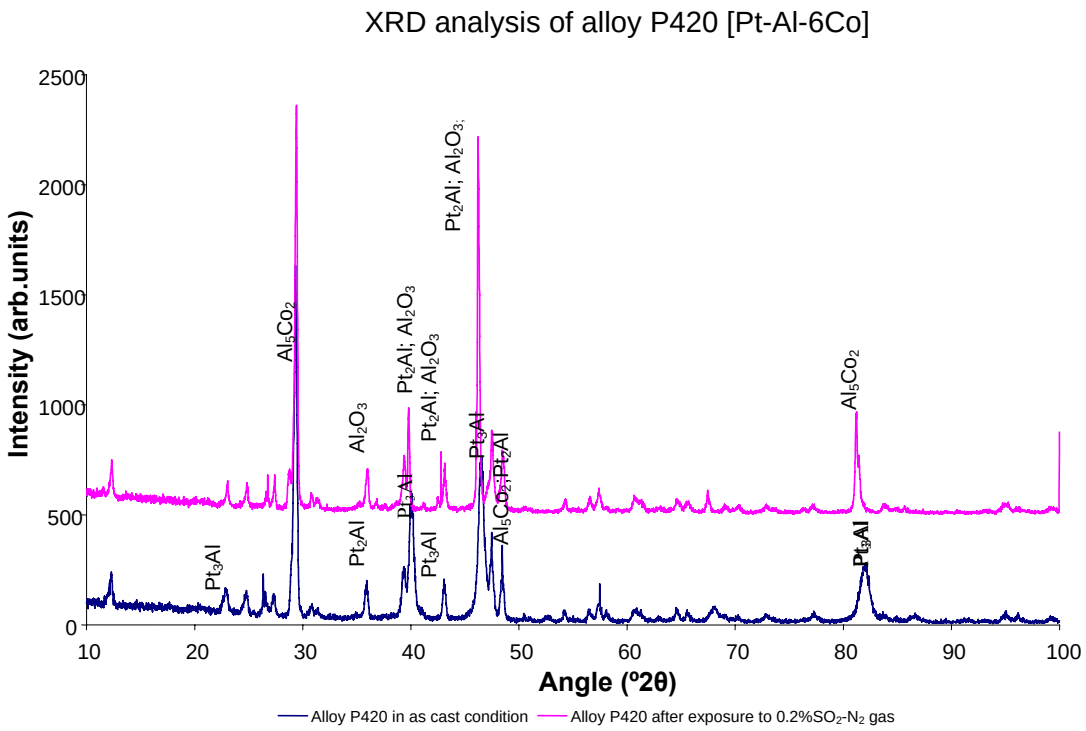


Figure 5.60 XRD spectrum performed on the external surface of alloy P420 [Pt-Al-6Co] before and after exposure to a 0.2% SO_2-N_2 atmosphere at 900ºC for a period of 60 hours

Different from alloys RS1, RS2 and RS3, there were slight changes on surfaces of alloys P420 and P421. Co-oxides were detected on the surface of these alloys after the sulphidation test, as indicated in figure 5.61. Alloy P421 underwent sulphidation and formed sulphides such as Al_2S and PtS.

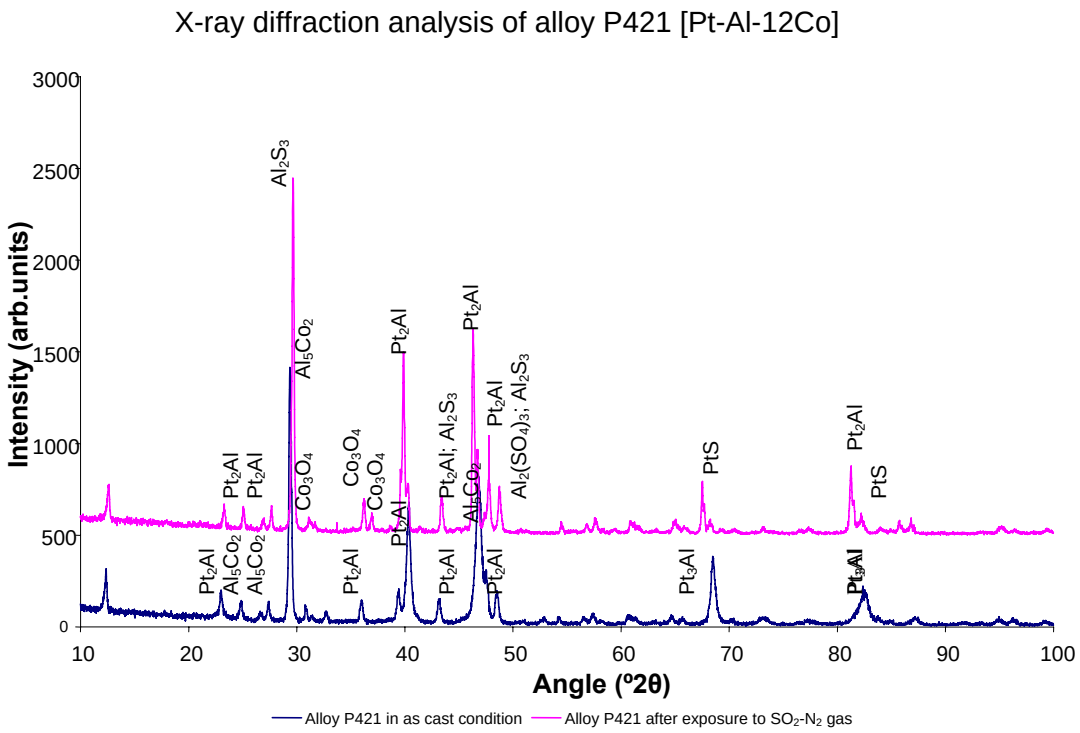


Figure 5.61 XRD pattern of alloy P421 in as-cast condition and after exposing the alloy to a gaseous environment of 0.2% SO_2-N_2 for duration of 60 hours

5.2.4 Raman Analysis

Raman analyses were performed on surfaces of the corroded alloys to validate compounds unidentified by techniques mentioned previously. Raman scans covered a range from 250-2500 cm^{-1}. The optical micrographs of corroded surfaces are placed next to each respective spectrum of the investigated alloys. The spectra are shown in figures 5.62-5.68. Two prominent peaks that are similar to all the investigated alloys occur within the 1026-1032cm^{-1} range and 1048-1062cm^{-1}. The peaks were assigned to molecular vibrations of SO_4^{2-} ions. Sulphates form prints in the 900-1250cm^{-1} and 570-680 cm^{-1} range. The Raman peak at 981 cm^{-1} wavenumber is due to the symmetric stretching mode, whilst the Raman peak at 1051 cm^{-1} is as a result of the asymmetric stretching mode [Kloprogge and Frost, 1999]. A broad peak at approximately 840cm^{-1} wavenumber is believed to be due to molecular vibrations of SO_4^{2-} ions. Co_3O_4 was detected on the surface of the two Co-containing alloys, alloy P420 and alloy P421.

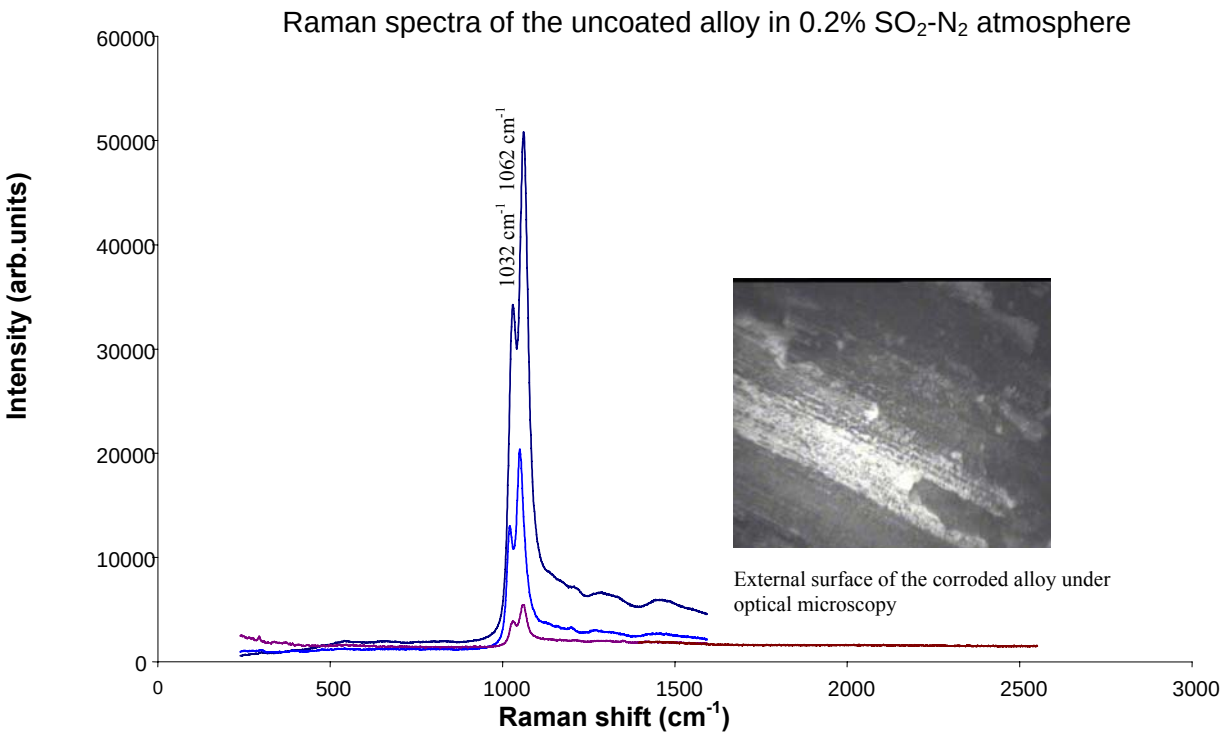


Figure 5.62 Raman spectra collected on the external surface of the uncoated alloy after sulphidation at 900°C for a period of 60 hours

In a study by Kloprogge and Frost (1998), the peaks at 1027 and 1029 cm^{-1} wavenumbers were assigned to N-O-Al bond vibrations. This suggested that traces of nitrates were also formed on the surfaces of corroded alloys.

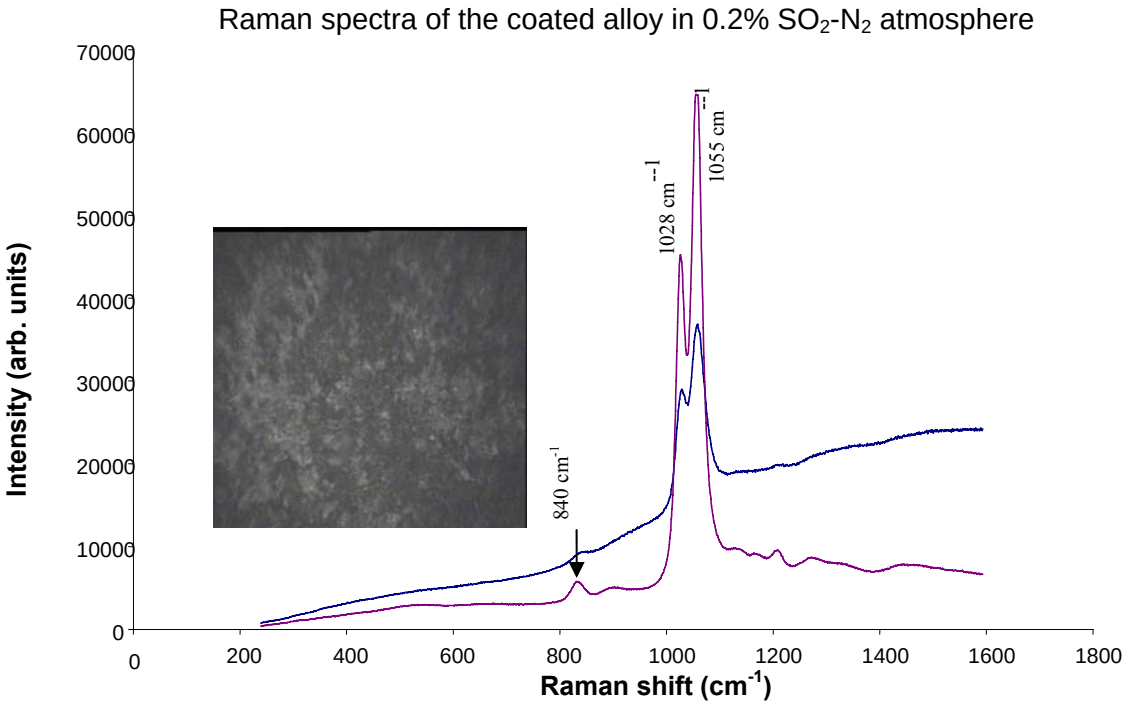


Figure 5.63 Raman spectra collected on the external surface of the coated alloy after sulphidation at 900°C for a period of 60 hours

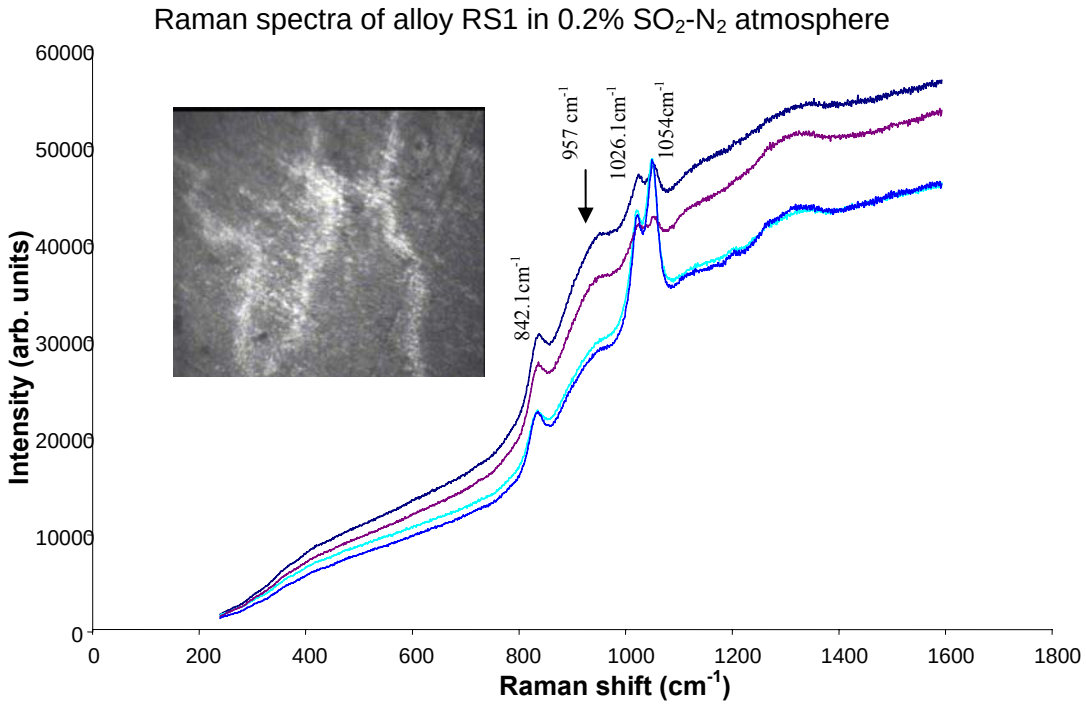


Figure 5.64 Raman spectra collected on the external surface of alloy RS1 after sulphidation at 900°C for a period of 60 hours

Peaks that formed on the surface of alloy RS2 were sharper and had higher intensities. Raman spectrum of alloy RS2 was similar to that of alloy RS3, as illustrated in figures 5.65 and 5.66. Table 5.2 tabulates the peaks that formed on the surface of alloys RS1, RS2, and RS3.

Table 5.2 Peak positions found on the surface of Pt-based superalloys after exposing the alloys to a corrosive gas

Samples	**Peak 1 (cm^{-1})**	**Peak 2 (cm^{-1})**	**Peak 3 (cm^{-1})**
Alloy RS1	842.1	1026.1	1054
Alloy RS2	834	1027	1056
Alloy RS3	836	1027	1057

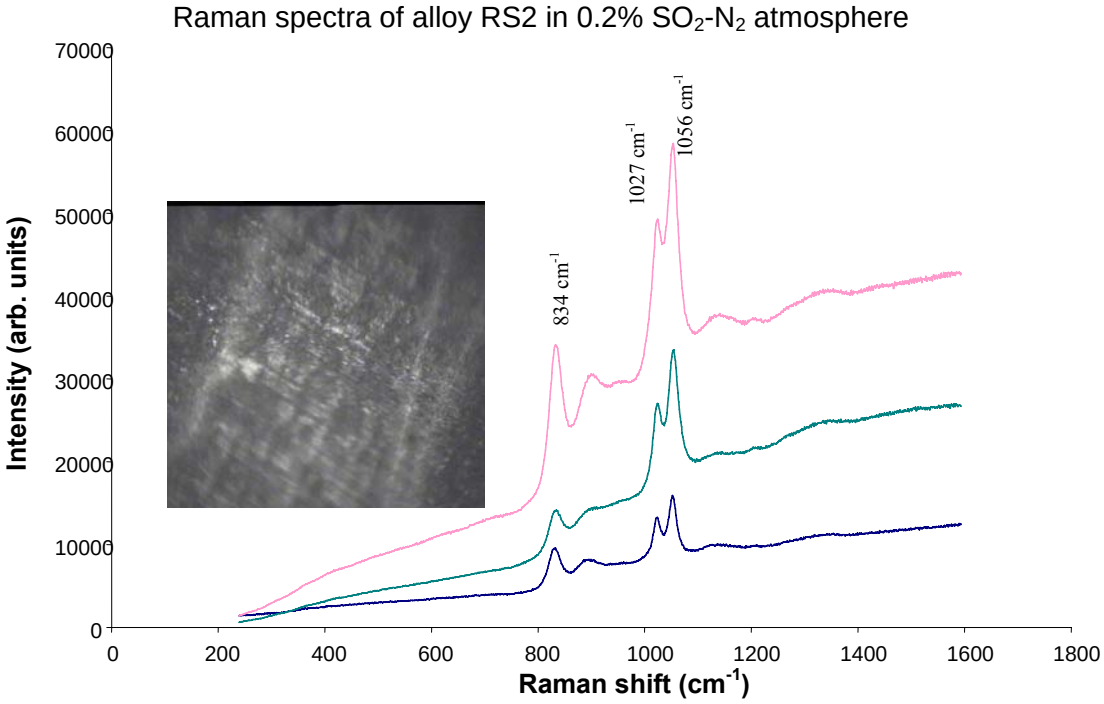


Figure 5.65 Raman spectra collected on the external surface of alloy RS2 after sulphidation at 900°C for a period of 60 hours

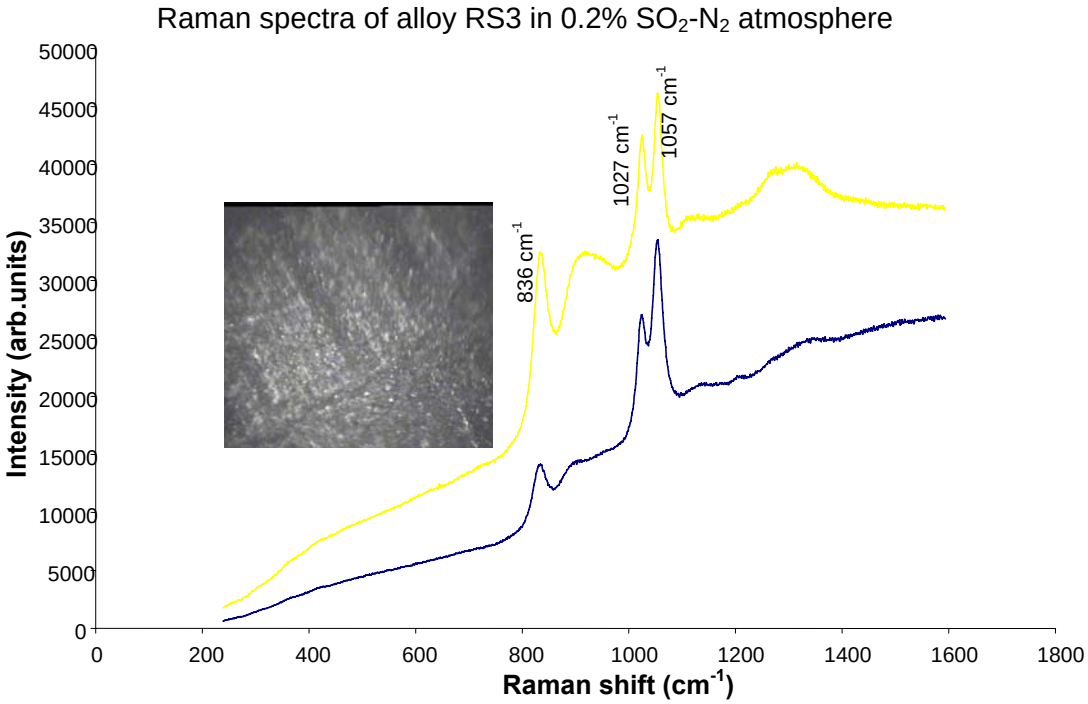


Figure 5.66 Raman spectra collected on the external surface of alloy RS3 after sulphidation at 900°C for a period of 60 hours

The Raman spectra of alloys P420 and P421 are nearly the same, and the spectra are depicted in figures 5.67 and 5.68. The four peaks at 486, 528, 629 and 699 cm^{-1} wavenumbers were assigned to blue Co_3O_4 as indicated in table 5.3. The peak at 194.4 due to F_{2g} vibrations is not observed because the spectral range started at $250cm^{-1}$.

Table 5.3 Raman shifts of the corroded alloy P420 exposed to 0.2%SO_2-N_2 corrosive gas at 900ºC

Co_3O_4	**Vibrational mode**	**Hadjiev *et al.*, 1988**	**This study**
	F_{2g}	194.4	
	E_g	482.4	486
	F_{2g}	521.4	528
	F_{2g}	618.4	629
	A_{1g}	691	699

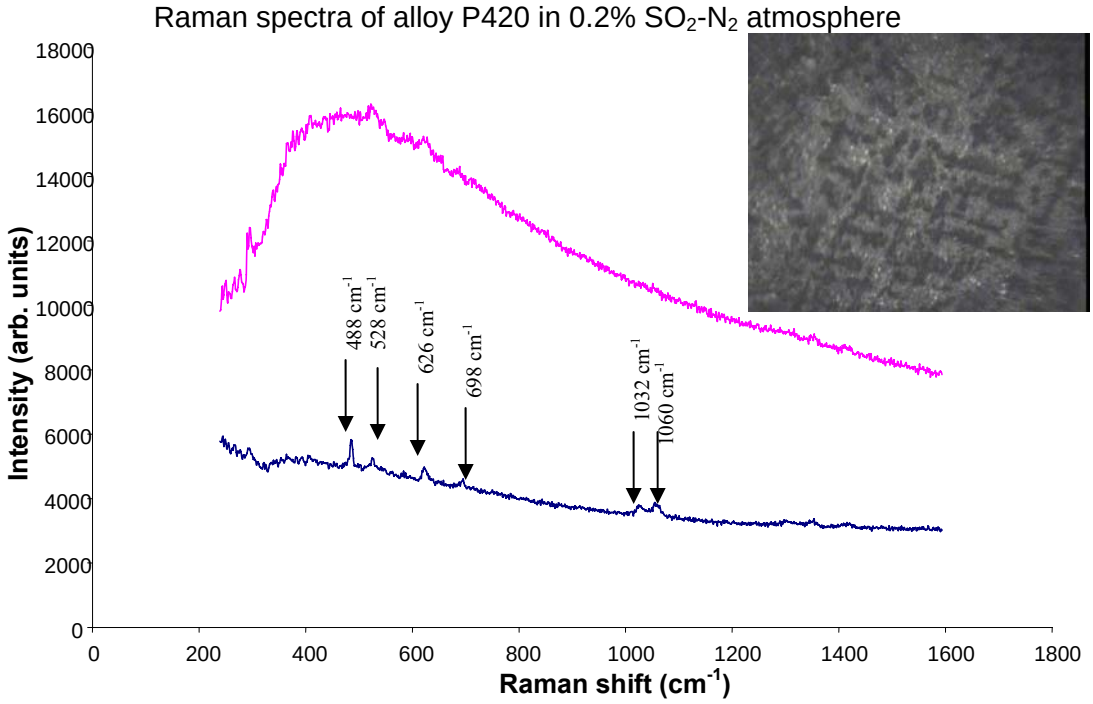


Figure 5.67 Raman spectra collected on the external surface of alloy P420 after sulphidation at 900°C for a period of 60 hours

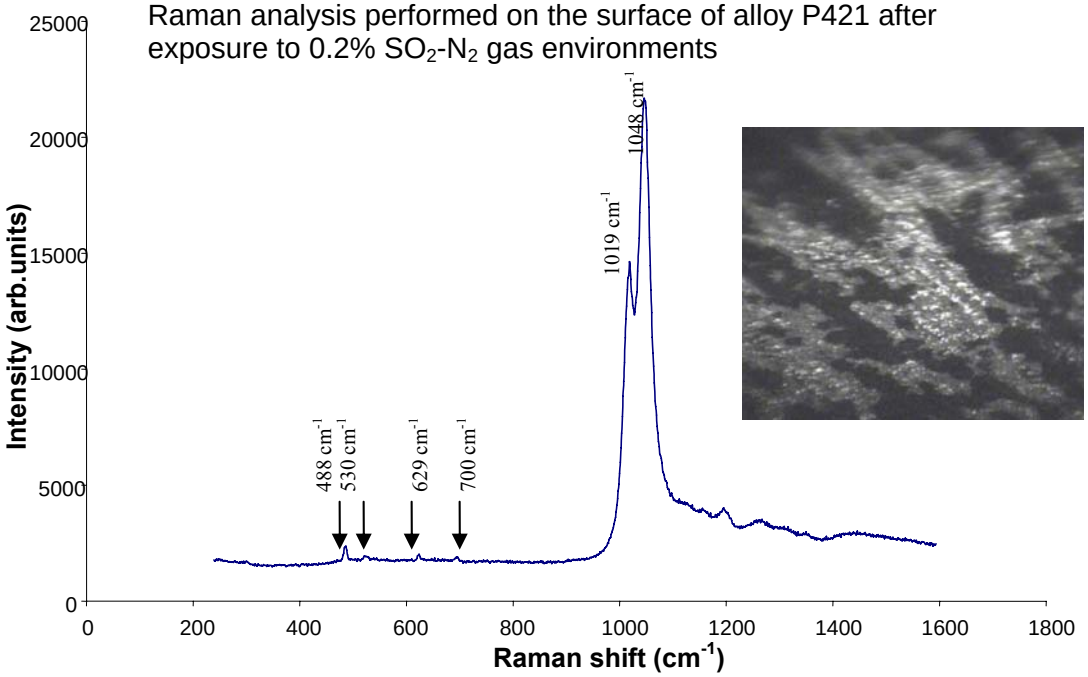


Figure 5.68 Raman spectra collected on the external surface of alloy P421 after sulphidation at 900°C for a period of 60 hours

The results obtained suggest that sulphate salts with possible traces of nitrates formed on the surfaces of the alloys.

6. DISCUSSIONS

Resistance against high temperature corrosion is offered by the formation of a tenacious, stable, non-porous oxide scale. Al_2O_3 is preferred because it is slow-growing and has good thermal stability at high temperatures. The oxide scale isolates the metal alloy from the environment, avoiding interactions between the alloy and its surroundings [Gurrappa, 2003].

6.1 Hot Corrosion

6.1.1 Degradation of the investigated alloys

The uncoated NBSA suffered severe attack following two stages, the initiation and the propagation stages as depicted in the corrosion kinetics curve in figure 5.1. It was during the propagation stage where accelerated attack was observed. The green colour change observed on the surface of the alloy was identified as NiO by XRD and Raman analyses. According to Eliaz *et al.* (2002), the green colour is characteristic of type I hot corrosion. On the other hand, Khajavi and Shariat (2004) stated that the green colour is characteristic of the presence of NiO and Cr_2O_3 in both type I and type II hot corrosion. NiO was the predominant oxide that formed. Al_2O_3 and Cr_2O_3 were able to form and these oxides further reacted with NiO to form spinels that were detected by XRD analysis.

An investigation by Rätzer-Scheibe and Winstone (1993) on single crystal alloys, showed that alloys with high a chromium content have better corrosion resistance compared to

alloys with low Cr composition. This is because Cr reacts to form chromates that consume sulphate ions and suppress the dissolution of Al_2O_3. Research studies have proven that both Al and Cr are the two main alloying elements that resist hot corrosion [Mévrel, 1989; Tzvetkoff and Gencheva, 2003; Ren *et al*., 2005]. Low Cr content in the CMSX-4 alloy made it difficult for the alloy to form a continuous protective oxide scale [Chen and Little, 1997; Gurrappa, 2003].

The coated alloy was able to offer better resistance to the underlying substrate for a longer period (540 hours) compared to the uncoated alloy, following a parabolic rate law. Coatings fail as a result of the inability to form an exterior protective scale [Guo *et al.,* 2006], hence it was thought that the coating failed once there was a depletion of protective oxide formers, primarily Al. Dissociation of the coating led to rapid attack and consumption of the substrate alloy which would eventually lead to possible loss of mechanical properties.

An intrinsic property of Pt is its excellence resistance to corrosion. Platinum's stability at high temperatures led to numerous high temperature applications, regardless of its high price. During the investigation, Pt-based superalloys displayed interesting results. The alloys displayed good corrosion resistance, recording the least weight gains, with minimum affected scale, and minimal external changes compared to their benchmark alloys. Outstanding performance was displayed by alloys RS1 [$Pt_{86}Al_{10}Cr_4$], RS2 [$Pt_{86}Al_{10}Ru_4$] and RS3 [$Pt_{84}Al_{11}Cr_3Ru_2$]. These alloys remained in the incubation stage for much longer period compared to the rest of the investigated alloys. Pt-based

superalloys were generally better performing, despite the different compositions which contributed towards different corrosion behaviours.

XRD analysis performed after hot corrosion identified Al_2O_3 as one of the corrosion compounds that formed on the surface of the alloys. Inward diffusion of oxygen from the gas-salt interface into the substrate led to internal oxidation, forming a somewhat continuous scale. Resistance towards environmental degradation by alloys RS1, RS2 and RS3 was due to the contribution by Al_2O_3, where the γ'-phase acted as a reservoir for aluminium.

Mass losses observed on alloys RS1 and RS3 were due to the formation of volatile oxides. Above 900°C, it is thermodynamically feasible for Cr_2O_3 to dissociate according to reaction 6.1 to form CrO_3.

$$Cr_2O_{3\,(s)} + \frac{3}{2} O_{2\,(g)} \rightarrow 2CrO_{3\,(g)} \qquad (6.1)$$

Despite good performance displayed by the Pt-based superalloys, not all of the developed Pt-based superalloys exhibited good corrosion characteristics. Co-containing alloys, (alloys P420 and P421), showed poor resistance amongst the Pt-based superalloys when subjected to molten salt. Alloy P420 was susceptible to crack formation, whilst P421 was the least resistant when exposed to molten salt after 792 hours and displayed the highest cumulative weight gain and linear corrosion behaviour.

At high temperatures, kinetics are increased and high mobility of ions lead to high diffusion rates. Co readily dissolves in alkaline media causing it to diffuse [Chen *et al.,* 2003] outwards and react with the molten salt, to form non-protective Co compounds identified by XRD analysis as $CoSO_4$. The suggested reaction occurring is given by equation 6.2 [Cutler, 1987].

$$Co_3O_4 + 3\ Na_2SO_4 \rightarrow 3CoSO_4 + 3\ Na_2O + ½\ O_2 \quad (6.2)$$

High degradation rates in Co-containing alloys could be influenced by the formation of low melting eutectics between $CoSO_4$ and Na_2SO_4 [Stringer, 1987].

6.1.2 Possible mechanism of failure

Molten salts are conductive and the reactions occurring in them are electrochemical in nature. The salt chemistry can either be basic or acidic, depending of the ions that are in high concentrations. The presence of molten salt in contact with metals led to fluxing of the protective scale [Stringer, 1987].

Refractory elements such as Mo and W tend to form oxides that are acidic in nature. The acidic medium influences acidic fluxing of the protective scale that leaves the alloy susceptible to failure. Failure of both NBSAs was governed by the acidic fluxing mechanism influenced by the corrosion compounds that formed. Acidic fluxing is generally more aggressive compared to basic fluxing. SO_3, the acidic component, diffuse into the surface and S react to form undesirable sulphides.

Al_2O_3 probably formed during the early stages of the investigation. These oxides were able to offer resistance to Pt-based superalloys. Oxides further reacted with the salt, forming non-protective oxides. Cr_2O_3 help reduce the rate of consumption of Al_2O_3, by consuming SO_4^{2-} [Ren *et al.,* 2003]. The effective roles of Cr and Al as alloying elements was evident in alloy RS1, since it exhibited better corrosion resistance than the rest of the investigated high temperature alloys.

Basic fluxing of the protective scale led to failure of the protective scale. Figure 6.1 shows a fluxed scale on the surface of alloy RS3. Basic fluxing of Cr_2O_3 and Al_2O_3 were described by Rapp (2002) as indicated in equations 6.3 and 6.4. Internal oxidation and the inability to form a continuous oxide scale contributed to failure of Pt-based superalloys.

$$Cr_2O_3 + O^{2-} = 2CrO_2^- \qquad (6.3)$$

$$Al_2O_3 + O^{2-} = 2AlO_2^- \qquad (6.4)$$

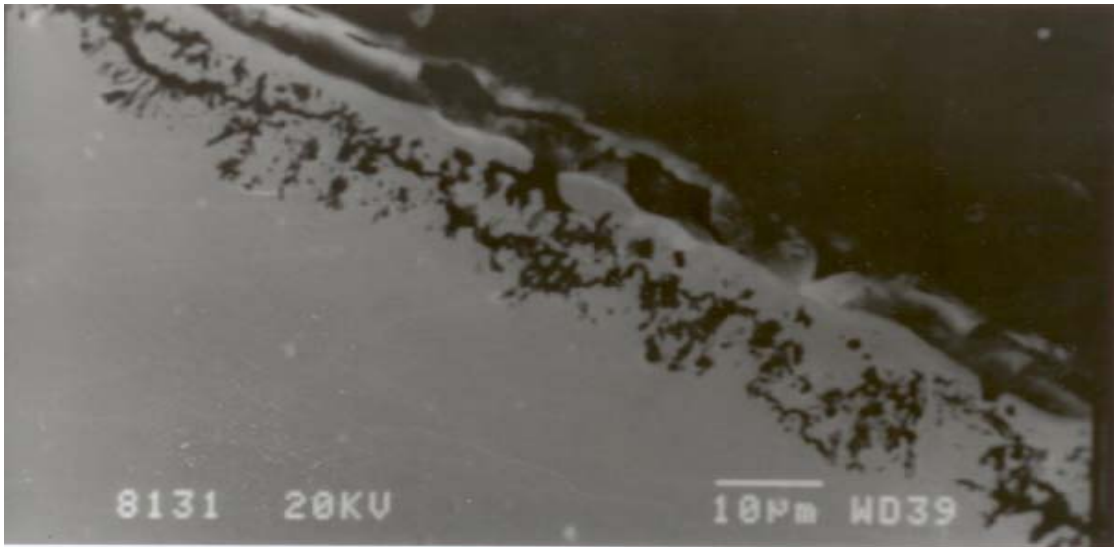


Figure 6.1 Cross section of alloy RS3 showing fluxing of the external scale when the alloys were immersed in molten Na_2SO_4 salt

6.1.3 Role of alloying elements in corrosion resistance

It is unquestionable that alloying elements have an effect towards corrosion behaviour of high temperature materials. Some alloying elements have beneficial effects towards corrosion resistance while others are essential to enhance mechanical properties. Different alloying elements in ternary and quaternary alloys were added to improve strength and stability of the alloys. Moreover, these alloys played a special role in improving the corrosion resistance of the Pt-based superalloys.

As already discussed, refractory elements such as Mo and W are good for improving strength. However, these alloying elements are poor in enhancing corrosion resistance, and instead they aggravate the conditions [Gurrappa, 2003]. Refractory elements impact negatively on hot corrosion resistance of NBSAs and this was noted with both the coated and the uncoated alloys.

Co improves hot corrosion resistance in high temperature materials and Co-based superalloys are known to have superior corrosion resistance over NBSAs [Stringer, 1987]. Co was added to ternary Pt-based superalloys, alloy P420 [$Pt_{79}Al_{15}Co_{6}$] and P421 [$Pt_{73}Al_{15}Co_{12}$] especially to improve the alloy's formability and strength. However, these alloys showed poor corrosion resistance compared to the other investigated Pt-based superalloys, forming a loose and porous oxide scale despite their higher Al content. Alloy P421 was the most unstable amongst the Pt-based superalloys. This observation indicates that there should be a minimum amount of Co added to these alloys and presently, the Co

content does not effectively improve corrosion properties of the two Co-containing ternary alloys.

Sulphides are undesirable, because of their detrimental effect towards brittleness of Pt-based superalloys. Sulphur activity is increased once oxygen activity is lowered as a result of oxide formation. The activity of O_2 was lowered as a result of the formation of oxides on the external surface of the alloys. The presence of S led to the formation of sulphide compounds such as $NaPtS_2$, PtS and $CoSO_4$, as detected by XRD on alloy P420. Cracks were visible on the surface of the alloy as depicted in figure 6.2. Scale spallation around the cracked area shows that the scale was porous with poor adherence.

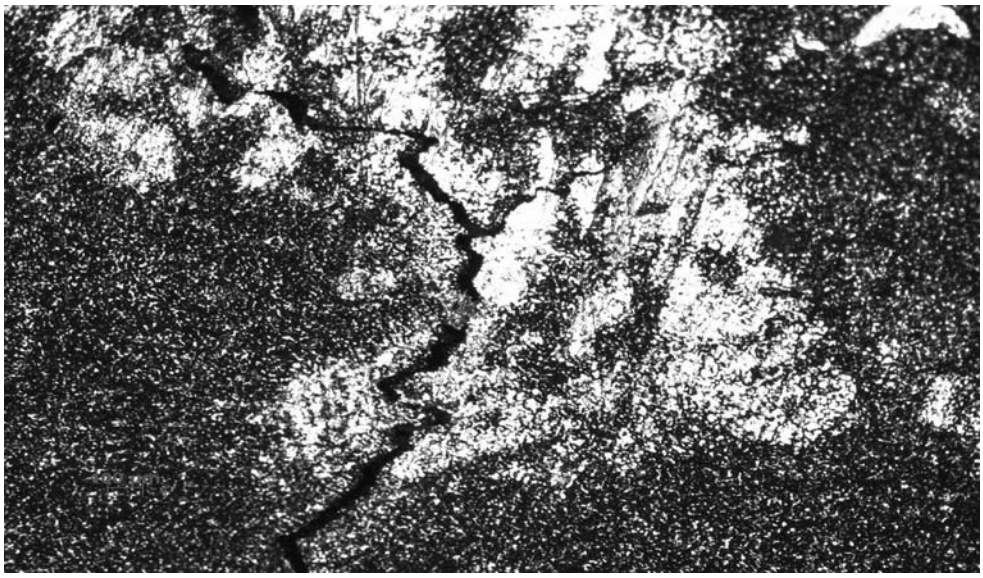


Figure 6.2 Spallation around the cracks on the surface of alloy P420 that was subjected to molten salts at 950ºC for a period of 540 hours

Crack resistance is one of the crucial properties a high temperature material should possess. Work conducted at Mintek showed that the Pt-Al-Z (where Z represents Cr and

Ru in the study) system had resistance against crack formation [Cornish *et al.,* 2004], but alloy P420 formed cracks on its surface, making the alloy undesirable for high temperature applications. Spallation of the oxide scale and crack formation was induced by thermal cycling and stresses in the alloy. Oxides spallation is due to the difference in thermal expansion coefficients or induced stresses [Mevrel, 1989].

The role of Al as an alloying element was excellent when oxidation of the developed materials were evaluated [Süss *et al.,* 2001]. Similar effects were noticed in both hot corrosion and sulphidation tests. Pt improves scale adhesion in coatings [Zheng *et al.,* 2006]. In this investigation it was noted that Pt was not reactive to the molten salt, hence the γ-phase contributed towards resistance of the alloys against hot corrosion.

Silica crucibles used during preliminary investigations were reacting with the molten salts and silica deposits were found on the surface of the alloys. These oxides formed a glazing on the surface of the alloys that offered resistance to the alloys.

Alloys RS1, RS2, RS3 are better performing compared to the rest of the investigated alloys. The results indicated that Pt-based superalloys could be ranked as follows: RS1, RS3, RS2, P420 and P421 according to their performance during hot corrosion evaluations.

6.2 Sulphidation

Coatings are commonly used in high temperature components to offer improved corrosion resistance and prevent degradation of materials. Aluminide coatings are

commonly used in gas turbines. These coatings are able to form Al_2O_3 due to the presence of adequate Al.

The coated alloy had the highest corrosion rates and suffered serious degradation compared to the other investigated alloys when subjected to a gaseous environment. β-NiAl oxidizes to form alumina depleting the substrate and subsurface region of Al, as expected of aluminide coatings. According to EDS analysis performed on the two phase region, phase transformation from β-NiAl to Ni_3Al took precedence and affected the corrosion resistance of the alloy, since β-NiAl offer better corrosion resistance than Ni_3Al because of its high alumina content. The four different regions distinguished in cross sections analysis indicated that there was a region beneath the Al_2O_3 scale that comprised of a mixed sulphides (Cr_xS_y and Ni_xS_y). This suggests that the scale was porous and allowed infiltration of sulphides from the atmosphere to react with the alloy.

A needle-like, topologically close packed (TCP) phase rich in W and other alloying elements such as Cr and Co formed next to the interdiffusion zone. Similar behaviour was observed during the oxidation investigation of Pt-aluminide coatings on CMSX-4 by Chen and Little (1997). These needle-like phases are brittle and can have deleterious effects on the mechanical behaviour of the alloy [Chen and Little, 1997]. EDS analysis performed on the TCP phases is presented in figure 6.3. It indicates that the coated alloy suffered internal sulphidation.

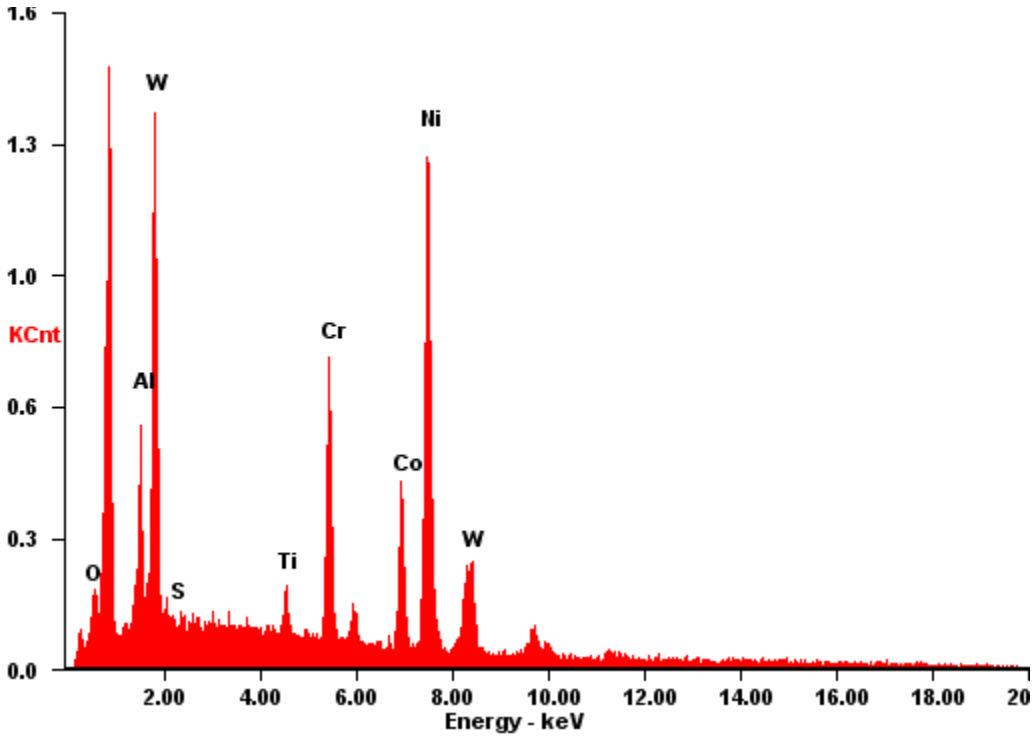


Figure 6.3 EDS spot analysis performed on the needles formed

The uncoated alloy formed cuboidal structures on the surface of the alloy, which comprised mostly of NiO. The formation of NiO hindered further reaction by slowing down corrosion rates. Below the external scale of NiO are a Cr-rich phase and a Ta-rich phase. Ta is soluble in Ni_3Al and is susceptible to oxidation [Pomeroy, 2005]. There was a decrease in the amount of Cr across the surface, suggesting that there was a depletion of alloying elements as a result of oxidation and possible volatilization.

The performances of the Pt-based superalloys were better than those of the NBSAs. Alloy RS2 outperformed all investigated alloys, and formed a stable oxide scale that protected the substrate alloy from further attacks. Alloy RS1 was also relatively stable compared to

the Co-containing alloys. Once again alloy P420 and P421 were prone to serious degradation attacks compared to other investigated Pt-based superalloys.

XRD analysis performed prior and after sulphidation tests indicated that there were not much change on surfaces of alloys RS1, RS2 and RS3. Scale of the Co-containing alloys was becoming darker and this was due to formation of oxides and diffusion of Co and other alloying elements. There was a region below the corroded surface that comprised of the γ-phase. The area was even larger for alloy P421 than for P420. This area increased with increasing exposure to the corrosive environment. Below the depletion zone was an area that comprised of a dendritic structure.

Sulphur was not detected on alloys RS1, RS2 and RS3. Thus these alloys suffered internal oxidation and not sulphidation. It is likely that SO_2 decomposed into S and O_2. O_2 reacted to form oxides; since they are thermodynamically more stable and was released into the atmosphere in a gaseous state.

Al was diffusing out of the alloys to form Al_2O_3. There was also a diffusion of Cr which could have formed volatile compounds. XRD analysis performed before and after the test indicated that there were changes in the microstructure of the alloys. The thin oxide scale that formed on the surfaces of alloy RS1 and RS3 did not prevent internal oxidation from taking place. Moreover, cracks were observed on cross section of alloy RS3.

7.1 CONCLUSIONS

The development of new high temperature materials was necessary in order to achieve desired efficiencies in gas turbines. However, these high operating temperatures have serious damaging effect towards mechanical integrity of high temperature alloys. Furthermore, it is difficult to engineer an alloy with both high temperature strength and corrosion resistance.

Higher degradation rates were observed in molten salt conditions than the gaseous environment. This indicates that salts are more aggressive than the gaseous environment. NBSAs have outstanding mechanical properties, however, their corrosion properties are not excellent. NBSAs exhibited poor performance under both test conditions because:

- Alloys have low chromium concentrations
- Refractory elements aggravate corrosion conditions in molten salts, advancing acidic fluxing
- Alloys form non-protective oxides that allows the corrosive environment to further react with alloying elements in the substrate
- Formation of undesirable brittle TCP phases led the alloys to be susceptible to corrosion attacks
- Once the coating is damaged, it cannot protect the alloy from further attacks

Pt-based superalloys have proved to perform better under both test conditions, showing better performance over the benchmark alloys. Effect of alloying elements showed to be crucial towards the performance of the developed high temperature alloys.

- Al is highly desirable because it forms a protective scale that protects the alloy from hot corrosion attacks, sulphidation and oxidation.
- Pt and Ru have good corrosion properties forming a passive layer. However, they are susceptible to higher temperatures and high velocity conditions.
- Alloy RS1, RS2 and RS3 showed better corrosion resistance than the NBSAs with long incubation periods, mainly due to the presence of Al and Cr.
- Pt-Al-Ru is most corrosion resistant in SO_2-N_2 gaseous environment and Pt-Al-Cr is the most corrosion resistant alloy in the molten salt environment.
- Cr forms a protective scale, however it has application limits.
- Longer exposure times than those used in this investigation could result in the degradation of Pt-based superalloys.
- Co-containing alloys were susceptible to crack formation both in salt and gaseous environments, making these ternary alloys undesirable for high temperature applications.
- Higher volume fractions of the ~Pt_3Al would be desirable, so that more Al can react to form a protective barrier between the environment and the alloys.

This research work was to serve as a material selection exercise for Pt-based superalloys for application in the gas turbine industry. It was established that Pt-based superalloys have long incubation periods when exposed to molten salts. Moreover, corrosion and

mechanical behaviour of alloy RS1 was consistent. It exhibited good corrosion resistance in molten salts and remained fairly stable when exposed to a gaseous environment. The effects of Al and Cr on the corrosion behaviour of Pt-based superalloys are substantial. Ru not only is added to stabilise the ~Pt_3Al phase, but also help in improving corrosion resistance of the developed high temperature alloys. However, Ru is not effective at temperatures exceeding 950ºC, because of the formation of volatile oxides. Co-containing alloys are susceptible to attack by sulphur, forming brittle PtS that causes the alloys to crack.

7.2 RECOMMENDATIONS

Pt-based superalloys are fairly resistant to corrosion attacks. However, Pt, Ir and Ru alloys tend to form volatile oxides in flowing gases at higher temperatures. It should be established if the developed alloys will be able to sustain high velocity gases. Thus a burner-rig test at high pressures and high velocities should be conducted on the desired alloy, which is an alloy with high volume fractions, surface stability and good mechanical properties.

High temperature electrochemical tests would be ideal in investigating the behaviour of Pt-based superalloys and give more insight that what can be deduced from mass loss tests.

Co improves corrosion resistance, moreover, it improves formability of alloys. However, with Pt-based superalloys, Co-containing alloys performed poorly. Other alloying elements should be considered that will stabilise Co and reduce its high diffusion rates.

Pt is faced with great competition by other materials such as composites that are highly desirable because of their light weight. Considerable reduction of the alloy's density should receive attention as well.

7.3 CONTRIBUTION OF THIS RESEARCH

Previous studies indicated that Ni-based superalloy analogues based on Pt are possible. These alloys proved to have acceptable mechanical properties under the investigated conditions. Pt-based superalloys are more corrosion resistant in aggressive environment (molten salts and SO_2-containing environment). Hot corrosion studies showed that Pt-based superalloys failed, following a fluxing mechanism. However, a Pt-Al-Cr alloy have better resilience towards degradation by molten salts. Pt is quite expensive and ideally, it would be of interest to operate these alloys without applying coatings so that low cost can be achieved. However, these alloys are not completely resistant to high temperature corrosion, therefore coatings applications would be necessary for Pt-based superalloys. This investigation is a further contribution to the development of suitable Pt-based alloys and coatings for ultimate use in high temperature corrosion environments.

8. REFERENCES

Ashby, M.F. and Jones, D.R.H. (1988), ***Engineering Materials 1***, Pergamon Press

Bhadesia, H.K.D.H (2003). Nickel Based Superalloys. INTERNET. http://www.msm.cam.ac.uk/phase-trans/2003/Superalloys/superalloys.html. Cited 01 March 2005

BowmanR.(2000).Superalloys.INTERNET.htttp://www.tms.org/Meetings/Speciality/Superalloys2000/SuperalloysHistory.html.Cited 16 March 2007

Bradford, S.A. (2002), ***Corrosion Control***, Second Edition, Casti Publishing Inc.

Bradley, E.F. (Editor), (1979), ***Source Book on Materials for Elevated-Temperature Applications***, ASM, American Society for Metals

Brandl, W., Toma, D., and Grabke, H.J., (1998), The Characteristics of Alumina Scale Formed on HVOF-Sprayed MCrAlY Coatings, ***Surface and Coatings Technology***, Vol. 108-109, pp 10-15

Callister, W.D., (1999), ***Materials Science and Engineering***, 5th edition, John Wiley & Son Inc.

Carter, T.J., (2005), Common Failures in Gas Turbine Blades, ***Engineering Failure Analysis,*** Vol.12, pp 237-247

Chatterjee, U.K., Bose, S.K., and Roy, S.K., (2001), ***Environmental Degradation of Metals***, Marcel Dekker Inc.

Chen, J.H., and Little, J.A., (1997), Degradation of the Platinum Aluminide Coating on CMSX4 at 1100°C, ***Surface and Coatings Technology***, Vol. 92, pp 69-77

Chen, Z., Wu, N.Q., Singh, J., and Mao, S.X., (2003), Effect of Al_2O_3 Overlay on Hot Corrosion Behaviour of Yttria-stabilized Zirconia Coating in Molten Sulphate-Vandate Salt, ***Thin Solid Films***, Vol. 443, pp 46-52

Choi, B., and Lockwood, D.J., (2005), Peculiarities of the Structural Phase Transitions in Na_2SO_4 (V): a Raman Scattering Study, ***Journal of Physics: Condensed Matter***, Vol. 17, pp 6095-6108

Chown, L. H., Cornish, L. A., and Joja, B., (2004), Structure and Properties of Pt-Al-Co Alloys, ***Microscopy Society of Southern Africa Conference Proceedings***, Vol. 34, p 9

Cornish, L.A., Hohls, J., Hill, P.J., Prins, S., Süss, R., and Compton, D.N., (2002), The Development of Platinum-Based Alloys and their Thermodynamic Database, ***34th IOC on Mining and Metallurgy***, pp 545-549

Cornish, L.A, Fisher, B., and Vőlkl, R., (2003), Development of Platinum-Group-Metal Superalloys for High Temperature Use, ***MRS Bulletin***, pp 632-637

Cornish, L.A., Süss, R., Chown, L. H., Taylor, S., Glaner, L., Douglas, A., and Prins, S.N., (2004), Platinum-Based Alloys for High Temperature and Special Applications, International Platinum Conference "Platinum Adding Value", ***South African Institute of Mining and Metallurgy****, Symposium Series, S38*, pp 329-336

Cutler, A.J.B., (1987), Corrosion Reactions in Molten Sulphates, ***Materials Science and Technology***, Vol. 3, pp 512-518

Deb, D., Iyer, S.R., and Radhakrishnan, V.M., (1996), Assessment of High Temperature Performance of a Cast Nickel Base Superalloy in Corrosive Environment, ***Scripta Materialia****,* Vol. 35, No. 8, pp 947-952

Dragos, U., Gabriela, M., Waltraut, B., and Ioan, C., (2005), Improvement of the Oxidation Behaviour of Electron Beam Remelted MCrAlY Coatings, ***Solid State Sciences***, Vol. 7, pp 459-464

Eliaz, N., Shemesh, G., and Latanision, R.M., (2002), Hot Corrosion in Gas Turbine Components, ***Engineering Failure Analysis***, Vol. 9, Issue 1, pp 31-43

Elliot, P. (1990), Practical Guide to High Temperature Alloys, ***Nickel Development Institute***, pp1-10

Formanek, B., Szymański, K., Szczucka-Lasota, B., and Włodarczyk, A., (2005), New Generation of Protective Coatings Intended for the Power Industry, ***Journal of Materials Processing Technology***, Vol. 164-165, pp 850-855

Fritscher, K., Leyens, C., and Peters, M., (1995), Development of a Low-Expansion Bond Coating for Ni-base Superalloys, ***Materials Science and Engineering A***, Vol. 190, pp 253-258

Gaskel, D.R., (1981), ***Introduction to Metallurgical Thermodynamics***, 2nd Edition, McGraw-Hill

Gitanjaly, Prakash, S. and Singh, S. (2002), Effects of MgO and CaO on Hot Corrosion of Fe Base Superalloy Superfer 800H in Na_2SO_4-60% V_2O_5 Environment, ***British Corrosion Journal***, Vol. 37, No. 1, pp 56-62

Goward, G.W., (1998), Process in Coatings for Gas Turbine Airfoils, ***Surface and Coatings Technology***, Vol. 108-109, pp 73-79

Guo, M.H., Wang, Q, M., Ke, P.L., Gong, J., Sun, C., Huang, R,F., and Wen, L.S., (2006), The Preparation and Hot Corrosion Resistance of Gradient NiCoCrAlYSiB Coatings, ***Surface and Coatings Technology***, Vol. 200, pp 3942-3949

Gurrappa, I., and Rao, A.S., (2006), Thermal Barrier Coatings for Enhanced Efficiency of Gas Turbine Engines, ***Surface and Coatings Technology***, Vol. 201, pp 3016-3029

Gurrappa, I. (2003), Influence of Alloying Elements on Hot Corrosion of Superalloys and Coatings: Necessity of Smart Coatings for Gas Turbine Engines, ***Materials Science and Technology***, Vol.19, No.2, pp 178-183

Gurrappa, I., (2001), Identification of Hot Corrosion Resistant MCrAlY Based Bond Coatings for Gas Turbine Engine Applications, ***Surface and Coatings Technology***, Vol. 139, Issues 2-3, pp 272-283

Hadjiev, V.G., Illiev, M.N., Vergilov, I.V., (1988), The Raman Spectra of Co_3O_4, ***Journal of Physics and Chemistry***: Solid State Physics, Vol. 21, pp 199-201

Hale, R. (2000). Properties and Typical Applications of Selected Nickel Alloys INTERNET http://www.engr.ku.edu.htm.Cited 01 April 2007

Hertzberg, R.W. (1989), ***Deformation and Fracture Mechanics of Engineering Materials***, 3rd, John Wiley & Son

Hill, P.J., Yamabe-Mitarai, Y. Murakami, H. Cornish, L.A., Witcomb, M.J., Wolff, I.M., and Harada, H., (2001), The Precipitate Morphology and Lattice Mismatch of Ternary (Pt)\Pt_3Al Alloys, ***TMS (The Minerals, Metals & Materials Society)***, pp 527-533

Huo, X., Zhang, J.S., Wang, B.L., Wu, F.J., and Han, Y.F., (1999), Evaluation of NiCrAlYSi Overlay Coating on Ni_3Al Based Alloy IC-6 After Engine Test, ***Surface Coatings and Technology***, Vol. 114, pp 174-180

Hüller, M., Wenderoth, M., Vorberg, S., Fischer, B., Glatzel, U., and Völkl, R, (2005), Optimisation of Composition and Heat Treatment of Age-Hardened Pt-Al-Cr-Ni Alloys, ***Metallurgical and Materials Transactions A***, Vol. 36, pp 681-689

Jones, R.H., (2001), ***Environmental Effects on Engineering Materials***, Marcel Dekker, Inc.

Kermanpur,A., Varahraam, N., Engilehel, E., Mohammadzadeh, M., and Davami, P., (2000), Directional Solidification of Ni Base Superalloy IN738LC to Improve Creep Properties, ***Materials Science and Technology***, Vol 16, No.5, pp 579-586

Khajavi, M.R., and Shariat, M.H., (2004), Failure of First Stage Gas Turbine Blades, ***Engineering Failure Analysis***, Vol. 11, Issue 4, pp 589-597

Kim, J.H., and Wang, Π, S., (2005), Development of an in Situ Raman Spectroscopic System for Surface Oxide Films on Metals and Alloys in High Temperature Water, ***Nuclear Engineering and Design***, Vol. 235, Issue 9, pp 1029-1040

Kloprogee, J.T., and Frost, R.L., (1998), Raman Microscopy Study of Basic Aluminium Nitrate, ***Spectrochimica Acta Part A: Molecular and Biomolecular***, Vol.55, Issue 1, pp 163-169

Kloprogee, J.T., and Frost, R.L., (1999), Raman Microscopy Study of Basic Aluminum Sulfate, ***Journal of Materials Science***, Vol.34, pp 4199-4202

Konter, M., and Thumann, M., (2001), Materials and Manufacturing of Advanced Industrial Gas Turbine Components, ***Journal of Materials Processing Technology***, Vol. 117, pp 386-390

Lee, W.H., and Lin, R.Y., (2002), Hot Corrosion Mechanism of Intermetallic Compound Ni_3Al, ***Materials Chemistry and Physics***, Vol. 77, pp 86-96

Levine, S.R., Opila, E.J., Halbig, M.C., Kiser, J.D., Singh, M., and Salem, J.A., (2002), Evaluation of Ultra-High Temperature Ceramics for Aero Propulsion Use, ***Journal of the European Ceramic Society***, Vol. 22, Issues 14-15, pp 2757-2767

Massalski, T.B., Murray, J.L., Bennett, L.H., and Baker, H., (1986), ***Binary Alloy Phase Diagrams***, American Society of Metals, Library Congress Cataloging in Publication Data, Vol.1, 1st Edition, pg 153

Miller, S., (1996), Advanced Materials Mean Advanced Engines, ***Materials World***, Vol.4, pp 446-449

McLean, M., Ardakani, M., Basoalto, H., Ghosh, R.N., and Shollock, B.A., (1999),A Continuum Damage Mechanisms Approach to Modelling Anisotropic Creep in Single Crystal Superalloys, ***Creep Behaviour of Advanced Materials for the 21st Century***, The Minerals, Metals and Materials Society, pp 13-22

Mévrel, R., (1989), State of the Art on High-Temperature Corrosion-Resistant Coatings, ***Materials Science and Engineering A***, Vol. 120, pp 13-24

Müller, J., and Neuschütz, D., (2003), Efficiency of α-Alumina as Diffusion Barrier Between Bond Coat and Bulk Material of Gas Turbine Blades, ***Vacuum***, Vol. 71, pp 247-251

Nicholls, J.R., Simms, N.J., Chan, W.Y., and Evans, H.E., (2002), Smart Overlay Coatings-Concept and Practice, ***Surface and Coatings Technology***, Vol. 149, Issues 2-3, pp 236-244

Pint, B.A., Di Stefano, J.R., and Wright, I.G., (2006), Oxidation Resistance: One Barrier to Moving Beyond Ni-Base Superalloys, ***Materials Science and Engineering A***, Vol. 415, pp 255-263

Pomeroy, M.J., (2005), Coatings for Gas Turbines Materials and Long Term Stability Issues, ***Materials and Design***, Vol. 26, Issue 3, pp 223-231

Prasad, B.D., Sankaran, S.N., Wiedemann, K.E., and Glass, D.E., (1999), Platinum Substitutes and Two-Glass Overlayers as Low Cost Alternatives to Platinum Aluminide Coatings, ***Thin Solid Films,*** Vol. 345, pp 255-262

Purvis, A.L., and Warnes, B.M., (2001), The Effect of Platinum Concentration on the Oxidation Resistance of Superalloys Coated with Single-phase Platinum Aluminide, ***Surface and Coating Technology***, Vol. 146-147, pp 1-6

Rapp, R. A., (2002), Hot Corrosion of Materials: A Fluxing Mechanism, ***Corrosion Science***, Vol. 44, No.2, pp 209-221

Ren, X., Wang, F., and Wang, X., (2005), High Temperature Oxidation and Hot Corrosion Behaviours of the NiCr-CrAl Coating on a Nickel Based Superalloy, ***Surface and Coating Technology***, Vol. 198, Issues 1-3, pp 425-431

Rätzer-Scheibe, H.J., and Winstone, M.R., (1993), Hot Corrosion Resistance of Coated Single Crystal Superalloys under Marine Conditions, ***Materials Science and Technology***, Vol. 9, pp 253-258

Saltykov, P., Fabrichnaya, O., Golczewski, J., and Aldinger F., (2004), Thermodynamic Modeling of Oxidation of Al-Cr-Ni Alloys, ***Journal of Alloys and Compounds***, Vol. 381, pp 99-113

Schneibel, J.H., (2001), Beyond Nickel-Base Superalloys.
INTERNET.http://www.ornl.gov/~wedworks/cppr/y2001/pres/122106.pdf. Cited 20 April 2007

Schultz, U., Leyens, C., Fritscher, K., Peters, M., Saruhan-Brings, B., Lavigne, O., Dorvaux, J., Poulain, M., Mévrel, R., and Caliez, M., (2003), Some Recent Trends in Research and Technology of Advanced Thermal Barrier Coatings, ***Aerospace Science and Technology***, Vol. 7, pp 73-80

Schweitzer, P.A., (1998), ***Encyclopedia of Corrosion Technology***, Marcel Dekker Inc. p 242

Sharafat, S., Kobayashi, A., Chen, Y., and Ghoniem, N.M., (2002), Plasma Spraying of Micro-Composite Thermal Barrier Coatings, ***Vacuum***,Vol. 65, pp 415-425

Shirvani, K. Saremi, M. Nishikata, A. and Tsuru, T. (2003), Electrochemical Study on Hot Corrosion of Si-Modified Aluminide Coated In-738LC in Na_2SO_4 -20 wt% NaCl Melt at 750ºC, ***Corrosion Science***, Vol. 45, Issue 5, pp 1011-1021

Sidhu, B.S. and Prakash, S. (2006), Studies on the Behaviour of Satellite-6 as Plasma Sprayed and Laser Remelted Coatings in Molten Salt Environment at 900°C Under Cyclic Conditions, ***Journal of Materials Processing Technology***, Vol. 172, pp 52-63

Sidhu, T.S., Agrawal, R.D., and Prakash, S., (2005), Hot Corrosion of Some Superalloys and Role of High-Velocity Oxy-Fuel Spray Coatings-A Review, ***Surface and Coatings Technology***, Vol. 198, pp 441-446

Sidhu, T.S., Prakash, S., and Agrawal, R.D., (2006), Hot Corrosion and Performance of Nickel-based Coatings, ***Current Science***, Vol. 90, No.1, pp 41-47

Siebert, B., Funke, C, Vaβen, R., and Stöver, D., (1999), Change in Porosity and Young's Modulus, Due to Sintering of Plasma Sprayed Thermal Barrier Coatings, ***Journal of Materials Processing Technology***, Vol. 92-93, pp 217-223

Sims, Chester, T. Stoloff, N.S. Hagel, and William C. (1972), ***Superalloys***, John Wiley & Sons Inc.

Sims, Chester, T. Stoloff, N.S. Hagel, and William C., (1987), ***Superalloys II***, High Temperature Materials for Aerospace and Industrial Power, John Wiley & Sons Inc.

Singh, H., Puri. D., and Prakash, S., (2005), Some Studies on Hot Corrosion Performance of Plasma Sprayed Coatings on a Fe-Based Superalloy, ***Surface and Coatings Technology***, Vol.192, Issue 1, pp 27-38

Stringer, J. (1987), High-Temperature Corrosion of Superalloys, ***Material Science and Technology***, Vol. 3, No. 7, pp 482-493

Süss, R., Hill, P.J., Ellis, P., and Cornish, L.A., (2001), The Oxidation Resistance of Pt-Base Superalloy Pt_{80}:Al_{14}:Cr_3:Ru_3 Compared to that of Pt_{86}:Al_{10}:Cr_4, ***Microscopy Society of Southern Africa-Proceedings***, Vol. 31, p 21

Süss, R., Freund, D., Vőlkl, R., Fisher, B., Hill, P.J., Ellis, P., and Wolff, I.M., (2002), The Creep Behavior of Platinum-Based γ/γ' Analogues of Nickel-based Superalloys at 1300ºC, ***Materials Science and Engineering A***, Vol. 338, pp 133-141

Süss, R., Cornish, L.A., Hill, P.J., and Hohls, J., (2003), Properties of a New Series of Superalloys Based on Pt_{80}:Al_{14}:Cr_3:Ru_3, ***TMS (The Minerals, Metals & Materials Society)***, pp 301-307.

Süss, R., Douglas, A., and Cornish, L.A., (2004), An Electron Microscopy Investigation of Tensile Samples of Pt-based Superalloys, ***Microscopy Society of Southern Africa Conference Proceedings***, Vol. 34, pg 10

Tsaur, C.C, Rock, J.C., Wang, C.J., and Su, Y.H., (2005), The Hot Corrosion of 310 Stainless Steel with Pre-Coated $NaCl/Na_2SO_4$ Mixtures at 750°C, ***Materials Chemistry and Physics***, Vol. 89, Issues 2-3, pp 445-453

Tvetkoff, T., and Gencheva, P., (2003), Mechanism of Formation of Corrosion Layers on Nickel and Nickel-Based Alloys in Melts Containing Oxyanions, ***Materials Chemistry and Physics***, Vol. 82, pp 897-904

Uy, D., Wiegand, K.A., O'Neill, A.E., Dearth, M.A., Weber, W.H., (2002), In situ UV Raman Study of the NO_x Trapping and Sulfur Poisoning Behavior of $Pt/Ba/\gamma\text{-}Al_2O_3$ Catalysts, Journal of Physics and Chemistry B, Vol. 106, pp 387-394

Viswanathan, R., (2001), An Investigation of Blade Failures in Combustion Turbines, ***Engineering Failure Analysis***, Vol.8, pp 493-511

Wang, Q.M., Wu, Y.N., Ke, P.L., Cao, H.T., Gong, C., Sun, C., and Wen, L.S., (2004), Hot Corrosion Behaviour of AIP NiCoCrAl(SiB) Coatings on Nickel Base Superalloys, ***Surface and Coatings Technology,*** Vol. 186, Issue 3, pp 389-397

Wing, R., (2000), White Hot Technology-A Turbine Revolution, ***Materials World***, pp 10-12

Wolff, I.M., and Hill, P.J., (2000), Platinum Metals-Based Intermetallics for High Temperature Service, ***Platinum Metals Review***, Vol. 44, pp 158-166

Yamabe-Mitarai, Y., Koizumi, Y., Murakami, Ro, Y., Maruko, T., and Harada, H., (1996), Development of Ir-base Refractory Superalloys, ***Scripta Materialia***, Vol. 35, No. 2, pp 211-215

Yamabe-Mitarai, Y., and Aoki, H., (2002), Solid-Solution Hardening of Ir by Pt and Ni, ***Materials Letters***, Vol. 56, pp 781-786

Yoshiba, M., (1993), Effect of Hot Corrosion on the Mechanical Performance of Superalloys and Coating Systems, ***Corrosion Science,*** Vol. 35, No. 5-8, pp 1115-1124

Zheng, D., Zhu, S., and Wang., F., (2006), Oxidation and Hot Corrosion Behaviour of a Novel Enamel-Al_2O_3 Composite Coating on K38G Superalloy, ***Surface and Coatings Technology***, Vol. 200, pp 5931-5936